CONCRETE MIXTURE PROPERTIES AFFECTING THE AGGREGATE INTERLOCK MECHANISM OF JOINTS AND CRACKS FOR RIGID PAVEMENT SYSTEMS

by

Luis Carlos Ramírez

B.S., Escuela Colombiana de Ingeniería, 2001

Submitted to the Graduate Faculty of

Swanson School of Engineering in partial fulfillment

of the requirements for the degree of

Master of Science

University of Pittsburgh

2010

UNIVERSITY OF PITTSBURGH

SWANSON SCHOOL OF ENGINEERING

This thesis was presented

by

Luis Carlos Ramírez

It was defended on

November 19, 2010

and approved by

Natasa Vidic, Ph.D., Assistant Professor
Department of Industrial Engineering

John Brigham, Ph.D., Assistant Professor
Department of Civil and Environmental Engineering

Julie Marie Vandenbossche, Ph.D., Assistant Professor
Department of Civil and Environmental Engineering
Thesis Advisor

CONCRETE MIXTURE PROPERTIES AFFECTING THE
AGGREGATE INTERLOCK MECHANISM OF JOINTS AND CRACKS
FOR RIGID PAVEMENT SYSTEMS

Luis Carlos Ramírez, M.S.

University of Pittsburgh, 2010

A high load transfer efficiency (*LTE*) across the joints and cracks is critical for the long-term performance of a concrete pavement system. One of the most important factors affecting the *LTE* of non-doweled joints and cracks is the natural but complex mechanism of aggregate interlock which is characterized by an aggregate interlock factor or joint stiffness (*AGG*). This mechanism has been found to be extensively controlled by the crack width and the surface texture of the cracked face. This surface texture is significantly influenced by critical concrete mixture properties such as water-to-cementitious material ratio, and the type, top size, and hardness of the coarse aggregate.

The determination of the aggregate interlock factor, *AGG*, can be an intricate procedure. Obtaining this factor is commonly performed through iteration in a finite element model, through back-calculation using field data, through constitutive models, or through the use of empirical models that have been established based on laboratory test results. In a similar manner, the determination of the *LTE* at the joints and cracks exhibits some level of complexity. *LTE* can only be determined for in-service pavements or large-scale slabs through the use of specialized equipment such as a falling weight deflectometer (FWD). Consequently, it is imperative to develop relationships that allow an estimation of these important parameters, *LTE* and *AGG*, as a function of critical concrete properties and known pavement characteristics.

The main focus of this study is to develop a relationship between key concrete mixture properties and the parameters *LTE* and *AGG* for different geometric and structural pavement conditions. In order to achieve this goal, first, different concrete mixtures were evaluated in the laboratory on their strength, fracture properties and surface texture characteristics. These results were then supplemented with laboratory and field data from previous studies, and a regression analysis for the complete data set was performed. As a result, an empirical model relating the critical concrete properties and the aforementioned surface texture of the transverse joints/cracks was created. Lastly, this model was incorporated into existing equations to establish a relationship between key concrete properties and the aggregate interlock parameters *LTE* and *AGG*.

TABLE OF CONTENTS

LIST OF TABLES

LIST OF FIGURES

ACKNOWLEDGEMENTS

I would like to express my gratitude to Dr. Julie Vandenbossche not only for her support and guidance during this research project but for her dedication and mentoring throughout my graduate studies. I must thank her for all of the time, resources, and knowledge that she extended to me along the way.

I would also like to thank the graduate students Somayeh Nassiri, Matthew Geary, and Tom Adams, as well as the undergrad student Gary Gehringer for their immense help with the laboratory phase of this study. In the same manner, I would like to note my gratitude to my colleagues Feng Mu, Manik Barman, Kerri Gatti, and the graduate students mentioned above for their support and help in navigating through graduate school.

Special thanks to my friends in Colombia. Their support and unconditional friendship is priceless to me. Much thanks to my parents Eliseo and Blanca, and siblings Paola, Jorge, and Cata whom from the distance have been my inspiration to fight every battle.

Infinite gratitude is owed to the most beautiful engineer: my wife Maria Carolina. Her love, support and technical contributions have been invaluable in the accomplishment of this endeavor.

Finally, thanks to my son Jacobo, who constantly reminded me that working hard is good but having fun is better.

1.0 INTRODUCTION

1.1 BACKGROUND

Effective pavement design is an elaborate process that involves the consideration of a large number of variables specifically determined from the unique conditions of a project. For this reason, the identification and optimization of critical factors affecting the performance of pavement systems is a vital task that needs continuous investigation. State-of-the-art design procedures –such as the Mechanistic-Empirical Pavement Design Guide (MEPDG)– consider a vast range of critical factors that affect the selection, construction, and performance of a pavement system. However, minor attention has been given to the integration of key concrete mixture properties into the structural design process, as well as to the recognition of the effect of these properties on the concrete fracture behavior. Typically, all concrete mixtures are assumed equivalent as long as their strength is similar, however, this is not always the case because variations in concrete components and proportions considerably influence different critical mixture properties, such as the resistance to crack propagation. Consequently, the consideration of concrete fracture properties in the design of pavement concrete mixtures as well as in the pavement structural analysis and predicted performance is an essential task toward the optimization of field performance of rigid pavement systems.

The long-term performance of a rigid pavement largely depends on the load transfer efficiency (*LTE*) of joints and cracks. Good *LTE* is typically reflected in a high quality ride due to small deflections and reduced pavement distresses, such as faulting, corner breaks, spalling, and punchouts. One of the most important factors affecting the *LTE* of non-doweled joints and cracks is the mechanism of aggregate interlock. This is a pure-shear mechanism that depends primarily on crack width and the roughness of the cracked surface. The latter, in turn, depends considerably on concrete mixture properties such as coarse aggregate type, size, and hardness, and water-to-cementitious material ratio (w/c). The variation of these properties affects the rate of concrete crack propagation, as well as the interaction between the different phases of concrete, i.e., coarse aggregate, interfacial transition zone (ITZ), and cement matrix.

An aggregate interlock factor or joint stiffness (*AGG*) is used to characterize the ability to transfer loads across the crack. The determination of this *AGG* value is typically performed through backcalculation of falling weight deflectometer (FWD) data obtained in the field, through iteration using finite element programs, through the use of constitutive models, or through empirical models that have been developed based on different types of large-scale laboratory tests. However, for the most part, these methods are only suitable for specific load magnitudes and frequencies, geometries, and pavement structures. In addition, the available constitutive models do not take into account the variations in concrete mixture proportions and materials that critically influence the *AGG* value.

1.2 RESEARCH OBJECTIVE

The primary objectives of this study are: 1) to develop an empirical model that relates key concrete mixture properties such as water–to-cement ratio and coarse aggregate type, top size, and hardness with the *LTE* of non-doweled joints and cracks for different crack widths and slab thicknesses. 2) To relate the key concrete mixture properties already mentioned with the *AGG* value for different pavement characteristics such as: subgrade support, radius of relative stiffness, crack width and slab thickness.

Additionally, this study will look into the influence of the above-mentioned concrete mixture properties on the fracture behavior of concrete, and the effect of the fracture mechanics parameters obtained for each concrete mixture on the pavement *LTE* and *AGG* value.

The result of this investigation can be used in a forward analysis of joints and cracks in rigid pavements as well as in the design of paving concrete mixtures to optimize field performance

1.3 RESEARCH APPROACH

To accomplish the stated objectives, a testing program was designed to complement data from studies performed by other researchers in order to account for a wide range of values of the considered variables. Different concrete mixtures were evaluated in the laboratory to determine their flexural strength as well as their fracture mechanics parameters, such as fracture toughness, fracture energy, and critical crack length. In addition, the surface texture of the cracked specimens was quantified using the Volumetric Surface Texture (VST) method. The results of

this laboratory tests were analyzed in combination with laboratory and field data from prior studies in order to establish the relationship between the key concrete mixture properties and *LTE* and joint stiffness. The relationship between surface texture and concrete fracture parameters is also explored using the collected data.

1.4 STRUCTURE OF THE THESIS

The structure of the thesis is as follows: Chapter 2 presents a literature review that includes a discussion on *LTE* in rigid pavements, concrete mixture properties and fracture mechanics parameters affecting aggregate interlock, methods to determine surface texture characteristics, and available models for the aggregate interlock mechanism. Chapter 3 describes the previous studies from which the supplemental data was obtained to incorporate into this study as well as the design of the laboratory study implemented in this investigation. Chapter 4 presents the data obtained from the laboratory study as well as the analysis of the complete data set that includes the data from the previous studies as well as this study. Chapter 5 presents the development of the empirical models relating the investigated concrete mixture properties with *LTE* and *AGG* and presents an analysis of the models' predictions. Chapter 6 presents an analysis of the concrete fracture parameters obtained for the concrete mixtures in this study and a previous study, along with a relationship between VSTR and concrete fracture parameters. Chapter 7 presents a complete summary of the research findings and recommendations for future research.

2.0 LITERATURE REVIEW

2.1 LOAD TRANSFER EFFICIENCY

Long-term pavement performance is greatly affected by the *LTE* of cracks and joints. Several distresses that affect the ride quality can be developed as a consequence of poor *LTE*. These distresses are corner cracking and excessive faulting of jointed concrete pavements (JCP) and punchouts of continuously reinforced concrete pavements (CRCP). On the contrary, pavement systems with high *LTE* typically do not exhibit pavement serviceability problems.

Traffic loads applied near a joint in a Portland Cement Concrete (PCC) pavement causes both loaded and unloaded slabs to deflect because a portion of the load applied to the loaded slab is transferred to the unloaded slab. Consequently, deflections and stresses in the loaded slab significantly less when compared to those that would develop if loaded at a free edge.

The *LTE* of a joint or a crack is determined based on the ratio of the deflection of the unloaded slab measured directly across and equidistantly away from the joint with respect to the deflection of the loaded slab. Deflection *LTE* (LTE_{δ}) is typically calculated using the following equations:

$$LTE_{\partial} = \frac{\partial_u}{\partial_l} * 100\% \qquad (2\text{-}1)$$

$$LTE_{\partial}* = \frac{2 \cdot \delta_u}{\delta_l + \delta_u} * 100\% \qquad (2\text{-}2)$$

where,

δ_u = Maximum deflection at the discontinuity of the unloaded slab.

δ_l = Maximum deflection at the discontinuity of the loaded slab.

Figure 1 depicts the *LTE* definitions in terms of deflections.

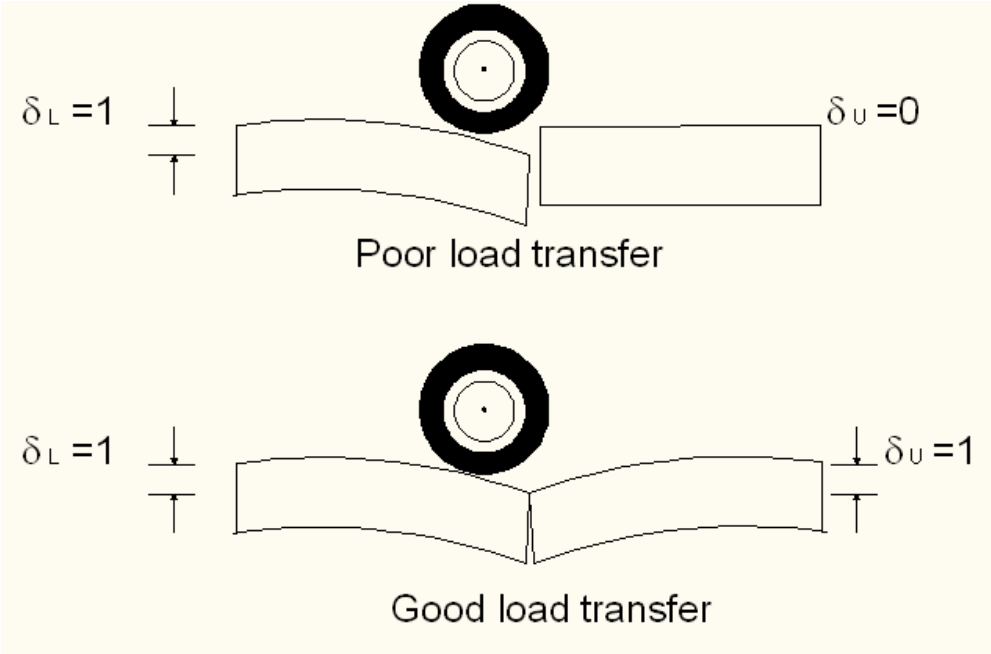

Figure 1. Diagram of poor and good load transfer.

Stress load transfer efficiency ($LTE\sigma$) is the ratio of the edge stress in the unloaded slab (σ_u) to edge stress in the loaded slab (σ_l) as defined in the following expression:

$$LTE_{\partial}* = \frac{\sigma_u}{\sigma_l} * 100\% \quad (2\text{-}3)$$

Load transfer between joints is accomplished through the aggregate interlock mechanism, and/or through dowels (for some pavements) and through the base and subgrade. *LTE* exhibits variation throughout the day and year because of the PCC temperature variation. When temperature decreases, a joint opens wider, which decreases contact between two slabs and also may decrease *LTE*, when no dowels exist. Also, PCC slab curling may change the contact between the slab and the underlying layer and affect measured load-induced deflections.(Khazanovich & Gotlif, 2003).

2.2 FUNDAMENTALS OF THE AGGREGATE INTERLOCK MECHANISM

Aggregate interlock was first recognized as a beneficial load transfer mechanism in the early 1900s, when the popularity of Portland cement concrete (PCC) as a paving material was beginning to increase. Aggregate interlock is a natural mechanism effective in transferring loads across discontinuities, such as joints and cracks in plain or reinforced pavements. Only a shear action is operative in this mechanism. In contrast, load transfer devices such as dowel bars also involve bending, thus creating an interest to investigate load transfer by aggregate interlock (Ioannides & Korovesis, 1990).

Because of its questionable long-term endurance record, aggregate interlock is not relied on as a primary load transfer mechanism in jointed concrete pavements, except perhaps in low volume roads. Abrasion and attrition of the aggregates coupled with temperature variations

causing a fluctuation in the size of the opening at the discontinuity can result in a significant decrease in the effectiveness of this mechanism over time (Ioannides & Korovesis, 1990)

Various experimental studies on aggregate interlock shear transfer in concrete pavements demonstrated that joint shear transfer effectiveness and endurance depend on many factors including joint width, slab thickness, load magnitude, foundation type, subgrade modulus, and aggregate shape

2.3 FACTORS AFFECTING THE AGGREGATE INTERLOCK MECHANISM

The aggregate interlock mechanism is influenced principally by two factors: Crack width and surface texture at the crack face. In addition, the surface texture at the crack is affected by several variables strictly related to the fracture behavior of concrete. These variables include properties of the coarse aggregate such as angularity, hardness, top size, and gradation; as well as properties and conditions that determine the strength and stiffness of the cement matrix such as time of cracking and water-to-cementitious material ratio.

This section discusses the influence of the above mentioned factors on the aggregate interlock mechanism as well as the effect of these factors on concrete fracture properties such as fracture toughness and fracture energy.

2.3.1 Effect of Crack Width on Aggregate Interlock

Crack width has been recognized by many researchers as one of the most influential parameter controlling the aggregate interlock effectiveness (Benkelman, 1933), (Colley & Humphrey,

1967), (Jensen & Hansen, 2001). The efficiency of the load transfer between crack faces is inversely related to the crack width. Jensen and Hansen (Jensen & Hansen, 2001) identified three different stages of the load transfer associated with the width of the crack. These include Stage I, which occurs when the crack width is smaller than 0.5 mm (20 mils) and the *LTE* is almost 100 percent. Stage II, occurs when crack widths are between 0.6 mm (24 mils) and 2.5 mm (99 mils). This is the crack width range where aggregate interlock plays a major role. Finally, Stage III, which represents the contribution of the foundation in the load transfer. This stage corresponds to a crack width larger than 2.5 mm (99 mils). These stages can be seen in Figure 2 where the differential deflections between the loaded and unloaded face of the cracks are presented for two concrete mixes with different top size aggregates.

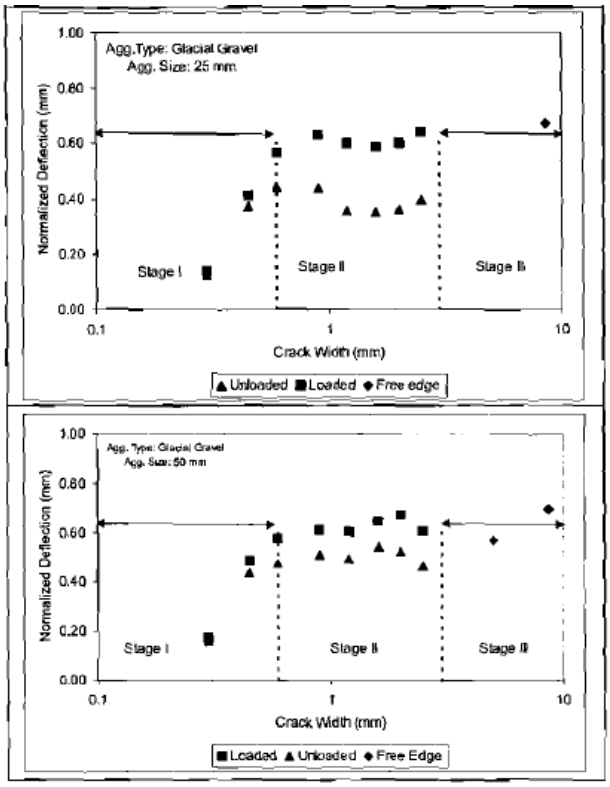

Figure 2. Deflection on the load and unloaded slab side versus crack width (Jensen & Hansen, 2001).

2.3.2 Effect of the Surface Texture of the Crack Face on Aggregate Interlock

The crack *LTE* for a given crack width is determined by the roughness or surface texture of the crack face. The relation between *LTE* and roughness is direct; rougher textures provide higher load transfer than smoother surfaces (Raja & Snyder, 1995). The crack surface texture is a function of the tortuosity of the crack path which is influenced by the fracture behavior of concrete. The fracture behavior is in turn determined by the interaction between the strength and stiffness of the different phases composing the concrete (i.e. cement matrix, aggregate, and ITZ).

Usually, cracks start at the matrix-aggregate interface, which is considered the weakest zone in concrete, and travel through the matrix. The crack then encounters coarse aggregate that can be fractured or can generate toughing mechanisms like bridging or also crack branching. However, since a crack will always propagate following the direction that requires the least work, variations in the strength and stiffness of the concrete phases can clearly influence this mechanism. This subsection discusses the effect of key concrete mixture design variables on the crack load transfer effectiveness, roughness of the crack surface, and the fracture behavior of concrete. These variables include the coarse aggregate angularity, hardness, top size, and gradation; as well as concrete water-to-cement ratio.

2.3.2.1 Coarse Aggregate Angularity

The angularity of the coarse aggregate, which is related to the sharpness of the edges and corners of the aggregate, has been found by several researchers as a variable that considerably affects the effectiveness of the crack load transfer. The load transfer increases as the aggregate angularity augments (Colley & Humphrey, 1967), (Nowlen, 1968). Figure 3 presents some of the results

that Colley and Humphrey obtained when comparing the joint effectiveness for natural and crushed aggregate.

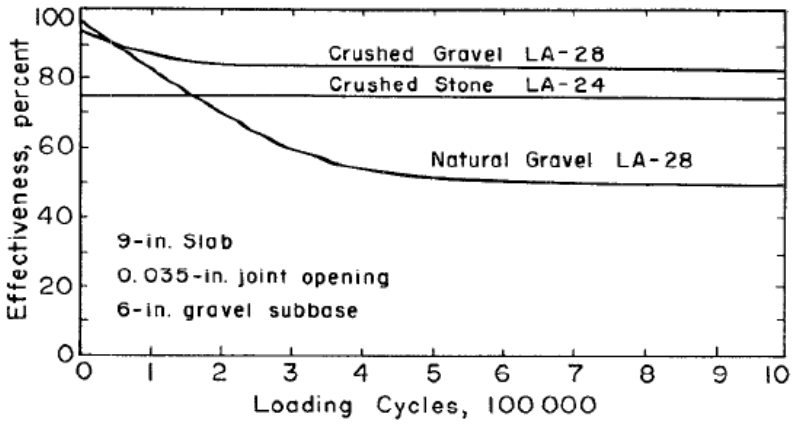

Figure 3. Influence of aggregate shape on joint effectiveness (Colley & Humphrey, 1967).

2.3.2.2 Coarse Aggregate Hardness

The aggregate hardness, which is related to the toughness and resistance to abrasion of the aggregate, is one of the most critical variables affecting the surface texture of the crack face and the concrete fracture behavior. Different studies have concluded that stronger aggregates produce rougher crack surface texture (Vandenbossche, 1999)(Chupanit & Roesler, 2005). Stronger aggregates produce greater surface texture since cracks tend to propagate around the stronger aggregate particles and not through them (Vandenbossche, 1999).

Raja and Snyder (Raja & Snyder, 1995), who studied the effect of coarse aggregate type, coarse aggregate gradation, and aggregate treatment (e.g. virgin or recycled) on the performance of transverse cracks in jointed reinforced concrete pavements, concluded that the *LTE* was

significantly higher for stronger aggregates (i.e. limestone and gravel) in comparison to weaker aggregates like slag. See Figure 4.

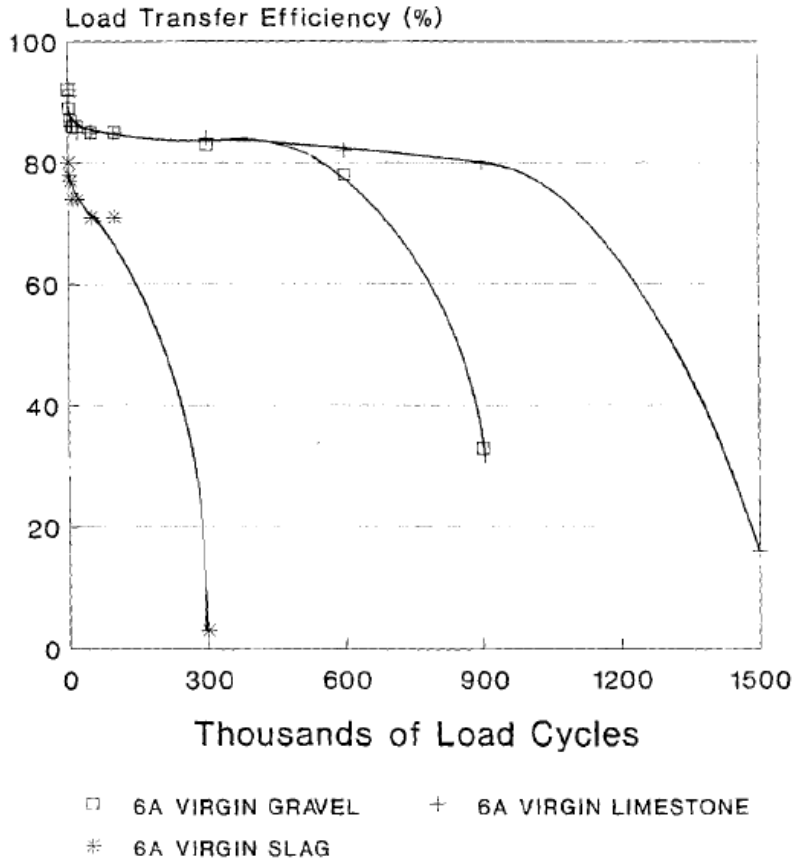

Figure 4. Influence of aggregate type on *LTE* (Raja & Snyder, 1995).

The aggregate hardness also has an influence on the concrete fracture parameters. The fracture energy for concrete with stronger aggregates is higher in comparison to the fracture energy obtained using weaker aggregates (Jensen & Hansen, 2001)(Chupanit & Roesler, 2005).

2.3.2.3 Coarse Aggregate Top Size

The top size of the coarse aggregate has an important effect on the roughness of the crack face. This property has been found to be directly related to the crack roughness, as the coarse aggregate top size is increased the roughness of the crack face augments (Vandenbossche, 1999). Concrete with larger size aggregates results in more tortuous crack patterns, which creates a rougher surface (Chupanit & Roesler, 2005). Figure 5 shows surface texture measurements for concrete containing limestone using the VSTR method performed on laboratory specimens by Vandenbossche (Vandenbossche, 1999). Figure 6 presents surface texture measurements of river gravel and trap rock using a parameter called Power Spectral Area Parameter (PSAP) (Chupanit & Roesler, 2005).

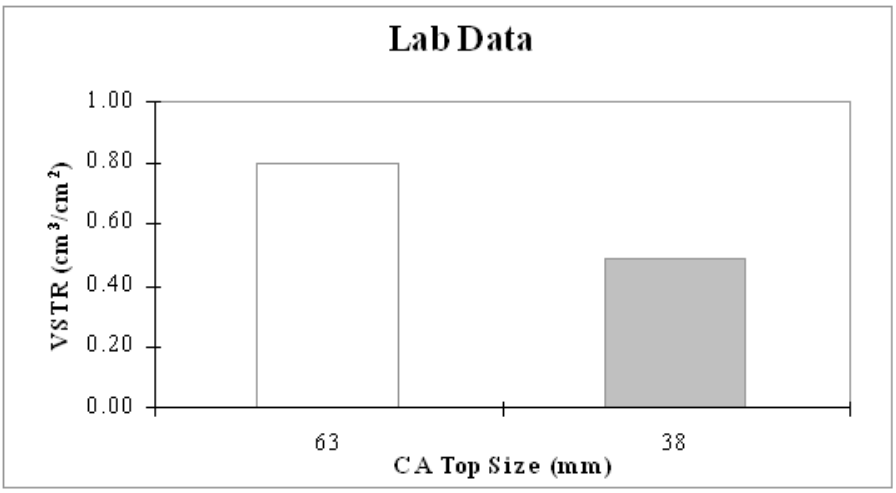

Figure 5. Effect of coarse aggregate top size on VSTR for lab specimens (Vandenbossche, 1999).

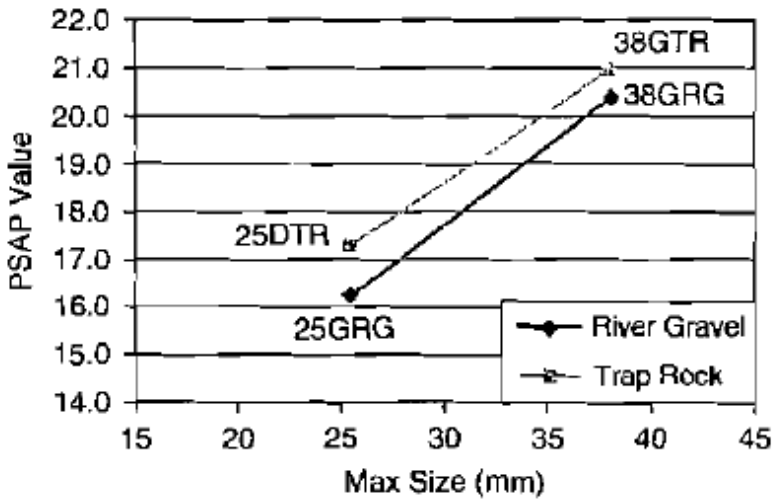

Figure 6. Effect of maximum aggregate size on crack surface roughness (Chupanit & Roesler, 2005).

Several studies have identified the effect of the aggregate top size on the effectiveness of the load transfer between opposite sides of the crack. The crack *LTE* increases as the top size is increased (Nowlen, 1968), (Raja & Snyder, 1995), (Jensen & Hansen, 2001). See Figure 7.

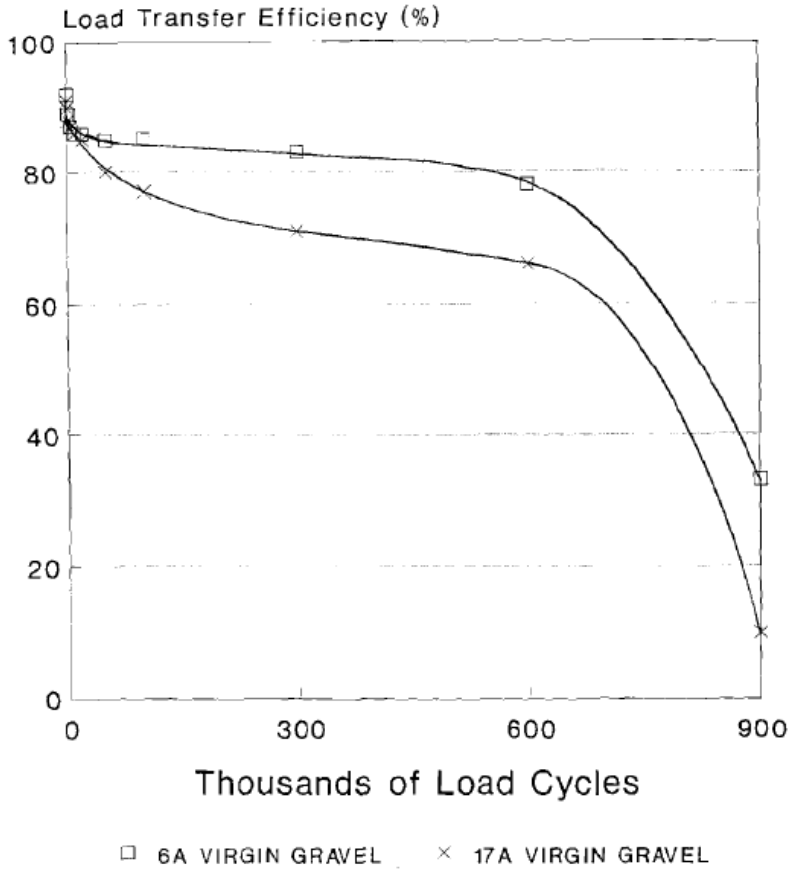

Figure 7. Influence of maximum aggregate size on *LTE* (6A 1 in nominal top size, 17A, 3/4 in nominal top size) (Raja & Snyder, 1995).

Additionally, the top size of the coarse aggregate has an important influence on the concrete fracture parameters. The concrete fracture energy is higher for concrete with large-sized coarse aggregate in comparison with concrete using smaller coarse aggregate (Chupanit & Roesler, 2005).

2.3.2.4 Coarse Aggregate Gradation

The gradation of the coarse aggregate has been recognized as a variable affecting the aggregate interlock mechanism. However, limited studies have investigated the isolated effect of gradation

on the crack surface roughness and the effectiveness of crack load transfer. Chupanit and Roesler studied the effect of two types of aggregate gradation (dense and gap) on the crack surface texture and concrete fracture energy. They concluded that the effect of gradation on the surface texture is negligible and that the concrete fracture energy for the concrete using gap gradation was slightly higher when compared with that of the concrete using a densely graded aggregate (Chupanit & Roesler, 2005).

Wattar et al. investigated the effect of gradation on crack surface roughness and joint stiffness. Two different gradation types were studied: Gap and Fuller. They concluded that gap-graded aggregates increase the crack surface roughness, enhancing the interlocking mechanism. Moreover, they concluded that joints with gap-graded aggregates have significantly higher joint stiffnesses in comparison to joints using well-graded aggregates (Wattar, Hawkins, & Barenberg, 2001).

2.3.2.5 Concrete Mixture Water-to-Cement Ratio

Concrete strength is largely controlled by the water-to-cement ratio. A limited number of studies have investigated the effect of this property on the aggregate interlock behavior. However, this property is strictly related to the time of cracking and concrete compressive strength which have been included by some researchers as studied variables.

Nowlen studied the influence of the time of cracking on joint *LTE*. He found that early-aged fractured joints have higher load transfer effectiveness when compared with joints which cracked at a later age. He stated that this condition is due to the nonexistence of fractured aggregates on the crack faces for the early-aged fractured joints (Nowlen, 1968). Figure 8 shows the *LTE* versus loading cycles for three different crack ages.

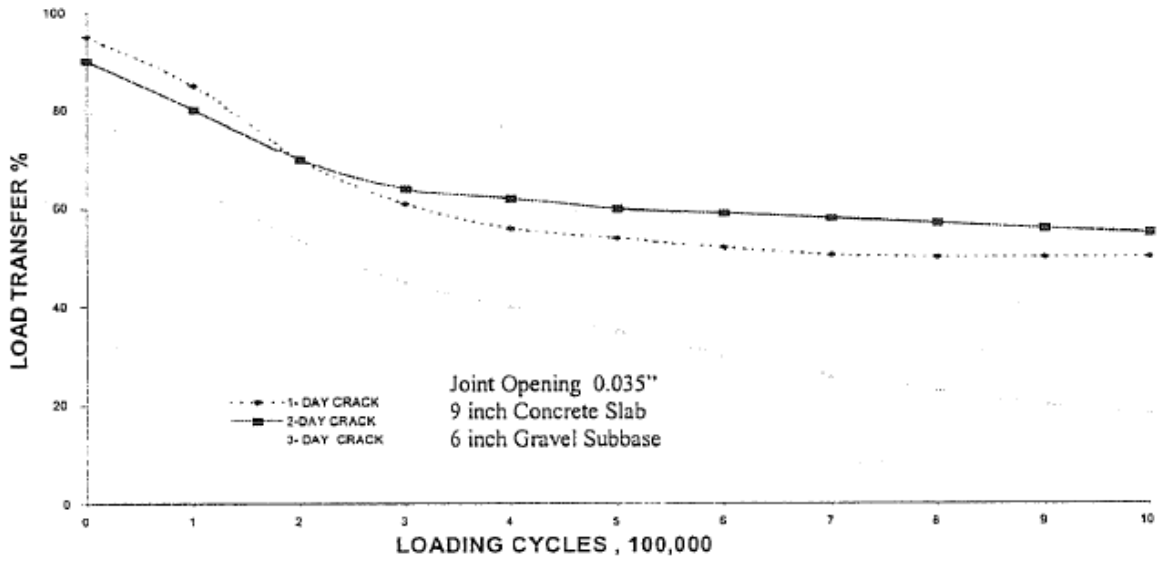

Figure 8. Influence of time of cracking on joint effectiveness (Nowlen, 1968).

Several researchers have investigated the effect of concrete compressive strength on the aggregate interlock mechanism. Bazant et al. (Bazant & Gambarova, 1980) and Walraven (Walraven, 1981) concluded that increasing concrete compressive strength improves the aggregate interlock behavior. In contrast, Wattar et al. (Wattar, Hawkins, & Barenberg, 2001) , who investigated the effect of concrete compressive strength on joint stiffness, concluded that increasing the compressive strength of concrete has little influence on the stiffness of the joints. These different observations are related to the relative strength of the three concrete phases and the interaction between them. For instance, if the strength of the aggregate is considerably lower than the strength of the mortar matrix, increasing the strength of the concrete will not have an important effect on the aggregate interlock behavior.

In the case of concrete fracture parameters, the relationship between the concrete strength and this fracture parameter is direct as seen in Figure 9. This figure presents results from the investigation by Giaccio et al. (Giaccio & Zerbino, 1998) on concrete failure mechanisms.

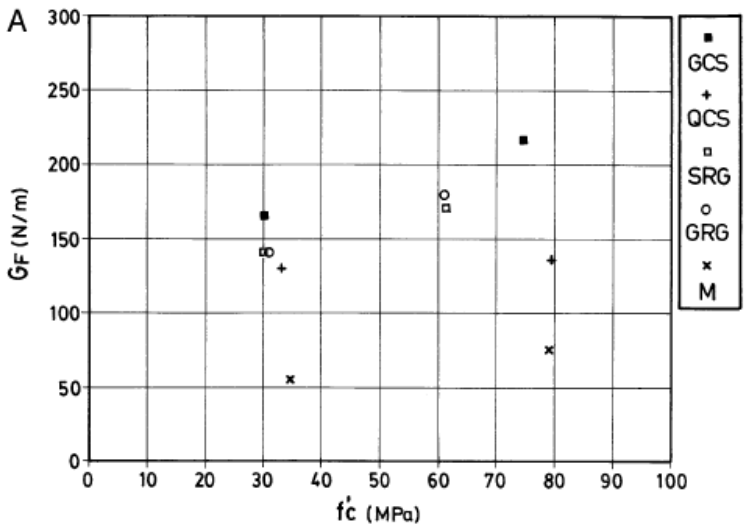

Figure 9. Variation of concrete fracture energy with concrete compressive strength (Giaccio & Zerbino, 1998).

2.4 SURFACE TEXTURE MEASUREMENT

The aggregate interlock mechanism is largely controlled by the crack surface texture or roughness. In order to be able to correlate the roughness of the crack with concrete mixture properties that affect this texture, it is critical to accurately quantify it. Although limited research has been performed on developing methods to quantify crack surface texture, there are some promising methods available. Among these methods are the Power Spectral Area Parameter (PSAP) (Chupanit P. , 1999), the Fractal Dimension method, and the Volumetric Surface Texture (VST) test (Vandenbossche, 1999).

This section presents a description of the concept of the VST method which is the test used to characterize the surface texture of the fractured faces included in this study.

2.4.1 Volumetric Surface Texture Test

The VST is a test developed at the University of Minnesota with the main purpose of estimating the load transfer potential of aggregates across a concrete fracture plane. The surface texture is quantified as the ratio of volume of texture per unit surface area in terms of a parameter called volumetric surface texture ratio (VSTR). To perform the test is necessary to use a probe or a laser profiler to measure a distance (d_i) from an arbitrarily selected datum to the crack surface. These distances are measured for each point of a matrix which has an area of about 25 in^2 and a distance between points of 0.125 in (see Figure 10).

The average of the distances (d_i) is calculated as follows:

$$d_{avg} = \frac{\sum_{1}^{n} d_i}{n} \tag{2-4}$$

where n is the number of d_i's measured on the fracture plane. The residual r_i, which is difference between the average distance to each individual distance (d_i), is calculated as Equation (2-5) shows.

$$r_i = d_i - d_{avg} \tag{2-5}$$

Then, the volume of each individual square is calculated using Equation (2-6).

$$V_i = r_i * A_i \tag{2-6}$$

where is V_i is the volume, r_i is the residual, and A_i is the area of each square in the matrix. A positive value of V_i represents the volume of material above the plane determined by $d_{avg.}$ On the other hand, a negative value of V_i represents the volume of the void below the mentioned plane.

To obtain the volume surface texture (VST), the volume of the solid material above the plane is added to the volume of voids below the plane as represented by the following equation:

$$VST = \sum_{1}^{n} abs(r_i * A_i) \tag{2-7}$$

where VST is the total volume of surface texture, n is the number of squares within the matrix, r_i is the residual, and A_i is the area. To be able to compare the VST value between different specimens it is necessary to normalize it by the tested area. The normalized value is called volumetric surface texture ratio (VSTR).

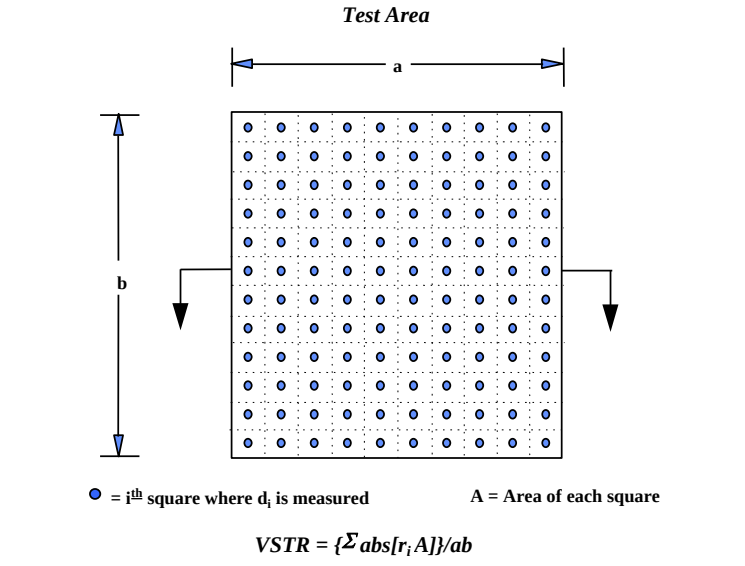

Figure 10. Graphical representation of VSTR measurements and calculations(Vandenbossche, 1999).

Vandenbossche carried out a study to validate the VST test; to investigate the effect of aggregate type, aggregate top size, and aggregate treatment on the cracks surface texture; and to determine the effects of the crack roughness on joint and crack performance (Vandenbossche, 1999). In this study, VST testing was performed on laboratory specimens, i.e. flexural beams, as well as on cores retrieved from several cracks and undoweled joints of pavements in different locations across the country.

As a result of this investigation, it was concluded that the VST method was a viable means of measuring and quantifying surface texture (Vandenbossche, 1999). In addition, the VST value was correlated with crack *LTE* and *AGG* of large-scale slabs tested in the laboratory and the *LTE* and *AGG* of cracks and undoweled joints of different pavements. Two foundations were evaluated in this study. The first foundation had a k-value of 100 psi/in and the second a k-value of 250 psi/in. Figure 11 presents the relationship between the VST value and crack *LTE* for specimens tested in the laboratory.

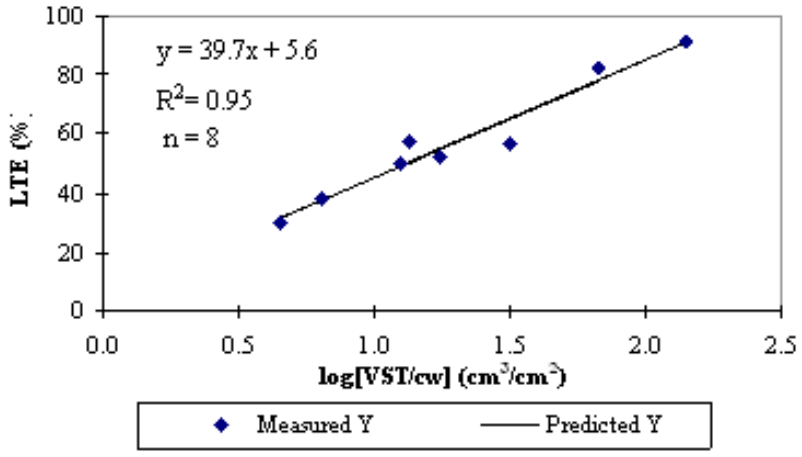

Figure 11. Regression model of *LTE* based on laboratory data (Vandenbossche, 1999).

Equation (2-8) presents the prediction equation for the relationship presented in the previous figure:

$$LTE\% = 39.7 \cdot \log\left(\frac{VST}{cw}\right) + 5.6 \qquad (2\text{-}8)$$

LTE% is the deflection load transfer efficiency in percentage, VST is the volumetric surface texture in cm^3/cm^2 and *cw* is the crack width in cm. As observed in the equation the VST was divided by the crack width to include the important effect of this parameter in the effectiveness of the load transfer. The importance of this equation lies on its ability to predict *LTE* based on VSTR measurements performed on beams failed in flexure after 28 days of curing, for an expected slab thickness, and a determined crack width.

Figure 12 presents the relationship between the VST value and *AGG* for specimens tested in the laboratory. The nondimensional joint stiffness parameter AGG/kl was obtained based on the measured load transfer efficiencies using the relationship established by Ioannides et. al (Ioannides & Korovesis, 1990) shown in Figure 15. This nondimensional parameter was multiplied by the radius of relative stiffness and the subgrade reaction of each pavement to establish a relationship between the measured surface texture and the joint spring stiffness *AGG*.

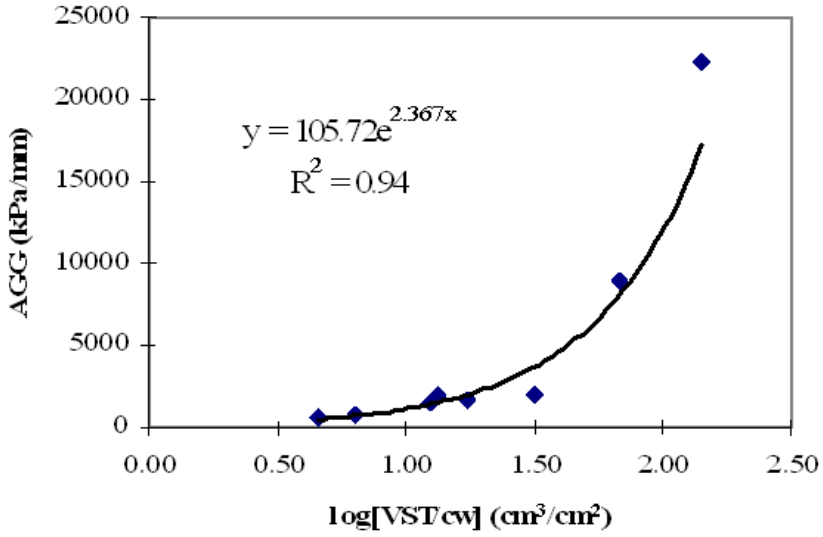

Figure 12. Regression model of *AGG* based on laboratory data (Vandenbossche, 1999).

Equation (2-9) presents the prediction equation for the relationship presented in the previous figure:

$$AGG = 105.72 \cdot e^{2.367 \cdot \log\left(\frac{VST}{cw}\right)} \quad (2\text{-}9)$$

AGG is the joint spring stiffness expressed in kPa/mm, the VST is the volumetric surface texture in cm^3/cm^2 and *cw* is the crack width in cm. The coefficient of determination, R^2, exhibited by this relationship is 0.94.

2.5 AGGREGATE INTERLOCK MODELS

Several researchers have attempted to model the aggregate interlock mechanism using different approaches. These models can be classified in two principal groups: Models mainly empirical in nature based on field investigations or laboratory studies, and theoretical models based on physical formulations of the crack mechanics. This section presents the fundamentals of some of the most widely used aggregate interlock models available in the literature.

2.5.1 Two-phase Model

The fundamentals of this theoretical model developed by Walraven (Walraven, 1981) are based on the representation of concrete as constituted by two different phases: A matrix (hardened cement paste) and the embedded aggregates which are modeled as spheres of distinct sizes. The strength and stiffness of the aggregate particles is assumed to always be greater than that of the matrix and the contact area between both phases, the ITZ. The ITZ is assumed to be the weakest link of the system. Consequently, cracking occurs commonly through the cement matrix, but along the periphery of the aggregate particles.

The formulation of this model is based on a statistical analysis of the crack structure and the associated areas of contact between the crack faces as a function of the crack width, the shear displacement, and the composition of the concrete mixture. The aggregate particles intersect the crack plane at various depths as a function of their statistical distribution within the concrete matrix as seen in Figure 13.

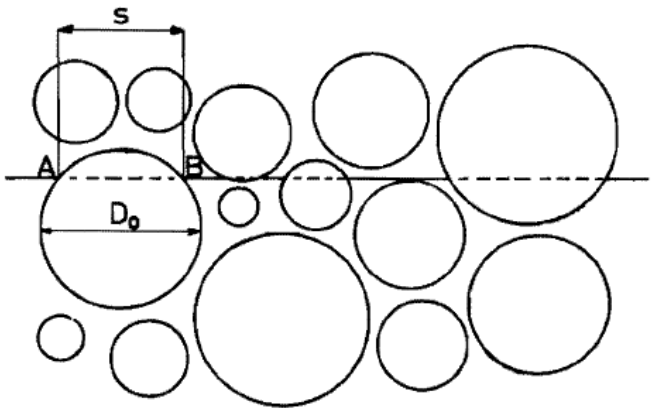

Figure 13. Contact areas in the crack plane (Walraven, 1981).

The micro-roughness of the crack, caused by the aggregate particles projecting from the crack plane was assumed to dominate the macro-roughness of the crack face. Due to the large plastic deformations of the cement paste due to pore-volume reduction, the cement paste was idealized as obeying a rigid-plastic stress-strain law. The aggregate particles were assumed to be incompressible.

As a result of the model assumptions, it is possible to consider a cracked concrete body as an assemblage of a large number of slices each of finite width, thus reducing the crack to a two dimensional problem of finite width. The stresses at the contact area are resolved into a stress normal to the contact area, σ_{pu}, and a stress tangential to the same area, $\tau_{pu,}$ as observed in Figure 14.

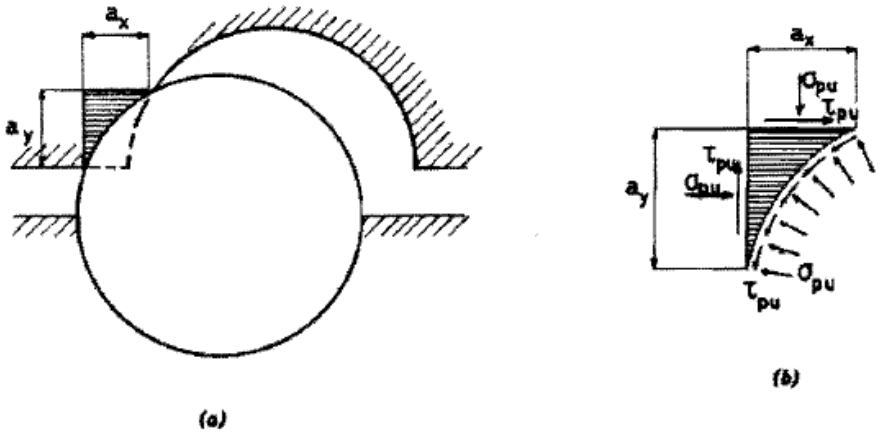

Figure 14. Stress conditions for the contact areas between matrix and aggregates (Walraven, 1981).

The stresses at the contact areas are interrelated by the condition that the areas of contact are about to slide and consequently:

$$\tau_{pu} = \mu \cdot \sigma_{pu} \tag{2-10}$$

where μ is the friction coefficient between the cement paste and the aggregate, and σ_{pu} corresponds to the ultimate strength of the paste which is determined by the following expression:

$$\sigma_{pu} = 6.39 \cdot f_{cu}^{\,0.56} \tag{2-11}$$

where f_{cu} is the concrete cube crushing strength in MPa.

The equilibrium of the crack plane requires that the contact forces be balanced as presented in the following equations:

$$F_y = \sigma_{pu} \cdot a_x - \tau_{pu} \cdot a_y \tag{2-12}$$

$$F_x = \sigma_{pu} \cdot a_y + \tau_{pu} \cdot a_x \tag{2-13}$$

where a_x and a_y are the projections in the x and y directions along the line of contact between the opposite crack faces as shown in Figure 14. If all particles over a unit crack length are considered, so the intersection circles of different diameters are encountered, the formulation can be generalized to

$$\sum F_y = \sigma_{pu} \cdot \sum \bar{a}_x - \tau_{pu} \cdot \sum \bar{a}_y \tag{2-14}$$

$$\sum F_x = \sigma_{pu} \cdot \sum \bar{a}_y + \tau_{pu} \cdot \sum \bar{a}_x \tag{2-15}$$

where $\sum \bar{a}_x$ and $\sum \bar{a}_y$ are the most probable, average projected contact lengths over the unit crack length considered.

Multiplying $\sum \bar{a}_x$ and $\sum \bar{a}_y$ by a unit width l, to consider a unit surface composed of an infinite number of lines of unit length, all which have the same expected average values of $\sum \bar{a}_x$ and $\sum \bar{a}_y$, the most probable contact areas $\bar{A}_x$ and $\bar{A}_y$ are obtained. The stresses σ and τ can be calculated as follows:

$$\sigma = \sigma_{pu}\left(\bar{A}_x - \mu \cdot \bar{A}_y\right) \tag{2-16}$$

$$\tau = \sigma_{pu}\left(\bar{A}_y + \mu \cdot \bar{A}_x\right) \tag{2-17}$$

The determination of the x and y projections is based on the statistical distribution of the aggregate in the concrete matrix, and the size of the spherical aggregate particles intersecting the crack plane at a given tangential and normal displacement.

A series of experiments were performed to compare their results with the theory. In these tests the crack width was maintained constant while the normal stress, the shear stress, and the shear displacement were measured. The values of σ_{pu} and μ were calculated to generate stress-

displacement curves for different crack widths. The experimental results showed good agreement with the theory.

2.5.2 Ioannides and Korovesis Model

Ioannides and Korovesis (Ioannides & Korovesis, 1990) investigated the behavior of jointed or cracked pavements which relied solely on aggregate interlock as the load transfer mechanism. As a result of this investigation, a dimensionless joint stiffness parameter, *AGG/kl*, was developed. The variable *k* is the modulus of subgrade reaction and *l* is the pavement radius of relative stiffness. Aggregate interlock was modeled using the finite element method software ILLI-SLAB with linear springs acting at each node along the discontinuity.

Several simplifications were adopted during the finite element method investigation with the aim of reducing the number of variables involved in the problem and thus improve the engineer's ability to understand and solve it. These simplifying assumptions are linear elasticity, plate theory, and a dense liquid foundation. The effect of the size of the loaded area was analyzed, as well as the effect of the slab length and width.

The major relationship established in this study presents the form of an S-shaped curve. This curve, depicted in Figure 15, is a non-dimensional plot of *AGG/kl* versus LTE_{δ}. As observed in this curve, LTE_{δ} is considerably sensitive and deteriorates rapidly as the non-dimensional joint stiffness (*AGG/kl*) variable falls below 10.

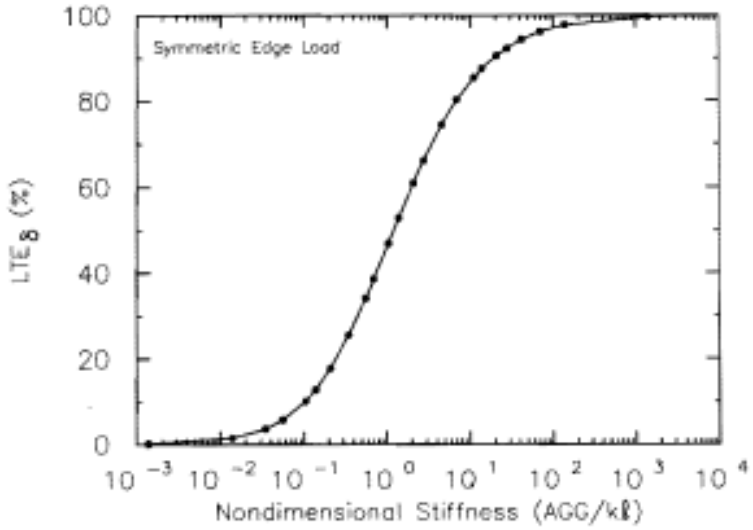

Figure 15. LTE_δ as a function of dimensionless joint stiffness (*AGG*/kl).

This relationship offers the possibility of investigating the factors influencing the joint stiffness *AGG*, which characterizes the aggregate interlock shear stiffness per unit length of crack. A large *AGG* value for a crack indicates that the crack is relatively stiff, and has good potential for aggregate interlock load transfer. The equation that describes the relationship between LTE_δ and *AGG*/kl is as follows:

$$LTE_\Delta = \frac{1}{1+\log^{-1}\left[\dfrac{0.214-0.183\left(\dfrac{\varepsilon}{l}\right)-\log\left(\dfrac{AGG}{kl}\right)}{1.180}\right]} \qquad (2\text{-}18)$$

where ε / l is the load size ratio.

Three loading conditions were analyzed: external only, curling only, and curling and external loading combined. Under curling conditions, joint stiffness caused by a pure-shear mechanism does not affect the response of either a short or a long slab. On the other hand, a mechanism involving bending also may be expected to increase the curling stresses, especially in shorter

slabs. Consequently, aggregate interlock provides a pure-shear load transfer mechanism that reduces edge stresses caused by the applied load, without increasing the curling-only stresses.

2.5.3 Jeong & Zollinger Aggregate Interlock Model

Based on the work executed by Ioannides and Korovesis (Ioannides & Korovesis, 1990), Jeong and Zollinger (Jeong & Zollinger, 2001; Zollinger & Soares, 1999; Ioannides, Alexander, Hammons, & Davis, 1996) investigated the main mechanisms causing joint deterioration (i.e. aggregate wear out, loss of dowel support, and the development of erosion for jointed concrete pavements or punch-out development in continuously reinforced concrete pavements.

The following expression was developed as a result of the investigation:

$$Log(J_{AGG}) = -4.00 \cdot \exp\left[-\exp\left(-\frac{J_s + 11.26}{7.56}\right)\right] - 28.85 \cdot \exp\left[-\exp\left(-\frac{s_o - 0.35}{0.38}\right)\right] + \quad (2\text{-}19)$$

$$+ 56.25 \cdot \exp\left[-\exp\left(-\frac{J_S + 11.26}{7.56}\right)\right] \cdot \exp\left[-\exp\left(-\frac{s_0 - 0.35}{0.38}\right)\right]$$

where,

J_{AGG} = *(AGG/kl)* = Non-dimensional joint stiffness on the transverse joint for the current increment.

J_s = Load transfer on the longitudinal joint between the PCC slab and shoulder.

s_o = Shear capacity equal to $ae^{-0.039w}$, with $0.55 < a < 1.3$ as a function of slab thickness = $0.0312h^{1.4578}$and, w equal to the joint width .

P = Wheel load.

τ = Shear stress on the crack face = s_0P/h^2.

h = Slab thickness.

The prediction of the deterioration of the aggregate interlock capacity is given by the following expression which is a function of load repetitions, joint stiffness, and critical slab features:

$$\Delta S_{ij} = \sum_i \sum_j \left(0.069 - 1.5317 \cdot e^{-wi/h}\right)\left(\frac{n_{ij}}{10^6}\right)\left(\frac{\tau_{stress}}{\tau_{ref}}\right) \quad (2\text{-}20)$$

where:

n_{ij} = Number of axle load applications for current sub increment *i* and load group *j*.

τ_{stress} = Transverse crack shear stress.

τ_{ref} = Reference shear stress derived from Portland Cement Association Results (Colley & Humphrey, 1967).

w_i = Crack width in sub-increment i.

τ_{stress} and τ_{ref} are calculated using the following expressions:

$$\tau_{stress} = \frac{sP}{h^2} \quad (2\text{-}21)$$

$$\tau_{ref} = 111.1 \cdot s = 111.1 \cdot \left[a + b \cdot \ln(J)^2 + c \cdot \ln(J) + de^{-1}\right] \quad (2\text{-}22)$$

where:

s = Nondimensional aggregate joint shear capacity.

J = Transverse crack joint stiffness.

a = 0.0848.

b = -0.000364.

c = 0.0188.

d = -0.006357.

Examining Equation (2-20), it is determined that below a value of 3.1 for the dimensionless term *w/h* the shear loss in negligible. From crack width data of continuously reinforced concrete pavements it was determined that a *LTE* of about 90 percent is associated with a value of *w/h* of 3.1. Consequently, it can be concluded that loss of shear capacity is insignificant when the *LTE* is above 90 percent. The deteriorated level of shear capacity can be calculated as follows:

$$s_{new} s_{old} - \Delta_S \tag{2-23}$$

s_{old} and s_{new} are the shear capacity before and after the loading increment, respectively. Δ_S is calculated using Equation (2-20).

This aggregate interlock model was adopted by the 2002 MEPDG faulting prediction model (ARA,I.,ERES Consultants Division, 2004). This model is used to predict the contribution of aggregate interlock in transferring loads across the joint/crack over the pavement design life. The model as presented above was modified for the inclusion in the MEPDG faulting prediction model as presented below.

Joint stiffness is calculated as follows:

$$Log(J_{AGG}) = -3.19626 + 16.09737 \cdot e^{-e^{-\left(\frac{s-0.35}{0.38}\right)}} \tag{2-24}$$

where J_{AGG} is the dimensionless joint stiffness (*AGG/kl*) and *s* is the nondimensional aggregate joint shear capacity. This joint shear capacity is a function of the joint width and the cumulative damage:

$$s = 0.05 \cdot h_{PCC} \cdot e^{-0.028 \cdot jw} - \Delta s_{tot} \tag{2-25}$$

where, *jw* is the joint width and Δs_{tot} is the cumulative loss in shear capacity.

The joint width is calculated for each month based on the set temperature of the PCC, the PCC drying shrinkage, and the PCC mean night time monthly temperature as follows:

$$jw = Max(12000 \cdot STSpace \cdot \beta \cdot (\alpha_{PCC} \cdot (T_{constr} - T_{mean}) + \varepsilon_{sh,mean}), 0) \quad (2\text{-}26)$$

where,

jw = Joint opening, mils.

$\varepsilon_{sh,mean}$ = PCC slab mean shrinkage strain.

α_{PCC} = PCC coefficient of thermal expansion, in/in/F°.

STSpace = Joint spacing, ft.

β = Joint open/close restraint coefficient assumed equal to 0.85 for a stabilized base and 0.65 for granular base.

T_{mean} = Mean monthly nighttime mid depth temperature, °F.

T_{constr} = PCC temperature at set, °F.

The cumulative loss of shear capacity is computed on a monthly basis as follows:

$$\Delta_{tot}^{tend} = \Delta s_{tot}^{b} - \sum_{i} n_i \cdot \Delta s_i \quad (2\text{-}27)$$

where,

Δ_{tot}^{tend} = Cumulative loss of shear capacity at the end of the current month is equal to the sum of the loss in shear capacity from every axle load application.

n_i = Number of applications of axle load i

Δs_i = Loss of shear capacity due to a single application of axle load i. When the joint width is smaller than $0.001 h_{PCC}$ Δs_i is zero. Otherwise, it is calculated using the following expressions:

$$\Delta s_i = \frac{0.005*10^{-6}}{1.0+(jw/h_{PCC})^{-5.7}}\left(\frac{\tau_i}{\tau_{ref}}\right) \text{ if } 0.001 < jw < 3.8\ h_{PCC} \quad (2\text{-}28)$$

$$\Delta s_i = \frac{0.068*10^{-6}}{1.0+6.0*(jw/h_{PCC}-3)^{-1.98}}\left(\frac{\tau_i}{\tau_{ref}}\right) \text{ if } jw > 3.8\ h_{PCC} \quad (2\text{-}29)$$

where,

h_{PCC} = PCC slab thickness, in.

jw = Joint opening, mils.

The predicted aggregate interlock *LTE* exhibits seasonal variation and a reduction over time. Seasonal variation is derived from the changes in joint opening due to the change in mean PCC temperature. The reduction over time results from the loss in shear capacity due to abrasion and an increase in joint opening due to drying shrinkage. An example of the predicted aggregate interlock *LTE* over time as predicted using the MPEDG is presented in Figure 16.

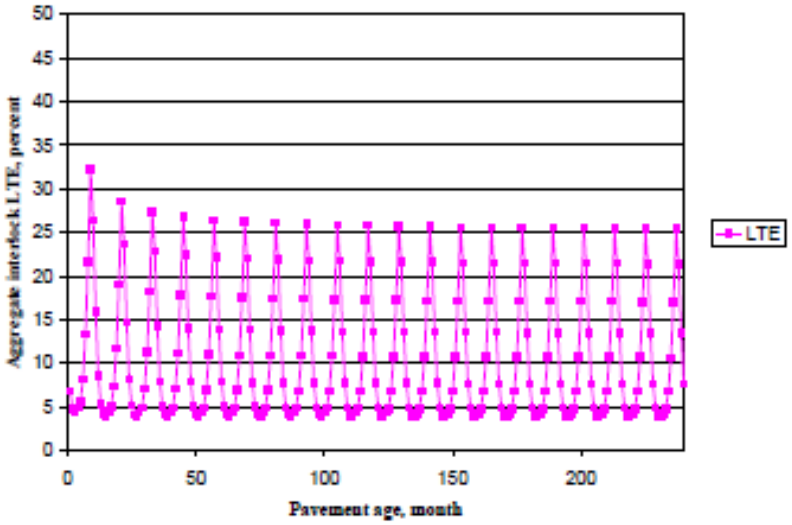

Figure 16. Example of predicted aggregate interlock *LTE* (ARA,I.,ERES Consultants Division, 2004).

2.6 TWO-PARAMETER FRACTURE MODEL TO DETERMINE CONCRETE FRACTURE PROPERTIES

A procedure to determine the fracture properties of the concrete was developed by Jenq and Shah (RILEM Comitee on Fracture Mechanics of Concrete-Test Methods, 1990) using a single-edge notched beam. The single-edge notched beam specimen is configured for three-point bending with the load (*P*) and crack mouth opening displacement (*CMOD*) being recorded. The specimen and load configuration for this test are presented in Figure 17.

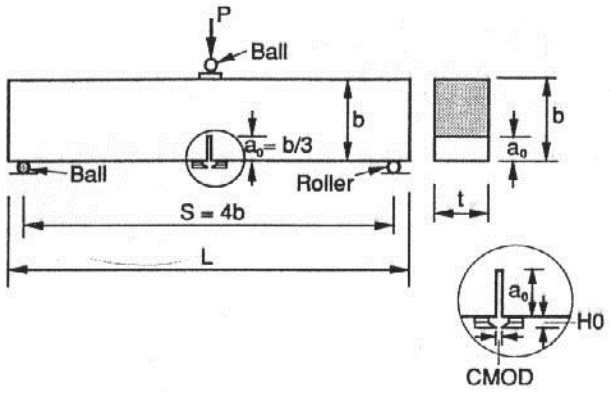

Figure 17. **Test setup for the Two-Parameter method (Shah, Swartz, & Ouyang, 1995).**

Jenq and Shah (Jenq & Shah, 1985) developed the Two-Parameter Fracture Model (TPFM) to determine two critical components: the critical stress intensity factor (K_{IC}^{S}) and the critical crack tip opening displacement ($CTOD_c$) of a monolithic beam based on an effective elastic crack approach.

From experimental results obtained using three-point bending beams, Jenq and Shah found that for beams with different sizes but made of the same material the values of K_{IC}^{S} and $CTOD_c$ are basically constant. Consequently, they proposed that these two parameters can characterize the critical fracture property of a quassi-brittle material.

The fundamentals of this method can be explained from load versus crack mouth opening displacement (*CMOD*) curves as presented in Figure 18. The relationship is linear until approximately half of the maximum load. In this linear relationship the *CTOD* is negligible and the stress intensity factor is less than 0.5 K_{IC}^{S} (Figure 18a). During the nonlinear stage, significant inelastic behavior and slow crack growth occur (Figure 18b). At the critical point, *CTOD* reaches a critical value, $CTOD_c$, and the stress intensity factor, K, is equal to K_{IC}^{S} (Figure 18c). Geometry greatly affects the critical point. K is also a function of the load, and the length of the notch. For plain concrete beams, the critical point occurs at a maximum load of 95% of the peak load on the descending end of the load vs. *CMOD* plot.

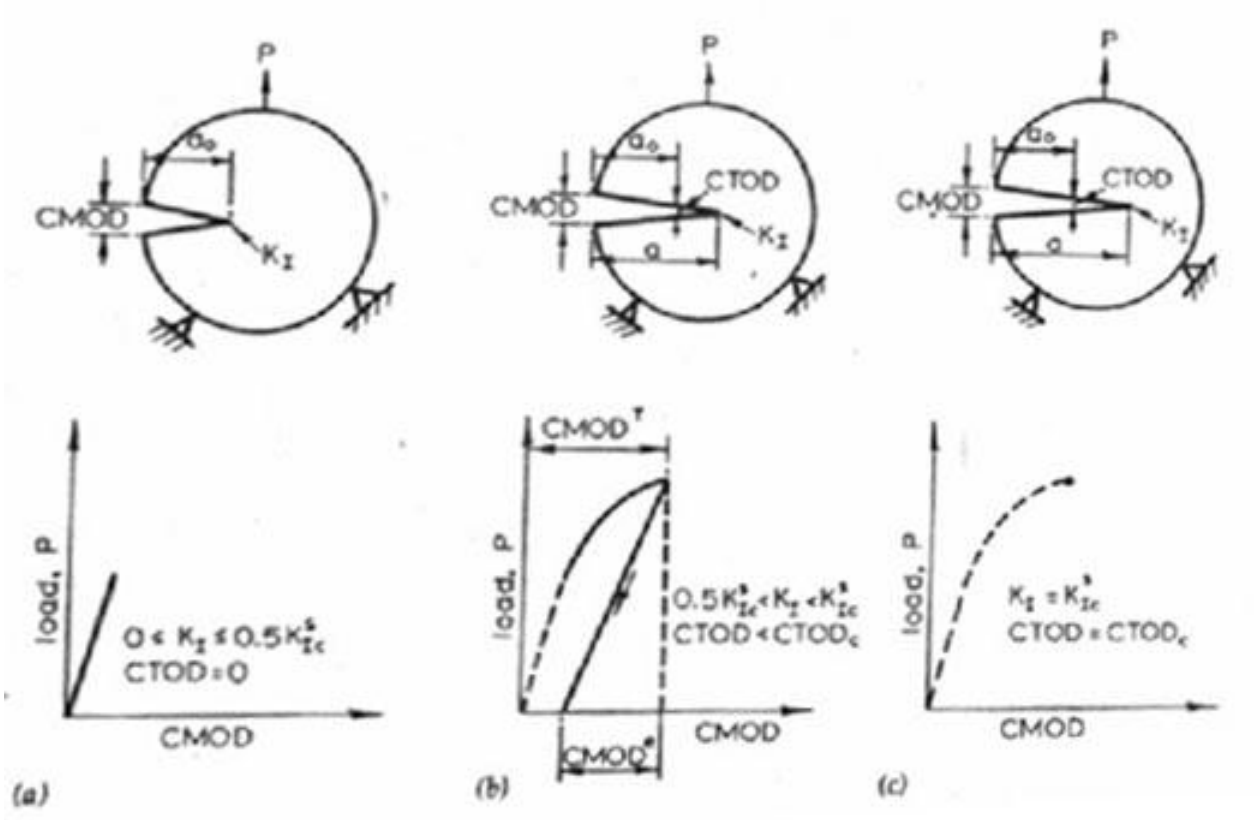

Figure 18. **Fracture resistance stages of plain concrete (Jenq & Shah, 1985).**

The equations and calculation process of the initial concrete fracture parameters using the TPFM are presented in Section 3.2.4.1.

3.0 EXPERIMENTAL SETUP

As a result of the literature investigation, four different concrete mixture design variables were selected to be included in this study due to the significance of their effect on the aggregate interlock mechanism. The variables are: Water-to-cementituos material ratio; and coarse aggregate top size, hardness, and angularity. Due to a lack of information available to accurately quantify the coarse aggregate angularity, it was decided to exclude this factor in the development of the main model subject of this investigation. However, a secondary model, relating the key concrete mixture properties already mentioned with surface texture was developed considering only angular aggregates. Consequently, an effort on gathering data that include a wide range of values for the three selected variables was the subsequent step. Taking into account that the volumetric proportion of the coarse aggregate can influence the aggregate interlock behavior, it was decided to maintain this factor as a constant to the extent possible for all of the mixtures included in this investigation. As a result, a target value of 45 percent (by volume) of the concrete mixture will consist of coarse aggregate.

This chapter presents a general description of previous studies from which the supplemental data included in this study was obtained. The additional data is presented along with the experimental design of the laboratory study performed in this research effort.

3.1 DATA SELECTED FROM PREVIOS STUDIES

Data from three different studies previously executed and one currently in execution were included in this investigation. The selection of these studies was performed based on the concrete mixture design properties, the availability of information relating the properties of the concrete components used, and the availability of VSTR data. The selected studies were as follows:

1. Factors Affecting Deterioration of Transverse Cracks in jointed Reinforced Concrete Pavements (Raja & Snyder, 1995). This study was performed at Michigan State University from 1991 to 1995 (referred to as "Study No.1" from this point forward).

2. Performance of Concrete Pavements Containing Recycled Concrete Aggregate (Wade, Cutell, Vandenbossche, Yu, Smith, & Snyder, 1997). This study was performed at University of Minnesota from 1994 to 1997 (referred to as "Study No.2" from this point forward).

3. Independent study on crack surface texture and concrete fracture parameters carried out at the University of Pittsburgh in 2006 (referred to as "Study No.3" from this point forward).

4. Establishing Appropriate Inputs When Using the Mechanistic-Empirical Pavement Design Guide (MEPDG) To Design Rigid Pavements in Pennsylvania. This study is currently being executed at the University of Pittsburgh (referred to as "Study No.4" from this point forward).

3.1.1 Study No. 1

Study No.1 was executed at Michigan State University between 1991 and 1995. The main purpose of this research effort was to evaluate the relative effects of several factors on transverse crack deterioration in JRCPs (Raja & Snyder, 1995). The analyzed factors were aggregate type

(virgin, recycled, and blended), treatment and gradation, foundation support, reinforcement type and quantity, and slab tension. The research study involved the collection and analysis of load transfer data from the testing of a series of large-scale pavement slabs that were subjected to repeated applications of loads replicating the passage of heavy-truck traffic. In addition to the large-scale concrete specimens, companion beams were cast to determine the flexural strength of the concrete as well to determine the VST of the fractured planes.

VST was measured for nineteen different concrete mixes, however, only the data of six of them is included in this study. The selection of these six concrete mixes was performed considering the available data, the possibility of using known correlations to determine unknown variables, as well as the use of only one type of virgin coarse aggregate in the mix. Virgin limestone, gravel and blast furnace slag were used in the six selected mixes. Table 1 presents the physical characteristics of these aggregates.

Table 1. Physical characteristics of coarse aggregates from Study No.1.

Description	**6A Limestone #2**	**4A Limestone #1**	**6A Gravel #3**	**6A Slag**
Aggregate Type	Limestone	Limestone	Gravel	Blast furnace slag
Maximum Aggregate Size (in)	1.5	2.5	1.5	1.5
Gradation	6A MDOT	4A MDOT	6A MDOT	6A MDOT
Bulk Specific Gravity (SSD)	2.62	2.67	2.67	2.39
Aborption Capacity (%)	2.2	0.5	1.05	2.34
Los Angeles Abrasion Value (%)	30	30	18	34

The concrete mixture design proportions as well as the fresh mixture properties of the six concretes mixtures selected are presented in Table 2. To identify each concrete mixture with its main properties a label system was used. Each label contains the coarse aggregate (CA) type, top size, Los Angeles abrasion (LA), and the water-to-cement-ratio as follows: CA type, CA top size, CA LA value, w/c ratio. The aggregate type is coded LS for limestone, SL for slag, G for gravel, and TR for trap rock. The CA top size code is the top size in inches. The CA LA value code is given as a percentage, and the w/c ratio is the decimal representing the water-to-cement-ratio.

Table 2. Concrete mixture design proportions (per yd^3) and fresh properties from Study No.1.

Slab No.	11	13	15	26	31	32
Concrete Mixture ID	LS_1.5_30_0.38	G_1.5_18_0.40	G_1.5_18_0.42	SL_1.5_34_0.46	G_1.5_18_0.47	LS_2.5_30_0.42
Aggregate Type	Limestone	Gravel	Gravel	Blast Furnace Slag	Gravel	Limestone
Maximum Aggregate Size (in)	1.5	1.5	1.5	1.5	1.5	2.5
Coarse Aggregate Volumetric Proportion (%)	46	43	46	43	44	43
Coarse Aggregate (lb)	2044	1972	2094	1758	1975	1922
Fine Aggregate (lb)	1132	1145	1211	1155	1076	1115
Cement (lb)	509	593	436	539	532	547
Fly Ash(lb)	16					
Water (lb)	198	235	184	247	248	230
Water-to-Cementituos Material Ratio	0.38	0.40	0.42	0.46	0.47	0.42
Fresh Mix Properties						
Air content (%)	6.4	5.0	6.8	5.3	5.4	5.2
Target Slump (in)	2--3	2--3	2--3	2--3	2--3	2--3

Table 3 shows the average of the modulus of rupture and VSTR for flexural beams tested for each of the selected concrete mixtures at 28 days of Study No.1.

Table 3. Flexural strength and VSTR results for the six concrete mixtures in Study No.1.

Slab No.	11	13	15	26	31	32
Concrete Mixture ID	LS_1.5_30_ 0.38	G_1.5_18_ 0.40	G_1.5_18_ 0.42	SL_1.5_34 _0.46	G_1.5_18_ 0.47	LS_2.5_30 _0.42
28-day Average Flexural Strength (psi)	873	796	738	625	713	480
28-day Average VSTR (in^3/in^2)	0.2859	0.1866	0.1785	0.0881	0.2353	0.5487

3.1.2 Study No. 2

Study No.2 was carried out at the University of Minnesota between 1994 and 1997. The main objectives of this research effort included the determination of causes of pavement distresses in concrete pavements related to the use of recycled concrete coarse aggregates as well as the development of guidelines for concrete mixture design using recycled aggregate (Wade, Cutell, Vandenbossche, Yu, Smith, & Snyder, 1997). A total of nine different projects across the country constructed with recycled aggregate were included in this investigation. Many of the projects included control sections that were constructed with virgin aggregate but maintained similar design features as the recycled aggregate sections. An important aspect of this research is that it included extensive field testing and laboratory testing on specimens retrieved from the field. As part of the laboratory study, VST testing was performed on cores retrieved from the cracks and undoweled joints representing 15 pavement sections. However, only the sections with virgin aggregate and which met the aggregate content criteria were included in this study. As a

result, only three of the sections containing the necessary information and meeting the criteria of volumetric percentage of coarse aggregate were selected to be part of this study.

Crushed trap rock and two different gravels were used in the concrete mixtures for the sections from Study No.2 that were included in this study. Table 4 shows the physical characteristics of these aggregates.

Table 4. Physical characteristics of coarse aggregates for Study No.2.

Description	**CT1-2**	**WY1-2**	**MN4-2**
Aggregate Type	Crushed Trap Rock	Gravel	Gravel
Maximum Aggregate Size (in)	1.5	1.5	1.5
Bulk Specific Gravity (SSD)	2.81	2.65	2.68
Absorption Capacity (%)	N/A	N/A	N/A
Uniaxial Compressive Strength (Mpa)	343	238	240
Los Angeles Abrasion Predicted Value (%)	16	22	20

As seen in the previous table the LA of the aggregates is predicted. This prediction was necessary due to the non existence of measured values for this aggregate property. The LA value was determined based on a relationship between the aggregates uniaxial compressive strength and the LA abrasion developed by Kahmaran et al. (Kahmaran & Fener, 2007). This relationship for sedimentary rocks is as follows:

$$s_{new}s_{old} - \Delta_S \; LA = 536.89 \cdot \sigma_c^{\,-0.60} \qquad (3\text{-}1)$$

where the LA is the Los Angeles abrasion value in percent and σ_c is the uniaxial compressive strength of the aggregate in MPa.

The concrete mixture design proportions as well as the fresh properties of the concrete are presented in Table 5.

Table 5. Concrete mixture design proportions (per yd^3) and fresh properties from Study No.2.

Concrete Mixture ID	**TR_1.5_16_0.45**	**G_1.5_22_0.44**	**G_1.5_20_0.46**
Aggregate Type	Crushed Trap Rock	Gravel WY1-2	Gravel MN4-2
Maximum Aggregate Size (in)	1.5	1.5	1.5
Coarse Aggregate Volumetric Proportion (%)	44	42	44
Coarse Aggregate (lb)	2065	1868	1965
Fine Aggregate (lb)	1080	1156	1101
Cement (lb)	610	588	469
Fly-ash (lb)			88
Water (lb)	275	258	258
Water-to-Cementituos Material Ratio	0.45	0.44	0.46
Fresh Mix Properties			
Air content (%)	4	5.5	5.5
Target Slump (in)	2.5	1.7	N/A

The laboratory-measured concrete compressive strength and VSTR values of the selected sections from Study No.2 are presented in Table 6.

Table 6. Strength properties and VSTR results for the three concrete mixtures of Study No.2.

Concrete Mixture ID	**TR_1.5_16_0.45**	**G_1.5_22_0.44**	**G_1.5_20_0.46**
Average Compressive Strength (psi)	5134	6483	6904
28-day Average Predicted Flexural Strength (psi)	685	800	834
Average 28-day VSTR (in^3/in^2)	0.1263	0.1189	0.0987

The concrete flexural strength presented in the previous table was predicted based on the compressive strength using the following relationship (Mindess, Young, & Darwin, 2003):

$$f'_r = 2.30 \cdot f'^{\,2.30}_c \qquad (3\text{-}2)$$

where f'_r is the concrete flexural strength in psi and f'_c is the concrete compressive strength in psi.

3.1.3 Study No. 3

This non-published study was executed at University of Pittsburgh in 2006. The objective of this study was to establish a relationship between the roughness of the fractured plane and concrete fracture energy, and to evaluate the effect of the strength, size and shape of aggregates on the fracture behavior of concrete. Four concrete mixtures were used in this investigation containing three different types of aggregates (blast furnace slag, gravel, and limestone) and two different aggregate top sizes (0.75 in and 2.5 in).

The physical characteristics of the coarse aggregates used in this investigation are presented in Table 7.

Table 7. Physical characteristics of aggregates of the Study No.3.

Aggregate type	Slag	Gravel	Limestone	Limestone
Maximum Aggregate Size (in)	0.75	0.75	0.75	2.5
Bulk Specific Gravity (SSD)	2.36	2.46	2.68	2.62
Absorption capacity (%)	2.92	2.69	0.50	1.19
Los Angeles Abrasion Predicted Value (%)	46	37	20	25

The concrete mixture proportions were selected in such a way as to maintain the volumetric proportions of each constituent constant for all of the mixes. Table 8 presents the mixture designs along with the fresh mixture properties measured for the four mixes.

Table 8. Concrete mixture design proportions (per yd^3) and fresh properties of the Study No.3.

Concrete Mixture ID	**SL_0.75_46_0.56**	**G_0.75_37_0.50**	**LS_0.75_20_0.50**	**LS_2.50_25_0.52**
Aggregate Type	Slag	Gravel	Limestone	Limestone
Top Aggregate Size (in)	0.75	0.75	0.75	2.50
Coarse Aggregate Volumetric Proportion (%)	45	45	47	47
Coarse Aggregate (lb)	1700	1737	1881	1871
Fine Aggregate (lb)	1129	1211	1248	1211
Cement (lb)	584	588	382	588
Ground Granulated Blast Furnace Slag (lb)			206	
Water (lb)	330	328	286	303
Water-to-Cementituos Material Ratio	0.56	0.56	0.50	0.52
Fresh Mix Properties				
Air content (%)	5.4	5.5	5.2	5.1
Slump (in)	5.5	2.25	2.0	N/A

The results of the laboratory measurements of flexural strength, VSTR, fracture toughness, and fracture energy for the four mixtures included in this study are presented in Table 9.

Table 9. Strength, VSTR, and fracture parameters for the concrete mixtures in Study No.3.

Concrete Mixture ID	SL_0.75_46_0.56	G_0.75_37_0.50	LS_0.75_20_0.50	LS_2.50_25_0.52
Average 28-day Flexural Strength (psi)	632	591	1,106	760
Average 28-day VSTR (in^3/in^2)	0.1000	0.1580	0.2770	0.2250
Average (18 to 24 hours) Fracture Toughness (psi $in^{1/2}$)	363	N/A	631	N/A
Average 28-day Fracture Toughness (psi $in^{1/2}$)	878	805	1,120	1,205
Average (18 to 24 hours) Fracture Energy (lb/in)	0.06	N/A	0.12	N/A
Average 28-day Fracture Energy (lb/in)	0.25	0.23	0.28	0.32

3.1.4 Study No. 4

Study No.4 is currently being executed at the University of Pittsburgh by Nassiri et al. (Nassiri & Vandenbossche, 2009). The main objective of this study is to assist the Pennsylvania Department of Transportation (PennDOT) in the implementation of the rigid pavement portion of the new Mechanistic Empirical Pavement Design Guide. One of the tasks of this research effort includes the instrumentation of four pavement sections and an extensive material characterization of the PCC for these sections. Two of these four projects were selected to be included in this study (Project 3 and 4). VST testing was performed on flexural beams that were tested 28 days after

casting. Limestone from the Hanson-Torrance quarry in Pennsylvania was used in the concrete for the two selected projects. Table 10 presents the physical characteristics of the coarse aggregate used in Projects 3 and Project 4 of Study No.4.

Table 10. Physical characteristics of the coarse aggregate of the Study No.4.

Description	Value
Aggregate type	Limestone
Maximum Aggregate Size (in)	1.5
Bulk Specific Gravity (SSD)	2.68
Absorption capacity (%)	0.52
Los Angeles Abrasion Value (%)	17

Table 11 shows the mixture designs as well as the fresh concrete properties measured in the field.

Table 11. Concrete mixture design proportions (per yd^3) and fresh properties for the Study No.4.

Concrete Mixture ID	LS_1.5_17_0.46	LS_1.5_17_0.44
Coarse Aggregate Volumetric Proportion (%)	48	48
Coarse Aggregate (lb)	1840	1860
Fine Aggregate (lb)	1166	1285
Cement (lb)	500	500
Fly Ash-Type F (lb)	88	88
Water (lb)	194.27	163.15
Water-to-Cementituos Material Ratio	0.46	0.44
Fresh Mix Properties		
Air content (%)	6	6.0
Slump (in)	1.25	1.25

The average concrete modulus of rupture and the average VSTR for the specimens tested at 28 days is presented in Table 12.

Table 12. Flexural strength and VSTR for the concrete mixtures included in Study No.4.

Description	Project 3	Project 4
Average 28-day Flexural Strength (psi)	770	808
Average 28-day VSTR (in^3/in^2)	0.2408	0.2070

3.2 LABORATORY STUDY

3.2.1 Design of the Laboratory Study

This section describes the design of the laboratory study executed specifically for this investigation. As mentioned before, three different concrete properties were selected as the major variables to be studied. These properties are: Water-to-cement ratio; and coarse aggregate top size, and hardness or resistance to abrasion. The main purpose of the laboratory study is to expand the data collected using the selected information from the previous studies already presented. This inclusion of additional data is intended to fill the "gaps" of conditions not contemplated in the previous studies. Moreover, the inclusion of supplementary data points allows a better understanding of the effects of the mentioned variables on the aggregate interlock and fracture behavior of concrete.

A summary of the data, in terms of the three critical variables, from previous studies selected for inclusion in this study is presented in Table 13.

Table 13. Summary of the data from previous studies to be included in this study.

Study	Mix ID	Aggregate Type	Top Size (in)	LA (%)	w/c ratio
1	Slab 11	Limestone	1.5	30	0.38
	Slab 13	Gravel	1.5	18	0.4
	Slab 15	Gravel	1.5	18	0.42
	Slab 26	Blast Furnace Slag	1.5	34	0.46
	Slab 31	Gravel	1.5	18	0.47
	Slab 32	Limestone	2.5	30	0.42
2	CT1-2	Crushed Trap Rock	1.5	16	0.45
	WY1-2	Gravel	1.5	22	0.44
	MN4-2	Gravel	1.5	20	0.46
3	075S	Blast Furnace Slag	0.75	46	0.56
	075G	Gravel	0.75	37	0.56
	075L	Limestone	0.75	20	0.5
	250L	Limestone	2.5	25	0.52
4	Project 3	Limestone	1.5	17	0.46
	Project 4	Limestone	1.5	17	0.44

The LA value as well as the w/c ratio were categorized in three groups in order to design the laboratory study by organizing the data in terms of similarity of the properties. The categories for each variable are shown in Table 14.

Table 14. LA value and w/c ratio categories.

LA (%)		w/c ratio	
Category	**Value**	**Category**	**Value**
High resistance to abrasion	≤19	High strength	≤0.42
Medium resistance to abrasion	20-30	Medium strength	0.43-0.49
Low resistance to abrasion	≥31	Low strength	≥0.50

The data presented in Table 13 was grouped in the categories shown in Table 14 to generate Table 15.

Table 15. Summary of collected data categorized.

LA Category	CA Top Size (in)	w/c ratio Category
Low resistance to abrasion	0.75	Low strength
	1.5	Medium strength
Medium resistance to abrasion	0.75	Low strength
	1.5	Medium strength
		High strength
	2.5	Low strength
		High strength
High resistance to abrasion	1.5	Medium strength
		High strength

It can be seen in the previous table that the concrete mixtures from the previous studies are represented in 9 different conditions combining the predetermined categories of abrasion resistance and concrete strength with the coarse aggregate top size. Based on the time and the economic resources of the present study it was decided to develop 5 different concrete mixtures to expand the available data. Therefore, it was necessary to identify the combinations of properties that contribute the most in studying the effect of each factor and the interactions of these factors on surface texture. In order to identify these 5 combinations, a full factorial experiment with the 3 selected factors each at 3 different levels was developed as shown in Table 16. This table shows 27 different combinations of the three selected variables. As observed in the 4^{th} column of Table 16, there are five different combinations that contain aggregate with a medium resistance to abrasion and only two containing low and medium resistance to abrasion. In the case of the aggregate top size there are five different combinations having a 1.5 in top size, and only two with a 0.75 in and a 2.5 in top size. In addition, for the concrete strength the

existing data from previous studies contains three combinations for each level of strength. In addition to the limit on the number of mixtures to use in the laboratory study, the following conditions influenced the selection of the five additional mixtures:

1. Aggregate with a top size of 2.5 in was not available to use in this study. Therefore, it was desired to balance out the number of combinations for the aggregate top sizes of 0.75 in and 1.5 in.
2. Two w/c ratios were preselected to be used: 0.40 and 0.45.
3. It was desired to balance out the number of combinations for each level of resistance to abrasion.

Based on the mentioned conditions, the combinations of properties for the concrete mixtures selected to use in the present study are checked on the 5^{th} column of Table 16. With the selection of these mixtures the results was five mixtures containing aggregate with a low and five with medium resistance to abrasion, while four mixtures containing aggregate with high resistance to abrasion. In the case of the aggregate top size, six mixtures containing 0.75 in and six containing 1.5 in top size were considered, with two mixtures with 2.5 in aggregate top size. The final number of mixtures containing low, medium, and high strength concrete is three, five, and six, respectively.

Table 16. Full factorial experiment matrix.

LA Category	CA Top Size (in)	w/c ratio Category	Existent	Present Study
Low resistance to abrasion	0.75	Low strength	X	
		Medium strength		X
		High strength		X
	1.5	Low strength		
		Medium strength	X	
		High strength		X
	2.5	Low strength		
		Medium strength		
		High strength		
Medium resistance to abrasion	0.75	Low strength	X	
		Medium strength		
		High strength		
	1.5	Low strength		
		Medium strength	X	
		High strength	X	
	2.5	Low strength	X	
		Medium strength		
		High strength	X	
High resistance to abrasion	0.75	Low strength		
		Medium strength		X
		High strength		X
	1.5	Low strength		
		Medium strength	X	
		High strength	X	
	2.5	Low strength		
		Medium strength		
		High strength		

3.2.2 Concrete Mixture Components and Proportions

3.2.2.1 Coarse Aggregate

In order to develop the five selected concrete mixtures presented in Table 16, it was necessary to obtain aggregates from two different sources, one having a low resistance to abrasion and the other a high resistance to abrasion. To characterize this aggregate property, the Los Angeles Abrasion test, was used according to the standard ASTM C131 (ASTM, 2004). The LA abrasion test involves impacting and abrading a coarse aggregate sample with steel spheres in a rotating drum for a determined period of time. The percentage of material passing the No.12 sieve relative to the initial weight of the sample is the LA abrasion. This value is inversely related to the abrasion resistance and toughness of the aggregate. The selection of this test to characterize the aggregate hardness was based on previous results from Study No.3 where two different tests were used to characterize the aggregate hardness: The LA abrasion test and the point load strength index. The results from this study showed a strong correlation (R^2=99 percent) between LA abrasion and VSTR while no correlation was found for the point load strength index results and VSTR.

The LA abrasion for a limestone locally available from Stone and Company Inc. and blast furnace slag from Beaver Valley Slag were determined. The LA abrasion for the limestone was 17 percent whereas for the slag was 34 percent. Since these values represent high and low abrasion resistance, respectively, the limestone and the slag were selected as coarse aggregates for the concrete mixtures included in this study.

The physical characteristics of the aggregates used in the concrete mixtures are presented in Table 17.

Table 17. Physical characteristics of the aggregates used in the present study.

Aggregate Type	Blast Furnace Slag	Limestone
Maximum Aggregate Size (in)	0.75 and 1.25	0.75
Gradation	AASHTO No. 57	AASHTO No. 57
Bulk Specific Gravity (SSD)	2.35	2.71
Absorption Capacity (%)	4.78	0.50
Los Angeles Abrasion Value (%)	34	17

According to the aggregates sources the gradation of the slag and limestone were AASHTO No. 57 which has a 1.5 in top size particle. However, the sieve analysis for the blast furnace slag yielded a top size of 1.25 in. Although this size was not the desired, it was accepted and was actually considered beneficial for the study as far as investigating the effect of the top size on the surface texture. For the mixtures with a top size of 0.75 in it was necessary to remove the particles exceeding 0.75 in. The gradation for these two types of coarse aggregates included in this study are presented in Appendix A.

3.2.2.2 Fine Aggregate

The fine aggregate used in the concrete mixes was sand from Stone and Company Inc. The absorption and bulk specific gravity (SSD) for this material was 3 percent and 2.60, respectively.

3.2.2.3 Concrete Mix Proportions and Admixtures

The concrete proportions used for the five selected mixtures presented in Table 16 were based on mixture designs utilized in Study No.1. The main consideration in developing the mixture designs used in Study No.1 was holding the total volumetric proportion of coarse aggregate as constant as possible, while maintaining a similar workability and air content.

To develop the mix designs for this study, the batch proportions used in Study No.1 were adopted. The mixture designs used in this study were as follows: CA:FA:water:cement (lbs/yd^3):

- 6A virgin gravel - 1972:1145:235:593
- 6A slag - 1758:1155:247:539

These mixture designs were adapted slightly in the lab to obtain the desired targets of w/c ratio (0.4 and 0.45), slump (1-3 inches), and air content (7 percent). The Portland cement used for all of the mixes was Type I. Additionally, the following admixtures were used to acquire the targeted workability and air content:

- Medium range water reducer: Polyheed 1020 by BASF.
- Air-entraining agent: Catexol AE 360 by Axim.

Table 18 presents a summary of the concrete mixtures included in this study as well as the fresh concrete properties measured for these mixtures. As observed in this table, the volumetric proportion of the coarse aggregate was kept constant whereas two different water-to-cement ratios and two types of coarse aggregate were used.

Table 18. Mixture proportions and fresh mix properties for the concrete used in this study.

Concrete Mixture ID	**LS_0.75_17_0.4**	**LS_0.75_17_0.45**	**SL_1.5_34_0.4**	**SL_0.75_34_0.4**	**SL_0.75_17_0.45**
Aggregate Type	Limestone	Limestone	Slag	Slag	Slag
Top Aggregate Size (in)	0.75	0.75	1.5	0.75	0.75
Coarse Aggregate Volumetric Proportion (%)	44	44	44	44	44
Coarse Aggregate (lb)	1999	1991	1736	1736	1738
Fine Aggregate (lb)	1136	1146	1136	1136	1146
Cement (lb)	593	546	593	593	539
Water (lb)	235	243	235	235	243
Water-to-Cement Ratio	0.40	0.45	0.40	0.40	0.45
Fresh Mix Properties					
Air content (%)	5.0	8.0	8.0	7.5	5.0
Slump (in)	1.0	2.0	2.5	1.25	1.0

For each mixture, several trial batches with different admixture proportions were performed in order to obtain the required workability and entrained air content. Additionally, due to the capacity of the concrete mixer, it was necessary to distribute the total volume of each mix in three consecutive batches.

3.2.3 Testing Program

A total of 11 beams were cast for each of the concrete mixtures presented in the previous section. Of the 11 beams, 8 were fracture energy beams with the following dimensions: 27.5 in, 3 in, and 6 in. These dimensions were based on the RILEM specifications of the Two-Parameter method (RILEM Comitee on Fracture Mechanics of Concrete-Test Methods, 1990). The other 3 beams were 24 in x 6 in x 6 in modulus of rupture beams [ASTM C78 (ASTM, 2004)].

The laboratory testing, conducted in the Pavement Mechanics and Materials Laboratory (PMML) at the University of Pittsburgh, consisted of fracture energy testing at 1 and 28 days, flexural strength testing at 28 days and VST testing on the fractured faces of the specimens tested at 28 days. The execution of the fracture energy test and the flexural strength are described in the following section.

3.2.4 Fracture Energy Test

For the fracture energy testing the specimens were demolded 21 hours after casting and placed in a curing room (97±3 percent of relative humidity and 73 ± 3°F). For the 1-day testing, the specimens were removed from the curing room at 23 hours and approximately a 2-in notch was saw-cut in the center of the beam. On each side of the notch, aluminum plates were adhered to the concrete using epoxy. Steel plates were screwed into aluminum plates with a thickness of 0.127 in, a length of 1 in, and a width of 0.94 in. Once a MTS clip gauge was attached to the beam using the steel plates, the beam was placed on a pin and roller with a 23.5 in span. The pin and roller were attached to an aluminum plate placed on the bottom crossbeam of the steel load frame. For the 28 day testing, the specimens were removed from the curing room the day of

testing and the same procedure already described was conducted. Pictures of the complete setup have been provided in Appendix B.

The test setup consists of a 25 kip MTS hydraulic actuator with a 50 kip Lebow load cell and a pin roller on the loading end attached to a steel frame. To provide a continuous closed loop feedback system, a MTS TestStar IIM controller was utilized. The load was controlled with the crack mouth opening displacement (*CMOD*) that was measured using the MTS clip gauge.

The fracture energy test was performed in accordance with the RILEM (RILEM Comitee on Fracture Mechanics of Concrete-Test Methods, 1990) standard for the two parameter method. According to this standard, four beams are tested for each age and mixture design. Once the beam was centered on the pin and roller, with the notch on the bottom of the specimen, the loading roller was lowered to the surface of the beam. The specimen was loaded at a rate so that 95 percent of the peak load was reached in approximately five minutes. The beam was then unloaded and several loading and unloading cycles continued. Each of the later loadings took approximately one minute for a full cycle. Once five loading cycles were executed, the beam was broken if the beam did not already break during one of the loading cycles.

3.2.4.1 Fracture Energy Data Calculation

For each specimen the relationship between load and *CMOD* was plotted. Figure 19 shows an example of the first and second loading cycles that are used to determine the initial compliance C_i and the unloading compliance C_u and calculate the initial fracture properties of the concrete.

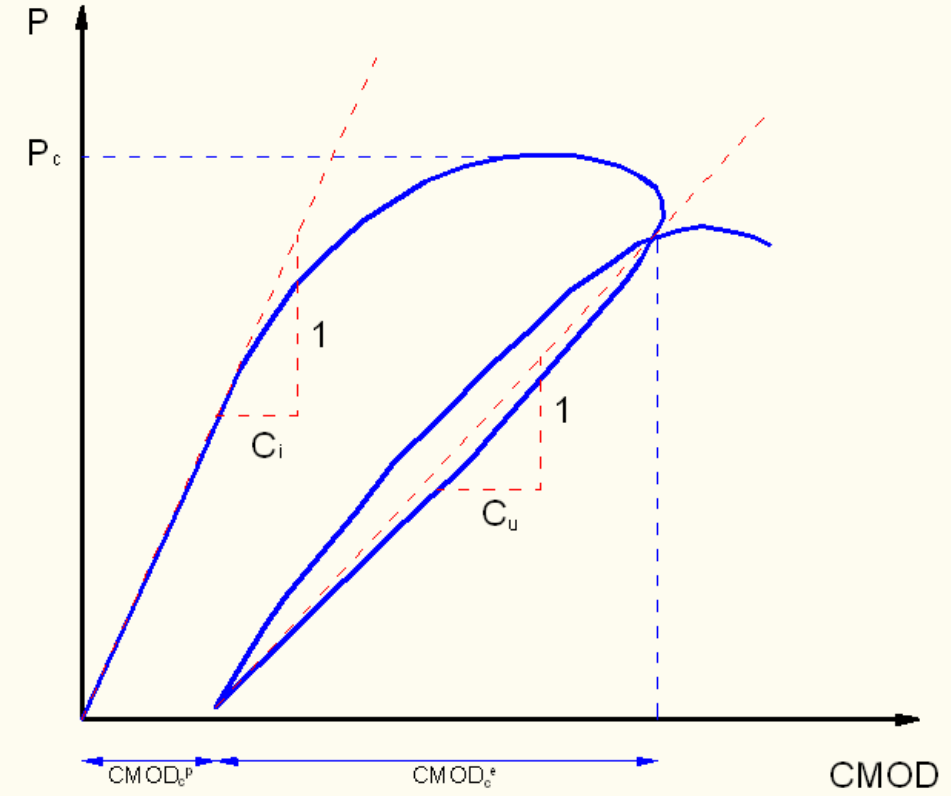

Figure 19. Loading and unloading procedure for the Two-parameter method.

The determination of the initial and unloading compliances is a process that is affected by the user subjectivity. The compliance slope could vary depending of the points selected along the curve. To avoid the variation derived from the user selection, different methods such as the focal point method by Jensen et al.(Jensen, Weiss, & Schleuchart, 2000) have been developed for the determination of the compliances. However, according to Jensen et al. (Jensen, Weiss, & Schleuchart, 2000) the variability of the calculated fracture parameters using this method was found to be similar to the variation observed using the traditional method where the user selects the points that establish the slope of the loading and unloading compliances. Consequently, for this particular study the initial compliance (C_i) in the linear elastic range was calculated as the inverse of the slope between 10 percent and 50 percent of the peak load. In the case of

discontinuities or initial seating different percentages of the peak load were used. The unloading compliance (C_u) was the inverse of slope of the unloading curve and was estimated between 10 percent and 80 percent of the peak load on the unloading curve.

The critical stress intensity factor or fracture toughness (K_{IC}^{S}) and the critical crack tip opening displacement ($CTOD_c$) were computed by first determining the critical effective crack length (a_c). This length can be obtained by equating the concrete's modulus of elasticity from the loading and unloading curves (E_i=E_u) as shown in the following equations:

$$E_i = \frac{6Sa_oV_1(\alpha_0)}{C_ib^2t} \tag{3-3}$$

$$E_u = \frac{6Sa_cV_1(\alpha_c)}{C_ub^2t} \tag{3-4}$$

where S is the span, $V_1(\alpha)$ is the opening displacement geometric factor presented in Equation (3-5), d is the depth of the beam, b the width of the beam, and a_0 the initial notch depth.

$$V_1(\alpha_o) = 0.76 - 2.28\alpha_o + 3.87\alpha_o^{\,2} - 2.04\alpha_o^{\,3.} + \frac{0.66}{(1-\alpha_o)^2} \tag{3-5}$$

where α_0 represents the following expression:

$$\alpha_o = \frac{a_o + Ho}{b + Ho} \tag{3-6}$$

H_0 is defined in Figure 17. To determine $V_1(\alpha_c)$, α_0 in Equation (3-5) is replaced by α_c which is a function of the critical crack length (a_c), Ho and b as defined in Equation (3-6).

With the critical crack length calculated the critical stress intensity factor or concrete fracture toughness K_{IC} can be computed using the following expression:

$$K_{IC}^{S} = 3(P_{MAX} + 0.5W)\frac{S(\pi a_c)^{1/2} F(\alpha)}{2b^2 t} \tag{3-7}$$

where P_{MAX} is the peak load applied, $F(\alpha)$ is calculated as follows:

$$\frac{1.99 - \alpha(1-\alpha)(2.15 - 3.93\alpha + 2.7\alpha^2)}{\sqrt{\pi}(1+2\alpha)(1-\alpha)^{3/2}} \tag{3-8}$$

with α being equal to

$$\alpha = \frac{a_c}{b} \tag{3-9}$$

and,

$$W = \frac{W_o S}{l} \tag{3-10}$$

where W_0 is the self-weight of the beam, S is the beam span and l is the length of the beam.

The *CTODc* can be calculated using the following expression:

$$CTOD_C = \frac{6P_{\max} S a_c V_1(\alpha)}{Ed^2 b}\left[(1-\beta)^2 + (1.081 - 1.149\alpha)(\beta - \beta^2)\right]^{1/2} \tag{3-11}$$

where β is defined as:

$$\beta = \frac{a_0}{a_c l} \tag{3-12}$$

The initial fracture energy can then be calculated relating the concrete modulus of elasticity and the concrete fracture toughness as follows:

$$G_{IC}^{s} = \frac{(K_{IC}^{S})^2}{E} \tag{3-13}$$

Jenq and Shanq (Jenq & Shah, 1985) introduced a material length, *Q*, which can be used as a brittleness index for the material and is proportional to the size of the fracture zone for the same material. This value *Q* is defined as:

$$Q = \left(\frac{E \cdot CTOD_C}{K_{Ic}^S} \right)^2 \tag{3-14}$$

The smaller *Q*, the more brittle the material. For concrete this value range from 4 to 14 in(Jenq & Shah, 1985).

3.2.5 Flexural Strength Test

The flexural beams were demolded 21 hours after casting and placed in the curing room for 28 days. The test was performed using a 400 kip Testmark compression machine following the standard ASTM C78 (ASTM, 2004). The beams were loaded until failure with a load rate of 100 lbs/sec. The test setup is depicted in Figure C 6 Appendix B.

3.2.6 VST Test

Vandenbossche (Vandenbossche, 1999) found that the VSTR measured for 28-day flexural beam breaks was more effective in predicting crack performance when compared to beams broken 18 hours after casting. Consequently, VST testing was performed on the fracture face of the fracture energy and flexural specimens fractured at 28 days. The fracture plane was saw-cut off perpendicular to the longitudinal axis of the beam approximately 2 in down from the lowest point on the fracture plane. Each cut specimen was placed on a linear traverse stage created by High-tech Metrology Products. A matrix program was used to run the linear traverse stage and a

laser profiler (AR600 from Acuity lasers) that measured the z distance. The surface was partitioned into a matrix of 5 in by 5 in for the flexural beams and 3 in by 3 in for the fracture energy beams. The distance in the x and y direction between points was set as 0.125 in in the matrix program. Once the program was initiated, the stage was automated and recorded the z distance data in a text file. After each run, the VSTR of the crack surface was calculated based on the equations presented in Section 2.4.1.

4.0 ANALYSIS OF THE EFFECT OF CRITICAL CONCRETE MIXTURE PROPERTIES ON THE CRACK ROUGHNESS FOR THE COMPLETE DATA SET

This chapter presents the results for the surface profiling tests executed as part of the laboratory study. Additionally, an analysis of the effect of the investigated concrete mixture properties on the surface roughness for the complete data set is included in this chapter.

4.1 VSTR RESULTS FOR THE PRESENT STUDY

Three beams for each mixture were tested for flexural strength beams broken at 28 days. The fractured surfaces of these specimens were used to determine the VSTR for each concrete mixture. Figure 20 presents a sample of the fractured surface for each of the five mixtures from the present study.

Figure 20. Samples of fractured surfaces for the five concrete mixtures of the present study.

The average VSTR for the flexural beams fractured at 28 days is presented in Table 19.

Table 19. Concrete mixture proportions and fresh mix properties.

Mixture	Average 28-day VSTR (in^3/in^2)
LS_0.75_17_0.4	0.1983 ± 0.0966
SL_1.25_34_0.4	0.2365 ± 0.1235
SL_0.75_34_0.45	0.1423 ± 0.0242
SL_0.75_34_0.40	0.1289 ± 0.0068
LS_0.75_17_0.45	0.2579 ± 0.1386

4.2 ANALYSIS OF THE VSTR RESULTS FOR THE COMPLETE DATA SET

This section discusses the results of the VST test for the complete data set including the four previous studies and the present study. This data set consists of a total of twenty data points, one for each concrete mixture. For the totality of the concrete mixtures the relationship between VSTR and the concrete mixture properties (coarse aggregate top size, type, and hardness, and w/c ratio) is analyzed. This analysis includes the isolated effect of each variable on the crack surface texture as well as the combined effect of the studied factors on texture.

Before presenting the results it is important to emphasize the complexity of crack propagation which determines the crack surface texture. Crack propagation is a function of not only a couple of parameters but it is determined by the properties of all concrete components and their interaction. Crack propagation typically starts at the ITZ, and the cracks then propagates through the matrix. Coarse aggregates arrest crack growth, producing branching and wandering of the cracks. The path of the main crack depends greatly on the relative differences in strength between the matrix, the aggregate and the ITZ as shown in Figure 21. Of the three phases of the concrete, the coarse aggregate is considered the strongest and the ITZ is considered the weakest. However, this is not always the case. The properties of the components of concrete and the interactions between them vary considerably. Figure 21 a) presents the case where the strength of the aggregate is larger than the strength of the matrix and the bond interface is poor resulting from the use of a smooth rounded aggregate. In this case, as the main crack grows, it encounters a relatively strong aggregate particle. This detains crack growth and forces the crack

to travel around the aggregate along the weakest path, which in this case is the ITZ. This condition augments the tortuosity of the crack which enhances the roughness of the crack face. In Figure 21 b) where the interface bond is strong due to the use of a rough angular aggregate, the crack growths thorough the matrix which in this case is the easiest path. When the strength of the coarse aggregate is much lower than the strength of the matrix as presented in Figure 21 c), the main crack makes its way through the aggregate resulting in a smoother crack surface texture. Figure 21 d) shows the case where the three phases exhibit similar strengths. In this situation, the crack path can be a combination of the three cases presented before.

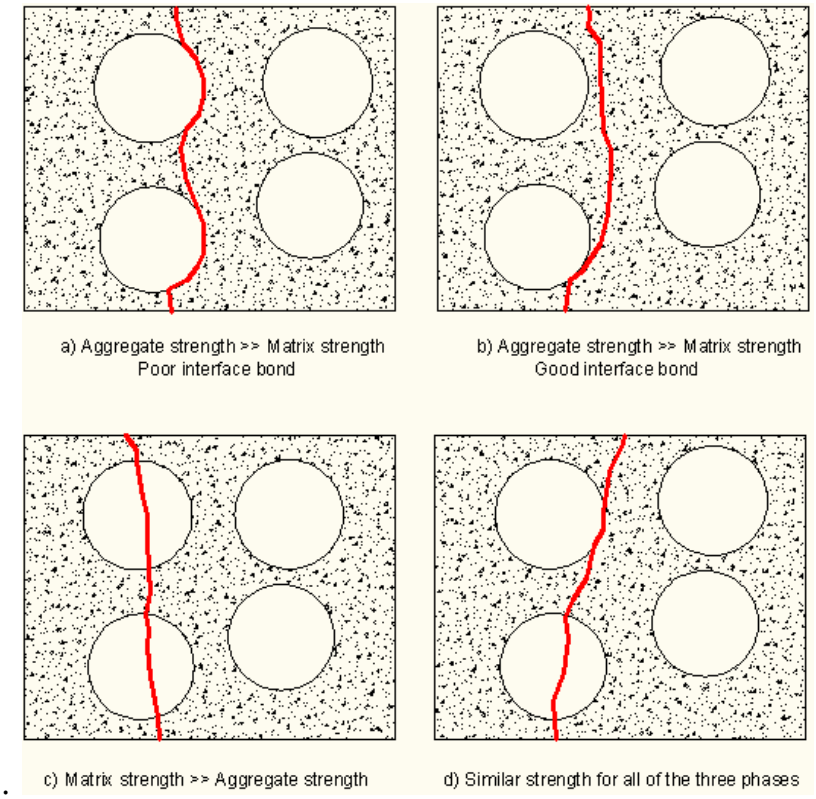

Figure 21. Potential modes of crack propagation.

In the analysis of the data presented below box plots are employed to observe variability and skewness of the data. In a box plot, the top and bottom points represent the maximum and minimum values of the data set, respectively. The top, middle, and bottom lines of the box present the 75th percentile, 50^{th} percentile or median, and 25th percentile values, respectively. Single data points are presented as horizontal lines, like the one observed in Figure 22 for the VSTR of the aggregate size of 1.25 in. Additionally, for the analysis of the effect of each variable on the surface texture, the statistical significance will be presented. Statistical significance is often determined by a p-value of a hypothesis test. In this case, a nonparametric hypothesis test called Mann-Whitney test (Johnson, 2005) will be used with the null hypothesis that the two population medians for each set of data are equal and the alternative hypothesis that the two population medians for each set of data points are different. If the p-value is less than 0.05 the statistic is said to be statistically significant. This implies that the data for each set is considered to come from different populations. The selection of the Mann-Whitnney test was based on the fact that the experimental data did not follow a normal distribution.

4.2.1 Effect of Coarse Aggregate Top Size on the Surface Texture

Figure 22 presents the effect of coarse aggregate top size on the crack surface texture quantified as VSTR. It can be observed in the figure that the overall relationship between aggregate top size with VSTR is positive. The roughness of the crack face increases as the coarse aggregate top size increases. This overall trend is in agreement with the results previously obtained by several researchers as presented in Section 2.3.2.3. In the majority of the cases the coarse aggregate is much stronger than the cement matrix. Consequently, cracks, which usually develop at the ITZ, propagate around the aggregates particles resulting in aggregate protrusions at the crack face. As

the coarse aggregate size increases, the crack travels through a more tortuous path. This behavior is responsible for the increase in roughness when augmenting the coarse aggregate top size.

There is an increase of 144 percent when varying the aggregate top size from 0.75 in to 2.5 in. However, based on a p-value of 0.2 given by the hypothesis test, it can be concluded that the data is considered to come from the same population. This implies that increase in surface texture due to increasing the aggregate top size is not statistically significant. This high p-value might be the result of the limited number of data points as well as the high standard deviation exhibited by the experimental data.

Analyzing not the overall trend but the change in VSTR when doing partial increments of the aggregate top size it can be observed that there is a non linear relationship between these two factors. This behavior implies that the same roughness of the crack face can be achieved by combining different concrete properties. For instance, two concrete mixtures, each with different aggregate top size, can result in the same crack surface texture. This can be explained considering that the propagation of the crack depends not only on one factor but on the properties and interactions of all of the concrete components combined.

Increasing the aggregate top size from 1.5 in to 2.5 in results in an increase of more than 112 percent in the median of VSTR. Nevertheless, based on the hypothesis test, it was found that this difference is not statistically significant.(p-value of 0.15) . For the same variation in top size Vandenbossche (Vandenbossche, 1999) found an increase in the VSTR of 66 percent.

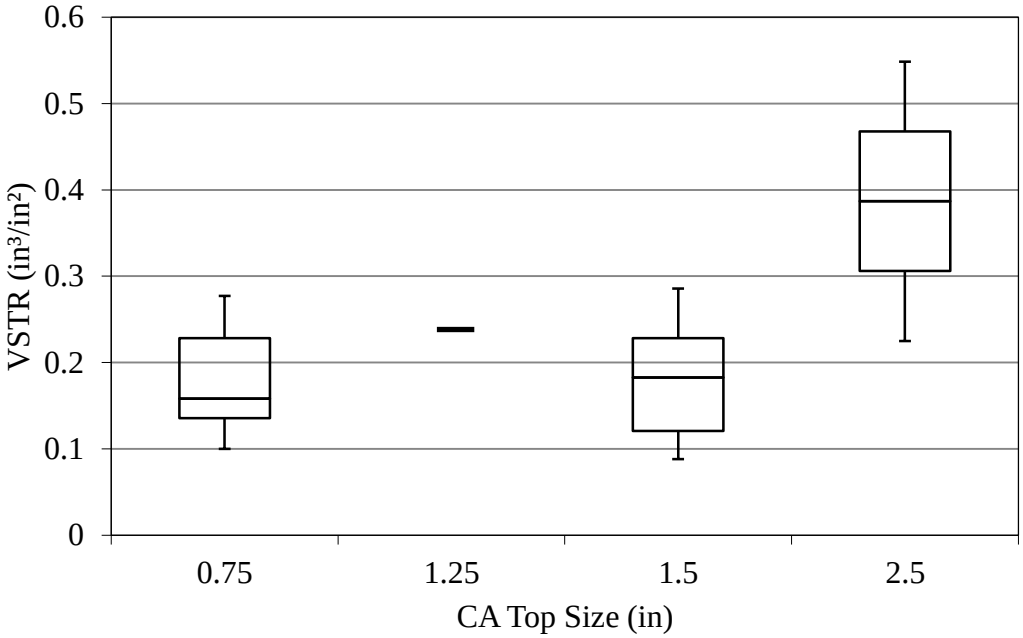

Figure 22. Effect of coarse aggregate top size on VSTR.

4.2.1.1 Effect of Coarse Aggregate Top Size on the Surface Texture for Different w/c Ratios

To further investigate the effect of aggregate top size on the roughness of the crack face, the VSTR results were grouped according to the three different ranges of w/c ratio previously defined for this study (e.i. w/c ratio less than or equal to 0.42, w/c ratio between 0.43 and 0.49, and w/c ratio greater than or equal to 0.50). Figure 23 presents the effect of the coarse aggregate top size on VSTR with respect to the strength of the matrix as characterized by the w/c ratio.

As observed in the figure, it is possible to identify changes in the surface texture for the three levels of matrix strength. For the high and low levels of matrix strength a positive relationship between aggregate top size and surface texture can be observed, while for the medium strength level this relationship is negative. However, there is no evidence to reject the

null hypothesis. This is based on the fact that the lowest p-value for the hypothesis tests conducted for the three levels of matrix strength was 0.3

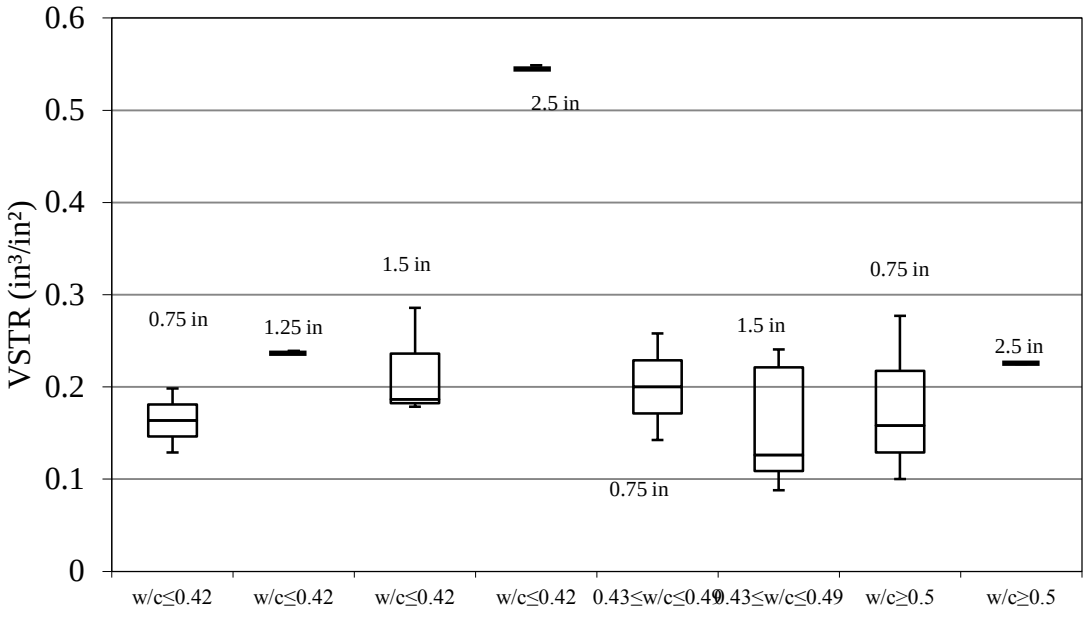

Figure 23. Effect of coarse aggregate top size on VSTR for different w/c ratios .

4.2.1.2 Effect of Coarse Aggregate Top Size on the Surface Texture for Different LA Abrasion Levels

Figure 24 presents the effect of the coarse aggregate top size on VSTR with respect to the hardness of the coarse aggregate determined by the LA abrasion. The VSTR results were arranged according to the three different levels of LA abrasion previously defined (e.i. LA abrasion less than or equal to 19 percent, LA between 20 and 30 percent, and LA abrasion greater than or equal to 31 percent).

It can be seen in Figure 24, that for the three levels of aggregate hardness there is an apparent reduction in the surface texture when increasing the aggregate top size from 0.75 in to 1.25in. Additionally, the effect of this change is less pronounced for stronger aggregates where the difference in the median VSTR is 14 percent, while this change for the medium and low levels of aggregate hardness is 60 and 35 percent respectively. Nevertheless, as similar to the data arrangement presented in Figure 23, there is not enough evidence to reject the null hypothesis. The lowest p-value from the hypothesis tests conducted to compare the significance of the difference in VSTR due to increasing the aggregate top size for different hardness levels was 0.4.

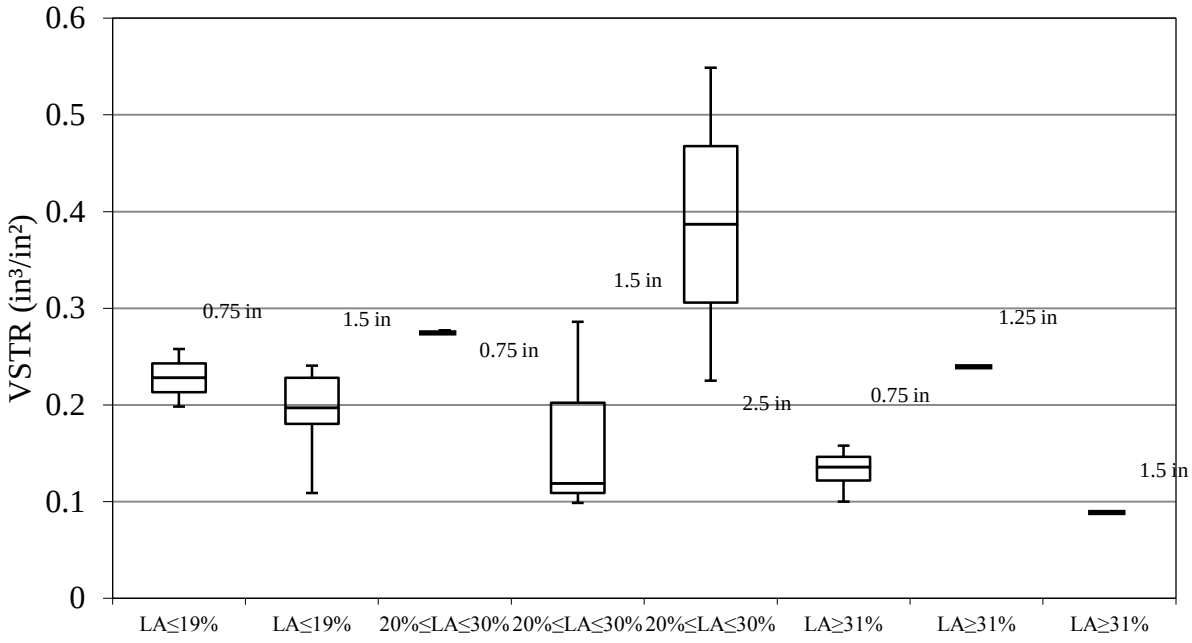

Figure 24. Effect of coarse aggregate top size on VSTR for different aggregate hardnesses.

4.2.2 Effect of Coarse Aggregate Hardness on the Crack Surface Texture

Figure 25 shows the effect of the coarse aggregate hardness, quantified by the LA abrasion, on the roughness of the crack face. As observed in the figure, for the three different levels of aggregate hardness, the largest VSTR was obtained for the stronger aggregates with high resistance to abrasion (i.e. LA≤19%) and the smallest VSTR was obtained for the weakest aggregates which have a low resistance to abrasion (i.e.LA≥31%). This overall trend agrees with the conclusions made by other researchers, as presented in Section 2.3.2.2., and can be explained by considering that for stronger aggregates the crack tends to propagate around the particle rather than through it. Nevertheless, it can be seen in the figure that the relationship between these two factors is not linear. The median value of the VSTR for the aggregates with a LA abrasion between 20 and 30 percent is higher than that of the two other categories. This implies that an equivalent crack surface texture can be obtained for different concrete mixtures, containing coarse aggregates with diverse hardness, when combined with other concrete components with specific properties.

The median VSTR for concrete mixtures with aggregates having a LA abrasion between 20 and 30 percent is 23 percent higher than for concrete mixtures containing coarse aggregates with a LA abrasion less than or equal to 19 percent. The hypothesis test conducted to compare the significance of this difference yielded a p-value of 0.5. Based on this it can be concluded that there is no evidence to reject the null hypothesis.

For the concrete mixtures with a weak coarse aggregate (i. e. LA≥31%), the median VSTR is 46 percent lower than that for the concrete with aggregates in the mid range of hardness (i.e. 20%≤LA≤30%). However, this difference is not considered statistically significant as a result of a p-value of 0.2obtained from a hypothesis test conducted with this data set. Comparing the

difference in surface texture when decreasing the aggregate hardness from the high level to the weak level a statistically significant (p-value 0.02) 33 percent decrease in the surface texture is obtained.

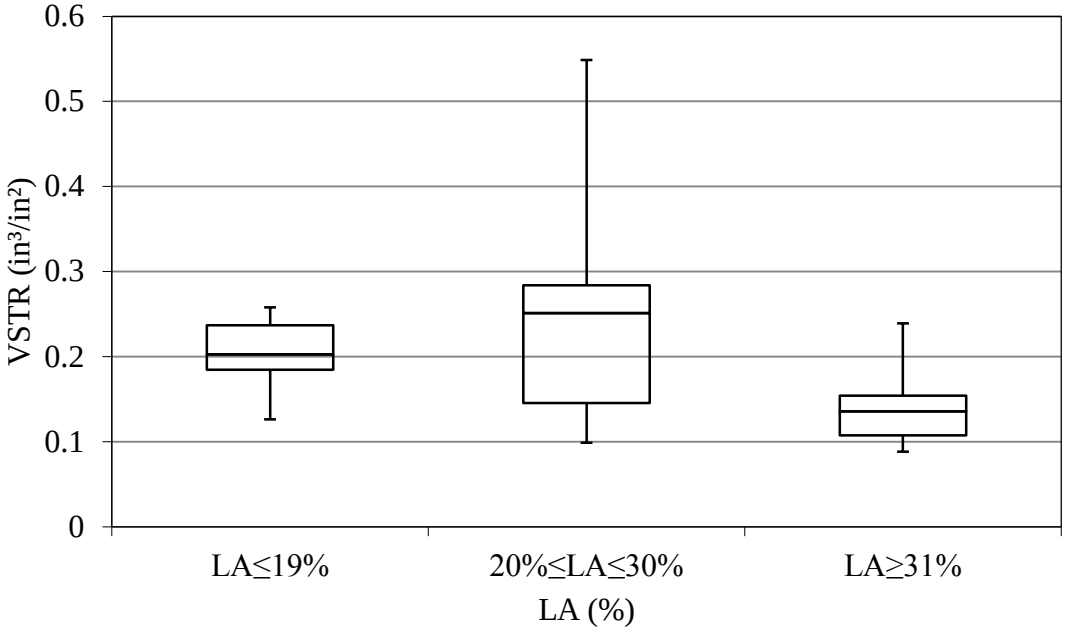

Figure 25. Effect of coarse aggregate hardness on VSTR.

4.2.2.1 Effect of Coarse Aggregate Hardness on the Surface Texture for Different Aggregate Top Sizes

The effect of the coarse aggregate hardness on the VSTR with respect to the different aggregate top sizes investigated is shown in Figure 26. As can be seen in the figure, for the aggregate with top size of 0.75in the trend for the three levels of aggregate hardness is similar to the overall trend presented in Figure 25. In this non linear trend the median VSTR for the concrete mixtures

with an aggregate hardness between 20 and 30 percent is higher than that of the other two categories. Varying the aggregate hardness from the first category (i.e.LA≤19%) to the third one (i.e. LA≥31%) results in a median VSTR which is 40 percent lower. A moderate level of statistical significance (p-value of 0.1) was found for this difference.

For the concrete mixtures using coarse aggregate with a top size of 1.5 in the relationship between aggregate hardness and VSTR is positive. A decrease in the aggregate hardness (i.e. increase in LA abrasion) results in a decrease in the VSTR. However, this difference is not considered statistically significant based on a p-value of 0.5 obtained from the hypothesis test conducted for this data set.

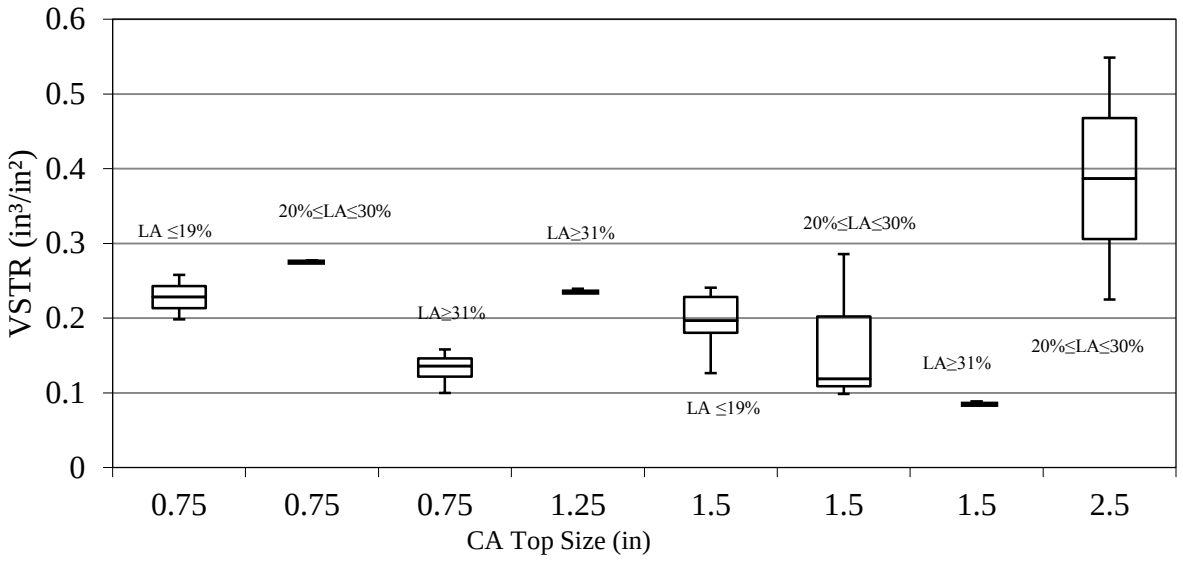

Figure 26. Effect of coarse aggregate hardness on VSTR for different aggregate top sizes.

4.2.2.2 Effect of Coarse Aggregate Hardness on the Crack Surface Texture for Different w/c Ratio Levels

The effect of the coarse aggregate hardness on the VSTR with respect to the three levels of w/c ratio previously defined is presented in Figure 27. As seen in the figure, for concrete mixtures with a w/c ratio less than or equal to 0.42 the relationship between LA abrasion and VSTR is non linear with the shape of a parabola that opens downward and has its vertex determined abrasion by the VSTR of concrete mixtures containing coarse aggregate with a LA abrasion between 20 and 30 percent. The median VSTR of the concrete mixtures with medium aggregate hardness (i.e. 20%≤LA≤30%) is 124 percent higher than that of the concrete with strong coarse aggregate (i.e LA≤19%); and it is 126 percent higher than that of the concrete with weak coarse aggregate (i.e. LA≥31%). The p-values obtained from the hypothesis tests to compare these differences in surface texture were 0.15 and 0.25 percent, respectively. These results imply that the evidence is not sufficient to reject the null hypothesis.

The trend determined by the relationship between LA abrasion and VSTR for the concrete mixtures with w/c ratio between 0.43 and 0.49 is a quadratic curve that opens upward with its vertex also determined by the VSTR of the concrete with medium hardness aggregate. The median of the VSTR for the medium hardness category is 53 percent lower than that of the concrete mixtures with stronger aggregate. This difference is considered to have a moderate level of significance (p-value of 0.08).

In the case of concrete mixtures with w/c ratio greater than or equal 0.5, the median VSTR of the mixtures with weaker aggregate is 49 percent lower than that of the concrete mixtures with medium hardness aggregate. The hypothesis test to compare this difference yielded a p-value of 0.25.

Comparing the absolute magnitude of the effect of varying the coarse aggregate hardness for the three levels of w/c ratio it can be concluded that the crack surface texture for the concrete mixtures with a w/c ratio less than or equal to 0.42 is more sensitive to the variation in aggregate hardness when compared to the other two predefined categories of that concrete property.

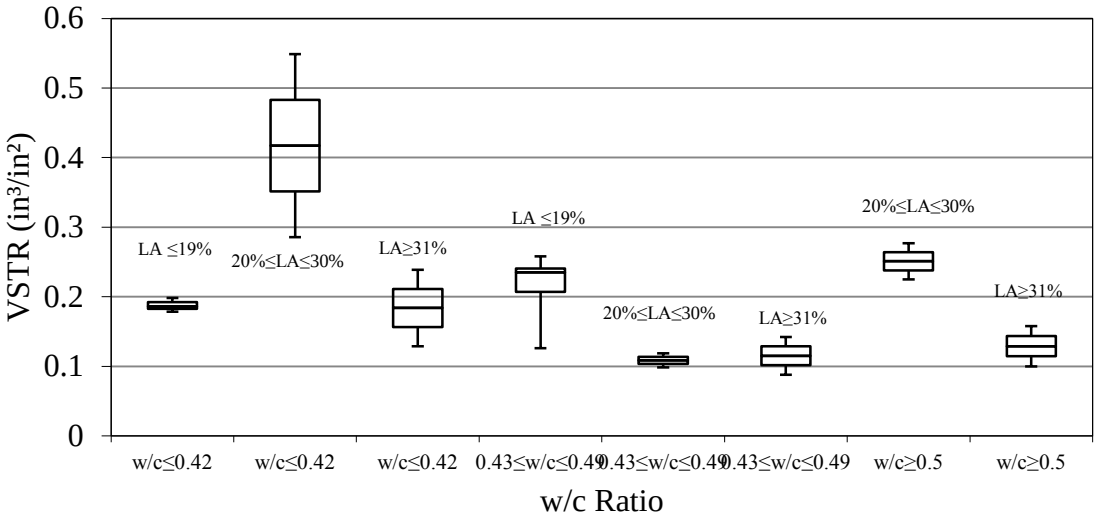

Figure 27. Effect of coarse aggregate hardness on VSTR for different w/c ratios.

4.2.3 Effect of Water-to-cementitious Materials (w/c) Ratio on the Surface Texture

The relationship between w/c ratio and VSTR for the complete set of data is presented in Figure 28. As observed in the figure, the overall change in surface texture, between the VSTR of concrete mixtures with a stronger matrix (i.e. w/c≤0.42) to the VSTR of concrete mixtures with a weaker matrix (i.e. w/c≥0.5), is very small (i.e. 3%). Additionally, this small difference was not found to be statistically significant.

In analyzing the trend delineated by the variation in VSTR for the three levels of w/c ratio it can be seen that there is a non linear relationship between these two factors. This non linear relationship has the form of a quadratic curve that opens upward with its vertex determined by the VSTR of the concrete mixtures with medium strength (i.e. $0.43 \leq w/c \leq 0.49$). This trend suggests that equivalent values of VSTR can be obtained for different concrete mixtures not having the same matrix strengths but combined with other components having specific properties which lead to similar crack surface textures.

Varying the w/c ratio from the high strength level to the medium strength level results in a decrease of the VSTR of 28 percent. The p-value obtained from the hypothesis test was 0.2. Additionally, varying the w/c ratio from the medium strength level to the low strength level results in an increase of the VSTR of 34 percent. However, this difference was found to be not statistically significant (p-value of 0.6).

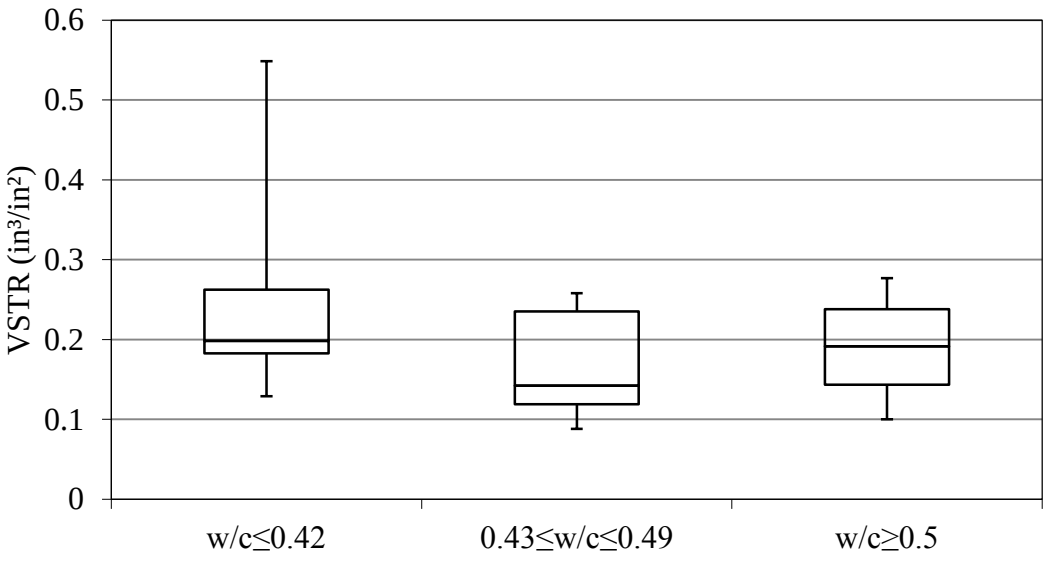

Figure 28. Effect of w/c ratio on VSTR.

4.2.3.1 Effect of w/c Ratio on the Surface Texture for Different Aggregate Top Sizes

As presented in Figure 29, the relationship between w/c ratio and VSTR for the concrete mixtures with coarse aggregate top size of 0.75 in exhibits the form of a quadratic curve that opens downward. This implies that for this set of concrete mixtures the largest values of VSTR are obtained when the w/c ratio lies within the medium strength range. For the concrete mixtures with a coarse aggregate top size of 1.5 in the relationship between w/c ratio and VSTR is positive, decreasing the matrix strength from the high strength level to the medium strength level results is a decrease 32 percent in the median VSTR.

In the case of concrete mixtures with a coarse aggregate top size of 2.5 in the relationship between w/c ratio and VSTR is also positive, decreasing the matrix strength from the high strength level to the low strength level results is a 59 percent decrease in the median VSTR.

Comparing the absolute magnitude of the effect of the variation in w/c ratio for the different coarse aggregate top sizes included in this study, it can be concluded that this variation is much more significant for the larger aggregate top size (i.e. 2.5 in) and less significant for the smaller aggregate top size (i.e. 0.75 in). However, the lower p-value obtained from the hypothesis tests conducted to compare these differences is 0.7. This implies that the totality of the data come from the same population. It is believed that the effect of varying the w/c ratio for the cases presented is being diminished by other factors.

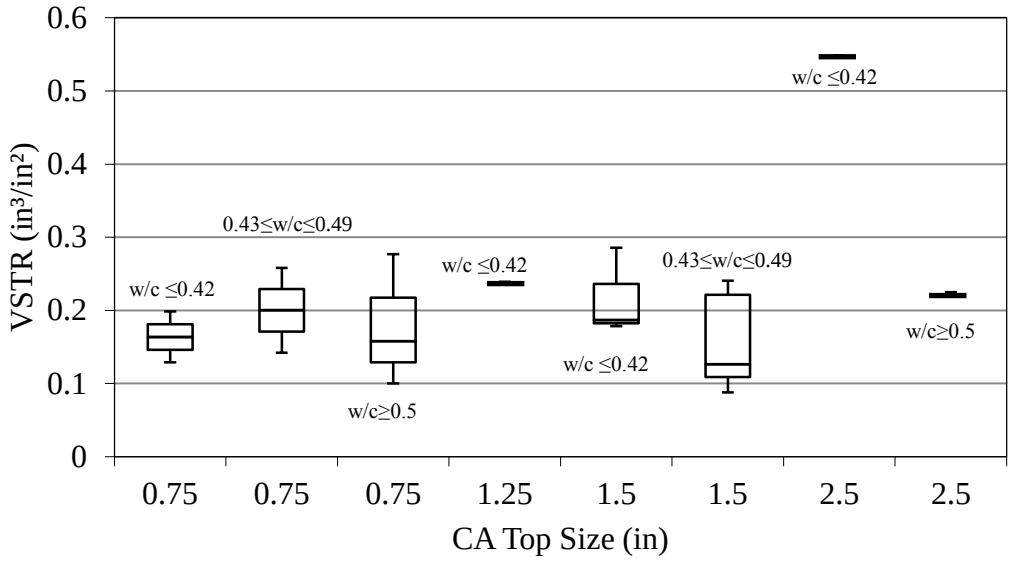

Figure 29. Effect of w/c ratio on VSTR for different coarse aggregate top sizes.

4.2.3.2 Effect of w/c Ratio on Surface Texture for Different Aggregate Hardnesses

Figure 30 presents the relationship between w/c ratio and VSTR for the three different levels of aggregate hardness previously defined for this study. As can be seen in the figure, for the concrete mixtures containing stronger aggregate hardness (i.e. LA≤19%) there is a negative relationship between matrix strength and VSTR, the larger the strength the lower the surface texture. However, this difference is not statistically significant as determined by a p-value of 0.25. For the concrete mixtures containing coarse aggregate hardness with an LA abrasion between 20 and 30 percent, the relationship between w/c ratio and VSTR exhibits the shape of a parabola that opens upward with its vertex defined by the VSTR of the medium concrete strength level mixtures. This implies that for this level of aggregate hardness the smother crack surfaces are obtained when using w/c ratios between 0.43 and 0.49. Varying the w/c ratio from the high strength level to the medium strength level results in a VSTR that is 74 percent lower.

Conversely, varying the w/c ratio from the medium strength level to the low strength level results in an increase in the VSTR by 130 percent. These differences are not statistically significant (p-value of 0.25).

For the concrete mixtures with a weaker coarse aggregate the exhibited trend between w/c ratio and VSTR has a similar shape compared to that of the concrete mixtures using aggregate with a LA abrasion between 20 and 30 percent. However, the magnitude of the effect of varying the w/c ratio is smaller and not statistically significant. Varying the w/c ratio from the high strength level to the medium strength level decreases the median VSTR by 37 percent; and varying it from the medium strength level to the low strength level results in a VSTR that is 12 percent higher.

Despite the fact that none of the differences presented in Figure 30 are statistically significant, it can be observed that concrete mixtures using coarse aggregate with an LA abrasion between 20 and 30 percent might be more sensitive to the variation in the matrix strength in comparison with the other two categories of aggregate hardness. Additionally, the variation of the w/c ratio might have a smaller effect on concrete mixtures with stronger aggregates.

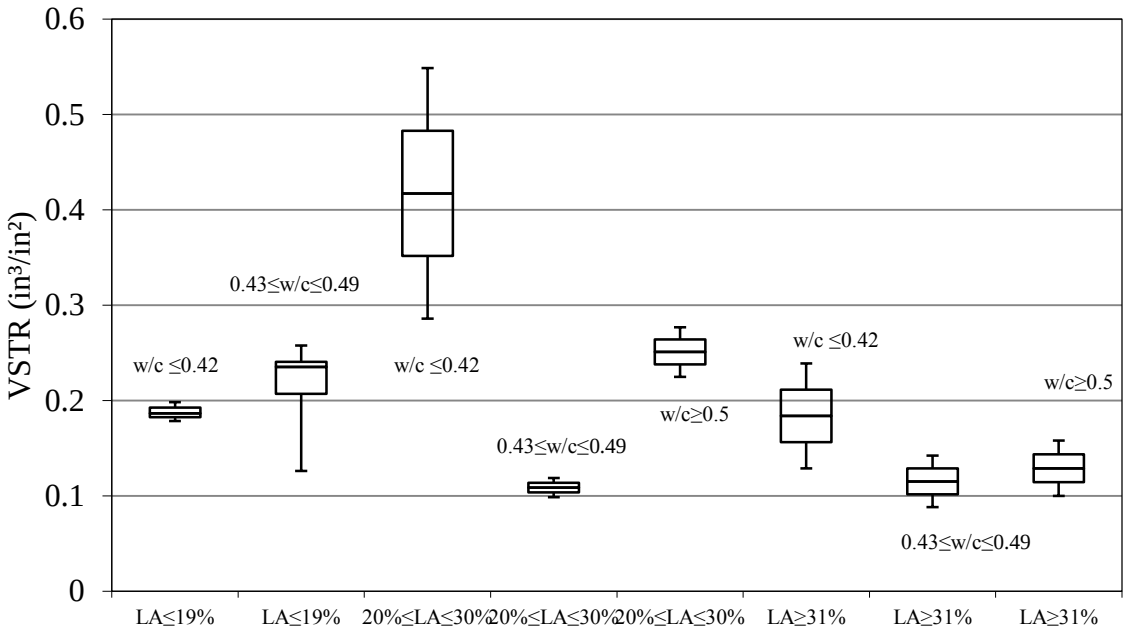

Figure 30. Effect of w/c ratio on VSTR for different aggregate hardnesses.

4.2.4 Effect of Aggregate Type on the Surface Texture

Besides the aggregate size and its hardness, there are aggregate properties that can influence the mechanism of crack propagation. For instance, as mentioned before, the aggregate surface texture can affect the strength of the matrix-aggregate interface. Smooth surfaces lead to a weaker bond in comparison with rough surfaces. Moreover, properties such as shape and angularity can affect fresh concrete properties, like workability, that eventually will affect the strength and properties of the ITZ. Such aggregate properties were not quantified in this study; however, the aggregate type can provide some information about the shape and texture of the aggregate. It is known that river gravel is composed of round particles and its texture depends on

its source. Siliceous gravels can be very smooth with low porosity whereas non-siliceous gravels can be rough with a high porosity. Blast furnace slag is angular, fairly cubical and its texture also varies depending on its components and production process. In general crushed limestone is angular, cubical and its texture varies according to it porosity. Trap rock tends to form polygonal vertical fractures mostly hexagonal.

Figure 31 presents the VSTR data for the four different coarse aggregate types included in this study. As seen in the figure, trap rock was used only for one concrete mixture. In the case of gravel it was used in six mixtures whereas limestone and slag were used for 8 and 5 mixtures, respectively. The figure shows that the concrete mixtures with limestone as the coarse aggregate achieve a higher VSTR value whereas concretes with slag and trap rock present the lower VSTR values. The median VSTR obtained for concretes with limestone is 50 percent higher than that for the concretes with gravel (p-value of 0.01). Additionally, the median VSTR for concretes with limestone is 93 percent higher than that for the concretes with slag (p-value 0.02). To isolate the effects of the other concrete components on the crack surface texture four different concrete mixtures with similar characteristics were investigated as discussed below.

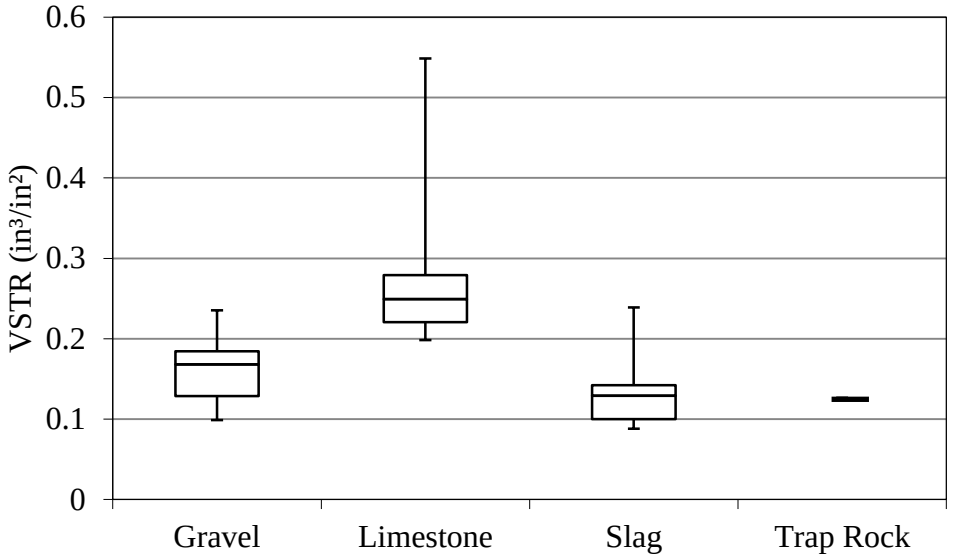

Figure 31. Effect of w/c ratio on VSTR for different aggregate hardnesses.

Figure 32 shows the VSTR for four different concrete mixtures that exhibit similar properties in terms of coarse aggregate hardness and top size as well as w/c ratio. The only remarkable difference between these mixtures is the aggregate type. As observed in the figure, the VSTR for the concrete containing limestone and gravel is very similar. The difference between the VSTR for the concrete containing gravel and the concrete using limestone with w/c ratio of 0.46 is only 2 percent. Based on this small difference it can be concluded that the shape of the aggregate does not affect the crack surface texture considerably. The VSTR obtained for the concrete containing trap rock is almost 40 percent lower than the average VSTR for the four concrete mixtures. This difference can be attributed to the strength of the aggregate-matrix interface which is function of the aggregate texture.

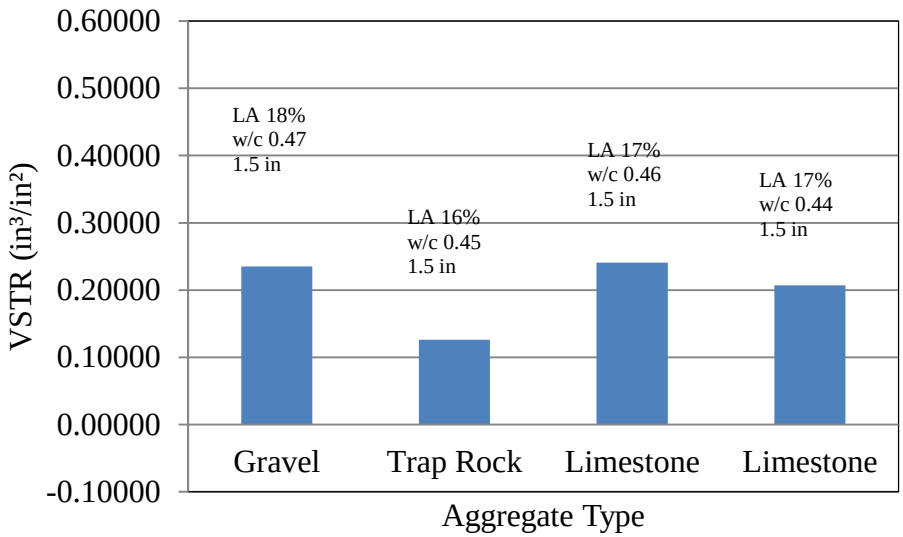

Figure 32. VSTR for concrete mixtures with similar properties and different coarse aggregate types.

5.0 DEVELOPMENT OF EMPIRICAL MODELS FOR VSTR, *AGG* AND *LTE* AND ANALYSIS OF THE MODEL PREDICTIONS

This chapter discusses the development of two models that predict *LTE* and *AGG* as a function of the concrete mixture properties investigated in this study (i.e. coarse aggregate top size, hardness, and w/c ratio) as well as a function of the VSTR and pavement characteristics such as: subgrade support, radius of relative stiffness, crack width and slab thickness. The development of these models includes the use of a statistical method of prediction and optimization as well as the use of models previously developed by other researchers as discussed in the following sections.

5.1 DEVELOPMENT OF THE VSTR MODEL

This section describes the development of a model that relates the VSTR of joints and cracks with the concrete mixture properties included in this study (i.e. coarse aggregate top size, hardness, and w/c ratio).

The model required the inclusion of one response (i.e. VTSR) and three predictors (i.e. coarse aggregate top size, hardness, and w/c ratio). Additionally, the analysis of the relationship between the studied variables and the quantified crack surface texture presented in Section 4.2 revealed that to accurately fit the experimental data it is necessary to include quadratic terms and interactions between the three predictors. In order to fulfill the requirements already mentioned,

a statistical method of prediction and optimization was selected. This method is commonly known as the Response Surface Method (RSM). The RSM is used to examine the relationship between one or more response variables and a set of quantitative experimental factors. This method is often employed after a "vital few" controllable factors have been identified and it is necessary to find the factor settings that optimize the response (Ledolter & Hogg, 2010). A statistical software Minitab was used to fit a model to the experimental data using the RSM. This method allows the selection of what predictor terms are included in the model which determines the linear or curvilinear aspects of the response surface. By including any second-order terms (i.e. square or interactions) it is possible to model curvilinear data. Considering the data trends presented in Section 4.2, a second-order polynomial equation was selected to express the VSTR as a function of the independent variables,

$$y = b_0 + b_1 x_1 + b_2 x_2 + b_3 x_3 + b_{11} x_1^2 + b_{22} x_2^2 + b_{33} x_3^2 + b_{12} x_1 x_2 + b_{13} x_1 x_3 + b_{23} x_2 x_3 \quad (5\text{-}1)$$

where y represents the VSTR in in^3/in^2, x_1 the coarse aggregate top size in inches, x_2 the inverse of the LA abrasion of the coarse aggregate expressed as a percentage, and x_3 represents the w/c ratio of the concrete mixture. Additionally, b_{ij} represents the regression coefficients.

Table 20 presents the 17 experimental data points that were used to fit the model. The original data set for all of the studies combined consisted of 20 data points. However, an investigation on the relationship between the quantified surface texture and factors controlling the mechanism of crack propagation lead to the exclusion of 3 data points. The relationship between VSTR and the ratio between the matrix strength and the aggregate strength (i.e.w/c ratio / LA abrasion) was studied for concrete mixtures containing the same aggregate top size. As a result of this investigation it was concluded that the concrete mixtures TR_1.5_16_0.45 and G_1.5_20_0.46 from Study No. 2, and the concrete mixture LS_1.5_30_0.38 from Study No.1 exhibit an

abnormal relationship between the surface texture and the mentioned ratio in comparison with the rest of the concrete mixtures with the same aggregate top size. Furthermore, the LA abrasion for the aggregates used in the mixtures was correlated rather than measured as discussed in Section 3.1.2.

Table 20. VSTR results for the complete data set.

CA Top size (in)	LA (%)	w/c ratio	Measured VSTR(in^3/in^2)
1.5	18	0.4	0.1866
1.5	18	0.42	0.1785
1.5	35	0.46	0.0881
1.5	18	0.47	0.2353
2.5	30	0.42	0.5487
1.5	22	0.44	0.1189
0.75	46	0.56	0.1000
0.75	37	0.56	0.1580
2.5	25	0.52	0.2250
0.75	20	0.5	0.2770
0.75	17	0.4	0.1984
1.25	34	0.4	0.2389
0.75	34	0.45	0.1424
0.75	34	0.4	0.1289
0.75	17	0.45	0.2579
1.5	17	0.46	0.2408
1.5	17	0.44	0.2070

The regression coefficients for the linear, quadratic, and interaction terms included in the second-order polynomial equation are presented in Table 21. In this table, TS represents the CA top size, LA the LA abrasion of the CA, and w_c the w/c ratio. The R^2 and the R^2 adjusted (i.e. modified R^2 that has been adjusted for unnecessary predictor terms in the model) for the second-order model with the regression coefficients shown in Table 21 are 91 and 86 percent, respectively. Additionally, the S value (root square of the mean square error) for the obtained

model was 0.039. The p-values presented in Table 21were obtained when the model was fitted. The null hypothesis in this case states that the regression coefficients are equal to zero while the alternate hypothesis states that at least one regression coefficient is different than zero. As observed in Table 21, the p-value for all of the terms is less than 0.05. Therefore, we can conclude that all the terms in the model are meaningful. However, previous regressions yielded a p-value above the cutoff level for the terms LA^2, TS/LA, and w_c^2. Consequently, those terms were not included in the subsequent regressions.

Table 21. Regression coefficients and p-value for the VSTR model.

Terms	Coefficient	p-value
Constant	0.3689	0.000
TS	0.5004	0.002
1/LA	-24.5162	0.000
w_c	-0.0540	0.001
TS^2	0.2049	0.000
TS*w_c	-2.2665	0.000
w_c/LA	61.5434	0.005

Table 22 presents the effect of the regression, linear, square and interaction terms on the VSTR model. As observed in the table, all of the terms exhibit p-values considerably lower than the predetermined α value (i.e. 0.05). This implies that the totality of the terms is contributing importantly to the prediction of the response.

Table 22. Effect of the regression, linear , square , and interaction terms on the VSTR model.

Source	p-value
Regression	0.0000
Linear	0.0010
Square	0.0010
Interaction	0.0000

The second-order polynomial equation describing the VSTR as a function of the concrete mixture properties investigated is as follows:

$$VSTR = 0.3689 + 0.5004 * TS - 24.5162 * (1/LA) - 0.0540 * w\_c + 0.2049 * TS^2 - 2.2665 * TS * w\_c + 61.5434 * (w\_c / LA) \quad (5\text{-}2)$$

where,

VSTR is the volumetric surface texture ratio expressed in in^3/in^2,

TS is the coarse aggregate top size expressed in in,

LA is the Los Angeles abrasion value, expressed in percentage, and,

w_c is the water to cementitous material ratio of the concrete mixture.

5.1.1 Analysis of the VSTR Model Predictions

Figure 33 shows the measured VSTR versus the predicted VSTR using the model presented in Equation (5-2). The R^2 describes the amount of variation in the measured response that is explained by the model. As mentioned before the R^2 for this model is 91 percent which is considered good. This model predicts the VSTR using w/c ratios between 0.38 and 0.56, coarse aggregate LA values between 16 and 46 percent, and coarse aggregate top sizes from 0.75 and 2.5 in.

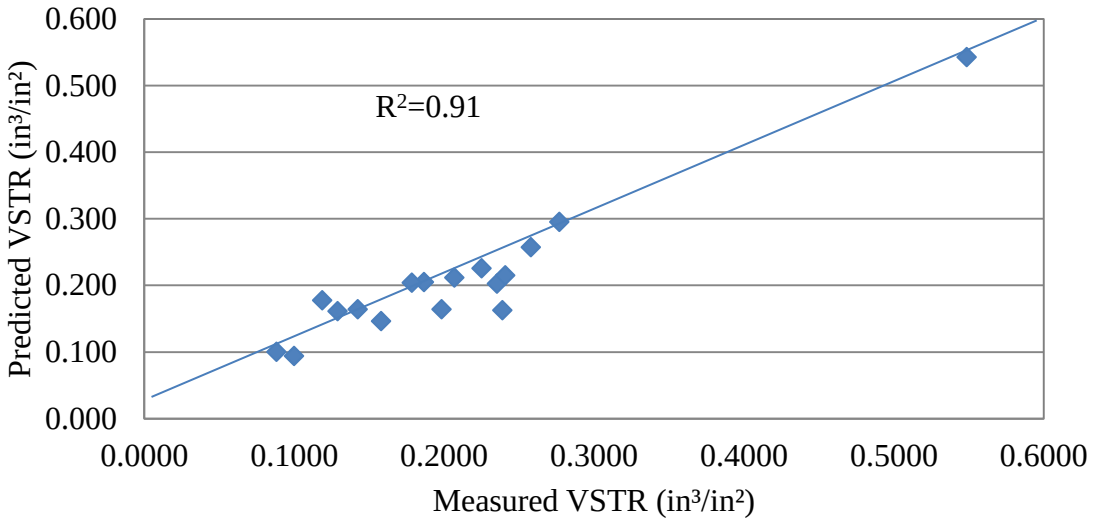

Figure 33. Measured VSTR vs. predicted VSTR.

5.1.1.1 Predicted VSTR as a function of the Coarse Aggregate LA abrasion and w/c ratio for a Constant Coarse Aggregate Top size

Figure 34 presents the predicted VSTR as a function of the coarse aggregate hardness and the w/c ratio for a constant coarse aggregate top size of 1.0 in. The predicted VSTR values shown in the surface plot range from 0.05178 in^3/in^2 to 0.3034 in^3/in^2. The lowest value corresponds to a concrete mixture with a w/c ratio of 0.5 and a coarse aggregate with an LA abrasion of 46 percent. The largest VSTR value corresponds to a concrete mixture with a w/c ratio of 0.50 and a coarse aggregate with a LA abrasion of 16 percent.

Except for concrete mixtures with a very strong aggregate, the relationship between matrix strength and surface texture shown in Figure 34 is positive. Increasing the matrix strength results in an increase in the surface texture. This trend supports findings of other researchers (Walraven, 1981),(Bazant & Gambarova, 1980) that concluded that increasing the concrete compressive strength improves the aggregate interlock joint behavior. However, the effect of

varying the matrix strength in the predicted VSTR is not the same for concretes with different aggregate hardnesses. As seen in Figure 34, for concretes with low-resistance-to-abrasion aggregates, increasing the matrix strength produces an increase in the surface texture, while for concretes with strong aggregates; increasing the matrix strength decreases the surface texture. It is believed that this behavior is related to the ratio between aggregate strength and matrix strength. In the case of concretes with stronger aggregates, a low-strength matrix results in cracks propagating around the aggregate particles. However, when increasing the matrix strength the crack can travel through some of the aggregate particles decreasing the surface texture. In the case of concretes with weaker aggregates, the crack propagates primarily thorough the aggregate particles, consequently, the contribution to the tortuosity of the crack is mainly provided by the matrix. It is believed , however, that for this particular case, where the porosity of the aggregate and the strength of the aggregate are high, the ITZ strength might be higher than the strength of the aggregate itself, which could contribute to the tortuosity of the crack path.

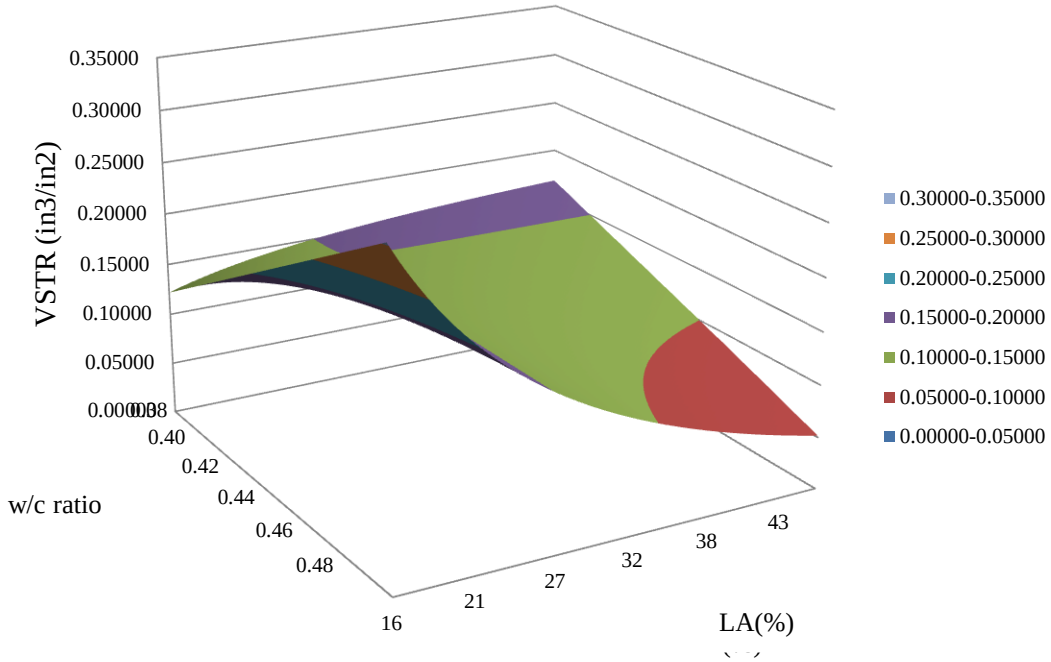

Figure 34. Predicted VSTR as a function of CA LA and w/c ratio for top size of 1.0 in.

5.1.1.2 Predicted VSTR as a function of the Coarse Aggregate Top size and w/c ratio for a Constant Coarse Aggregate LA Abrasion

Figure 35 presents the predicted VSTR as a function of the coarse aggregate top size and the w/c ratio for a constant LA of 30 percent. The predicted VSTR values shown in the surface plot range from 0.0635 in^3/in^2 to 0.69017 in^3/in^2. The lowest value corresponds to a concrete mixture with a w/c ratio of 0.5 and a coarse aggregate top size of 1.60 in. The largest VSTR value corresponds to a concrete mixture with a w/c ratio of 0.38 and a coarse aggregate top size of 2.50 in.

As observed in Figure 35, increasing the aggregate top size in the concrete mixture results in an increase in the surface texture. This trend agrees with the results previously obtained

by other researchers as presented in Section 2.3.2.3. This behavior is the result of the greater path length as the crack propagates around the aggregate particles.

The relationship between w/c ratio and surface texture shown in Figure 35 establishes that increasing the matrix strength results in a higher surface texture. As mentioned before, this trend is in agreement with other studies (Walraven, 1981), (Bazant & Gambarova, 1980). Furthermore, this variation in surface texture due to changes in the matrix strength is more prominent for concrete mixtures with larger aggregate top size. This might be caused the result of concrete having larger aggregates exhibiting more variability probably due to higher tendency of segregation (Mindess, Young, & Darwin, 2003).

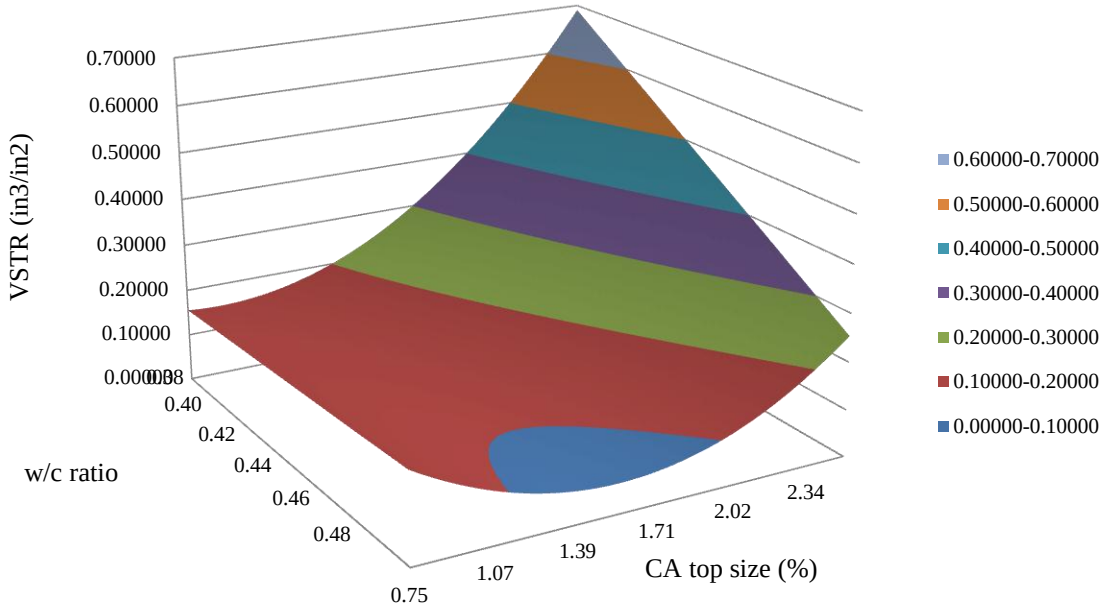

Figure 35. Predicted VSTR as a function of CA top size and w/c ratio for CA LA abrasion of 30 percent.

5.1.1.3 Predicted VSTR as a function of the Coarse Aggregate Top size and Coarse Aggregate LA Abrasion for a Constant w/c ratio

Figure 36 presents the predicted VSTR as a function of the coarse aggregate top size and the coarse aggregate LA abrasion for a constant w/c ratio of 0.45. The predicted VSTR values shown in the surface plot range from 0.0844 in^3/in^2 to 0.52586 in^3/in^2. The lowest value corresponds to a concrete mixture with coarse aggregate LA abrasion of 46 percent and a coarse aggregate top size of 1.28 in. The largest VSTR value corresponds to a concrete mixture with coarse aggregate LA abrasion of 16 percent and a coarse aggregate top size of 2.50 in. As seen in the figure, there is a direct relationship between aggregate top size and surface texture. Increasing the aggregate top size results in an increase in the VSTR. As discussed in Section 5.1.1.2 the higher surface

texture that results when increasing the aggregate top size is a function of the longer path of the crack when propagating around aggregates.

Additionally, it can be seen in Figure 36 that the relationship between aggregate hardness and surface texture is direct as was observed in Figure 34. Increasing the aggregate hardness results in a higher surface texture. As explained before, this behavior is related to the tendency of cracks to propagate around the aggregate particles when the strength of the aggregate is higher than the strength of the matrix and ITZ.

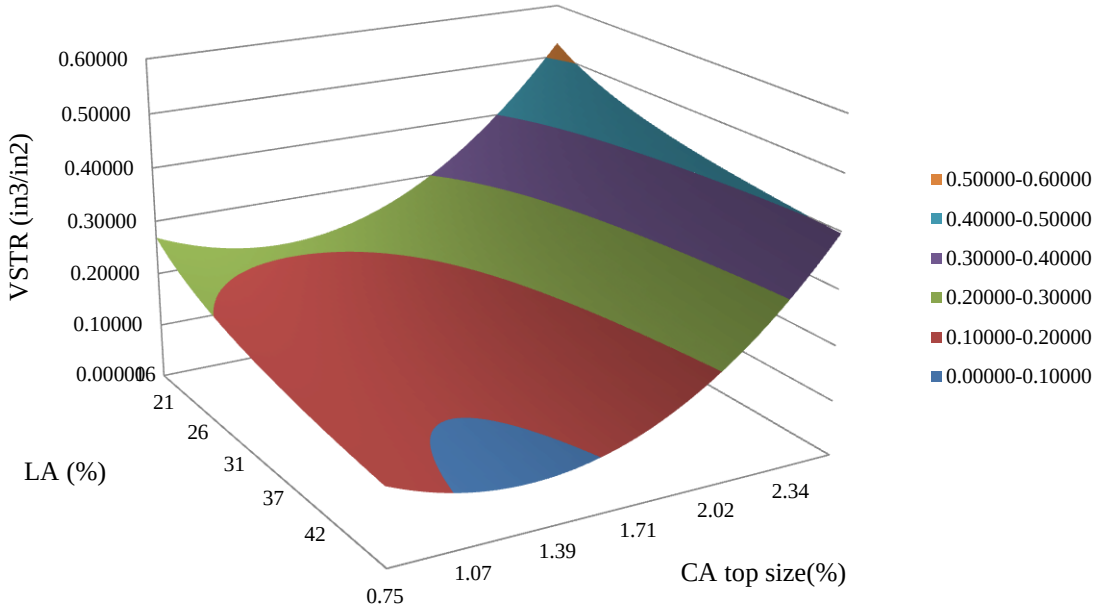

Figure 36. Predicted VSTR as a function of CA top size and CA LA for w/c ratio of 0.45.

5.2 DEVELOPMENT OF THE *LTE* MODEL

This section describes the development of a model that relates *LTE* of cracks and undoweled joints with the concrete mixture w/c ratio, the coarse aggregate top size, and hardness, and the joint/crack width. This model is based on the VSTR model presented in the previous section (Equation 5-2), and a model that relates VST and crack/joint width with the *LTE* of joints or cracks which was developed by Vandenbossche (Vandenbossche, 1999) and it was presented in Section 2.4.1 (Equation (2-8)). As shown in Figure 11, this model has a coefficient of determination, R^2, of 95 percent. In order to directly relate the concrete mixture properties already mentioned with *LTE* it is necessary to embed Equation (5-2) into Equation (2-8). Therefore, the VSTR has to be converted to VST.

As explained before, the VSTR is obtained by normalizing the VST by the test area. Consequently, to calculate the VST of a crack or joint face based on the VSTR it is necessary to multiply the VSTR by the "effective" pavement thickness. The effective pavement thickness refers to only that portion of the fractured slab face that contains crack texture (Vandenbossche, 1999). For instance, the effective pavement thickness is reduced at joints because the texture provided by the propagation of the crack starts at the bottom of the saw cut. The effective slab thickness is also reduced when the top and/or bottom of the slab is spalled (Vandenbossche, 1999). The VSTR multiplied by the effective slab thickness is referred to as the volumetric surface texture (VST) and it represents the volume of surface texture per unit width of the cracked slab face (Vandenbossche, 1999).

Embedding Equation (5-2) into Equation (2-8) results in the proposed *LTE* model as follows:

$$LTE = 39.7 \cdot \log[\frac{\{(0.3689 + 0.5004 * TS - 24.5162 * (1/LA) - 0.0540 * w\_c + 0.2049 * TS^2 - 2.2665 * TS * w\_c + 61.5434 * (w\_c / LA)\} * a * ST}{cw}] + 5.6 \quad (5\text{-}3)$$

where,

LTE is the joint/crack load transfer efficiency expressed in percentage,

TS is the coarse aggregate top size expressed in in,

LA is the Los Angeles abrasion value, expressed in percentage,

w_c is the water to cementitous material ratio of the concrete mixture,

a is constant equal to 2.54for units conversion,

ST is the slab thickness expressed in cm, and,

cw is the crack width expressed in cm.

This model is valid for concrete mixtures with w/c ratios between 0.38 and 0.50, coarse aggregate LA abrasion between 16 and 46 percent, and coarse aggregate top sizes from 0.75 and 2.5 in. Additionally, it is important to highlight that in the development of the relationship between LTE and VST presented in Equation (2-8) two foundations were evaluated. The first foundation had a stiffness of 100 psi/in and the second a stiffness of 250 psi/in.

5.2.1 Analysis of the *LTE* Model Predictions

5.2.1.1 Predicted *LTE* as a function of the Coarse Aggregate LA Abrasion and w/c ratio for a Constant Coarse Aggregate Top size, Crack Width, and Slab Thickness

Figure 37 presents the predicted *LTE* as a function of the coarse aggregate LA abrasion and the w/c ratio for a constant coarse aggregate top size of 1.0 in, a crack width of 0.08 in, and a slab

thickness of 11in. The predicted *LTE* shown in the surface plot ranges from 55 to 90 percent. The lowest value corresponds to a concrete mixture with a w/c ratio of 0.5 and a coarse aggregate with LA abrasion of 46 percent. The largest *LTE* value corresponds to a concrete mixture with a w/c ratio of 0.5 and a coarse aggregate with a LA abrasion of 16 percent. Comparing Figure 37 with Figure 34 it can be seen that the *LTE* response reflects the variation in the joint/crack surface texture determined by the VSTR. As seen in Figure 37, for aggregates with a low resistance to abrasion decreasing the matrix strength results in a decrease of the VSTR, whereas for stronger aggregates decreasing the matrix strength results in an increase of the VSTR.

One of the possible applications for this LTE model in pavement engineering can be explained using Figure 37. For instance, the coarse aggregate to be used in a concrete mixture for an 11-in thick non-doweled PCC pavement has a top size of 1.0 in and a LA abrasion of 35 percent. The maximum predicted joint width is 0.08 in. The designer wants to maximize the long-term expected *LTE* of the pavement to ensure a good pavement performance over time. As seen in Figure 37 this can be achieved by modifying the concrete proportions to obtain the w/c ratio that result in the higher *LTE* for the mentioned conditions. For this hypothetical case, a w/c ratio of 0.38 results in the highest *LTE*.

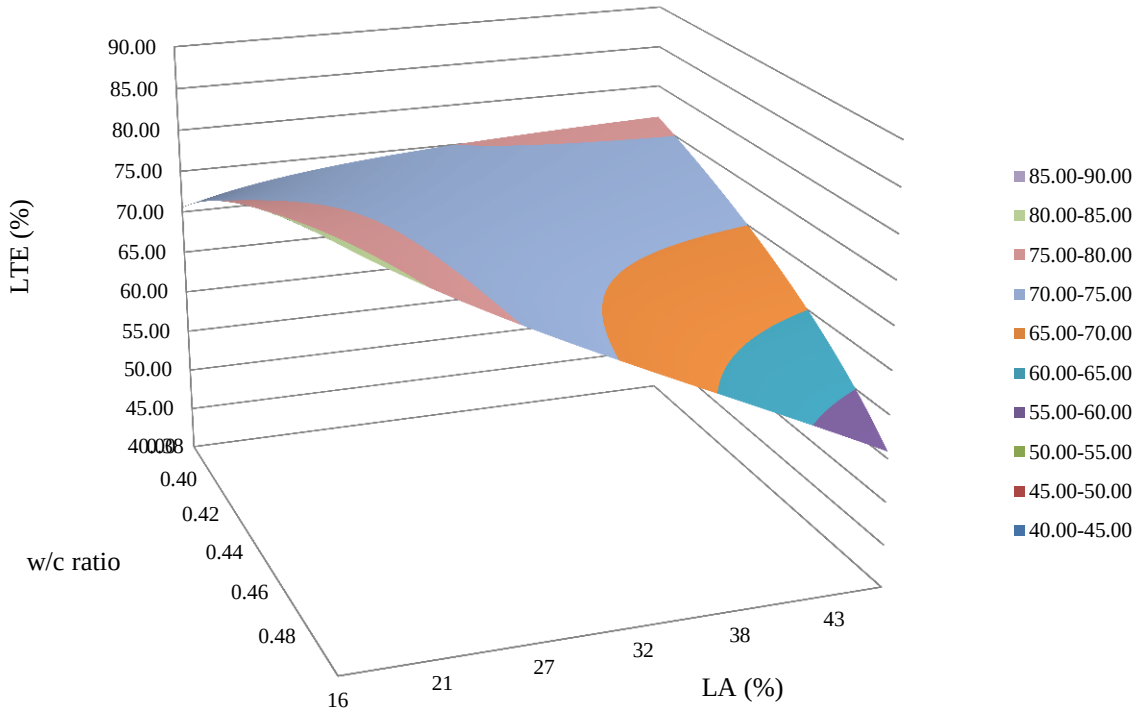

Figure 37. Predicted *LTE* as a function of CA LA abrasion and w/c ratio for CA top size of 1.0 in, a crack width of 0.08 in, and a slab thickness of 11 in.

5.2.1.2 Predicted *LTE* as a Function of the Coarse Aggregate Top size and w/c ratio for a Constant Coarse Aggregate LA Abrasion, Crack Width, and Slab Thickness

Figure 38 presents the predicted joint/crack *LTE* as a function of the coarse aggregate top size and the w/c ratio for a constant coarse aggregate LA abrasion of 20 percent, a crack width of 0.08 in, and a slab thickness of 11in. The predicted *LTE* values shown in the surface plot range from 70 to 98 percent. The lowest value corresponds to a concrete mixture with a w/c ratio of 0.38 and a coarse aggregate top size of 0.75 in. The highest *LTE* value corresponds to a concrete mixture with a w/c ratio of 0.38 and a coarse aggregate top size of 2.50 in. It can be seen in

Figure 38, that for these specific conditions, the variation in *LTE* when varying the matrix strength is almost the same regardless of the aggregate top size in the concrete mixture.

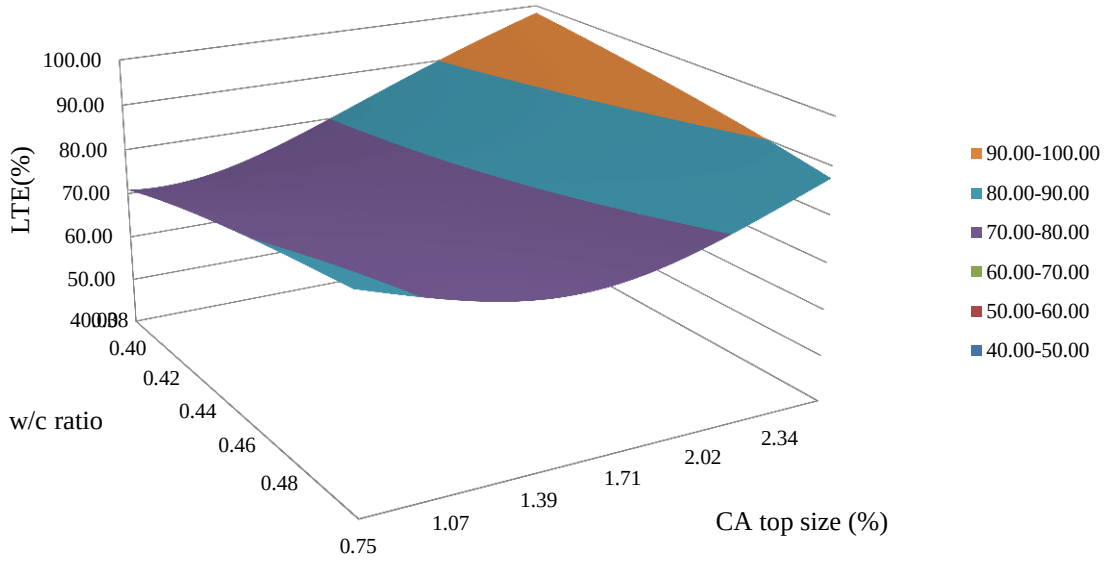

Figure 38. Predicted *LTE* as a function of CA top size and w/c ratio for CA LA abrasion of 20 percent, a crack width of 0.08 in, and a slab thickness of 11 in.

5.2.1.3 Predicted *LTE* as a function of the Coarse Aggregate Top size and Coarse Aggregate LA Abrasion for a Constant w/c ratio, Crack Width, and Slab Thickness

Figure 39. presents the predicted *LTE* as a function of the coarse aggregate top size and the coarse aggregate LA abrasion for a constant w/c ratio of 0.45 a crack width of 0.08 in, and a slab thickness of 11in. The predicted *LTE* values shown in the surface plot ranges from 64 to 96 percent. The lowest value corresponds to a concrete mixture with coarse aggregate LA of 46 percent and a coarse aggregate top size of 1.26 in. The largest VSTR value corresponds to a concrete mixture with coarse aggregate LA abrasion of 46 percent and a coarse aggregate top

size of 2.50 in. As seen in the figure, for concretes with CA top size larger than 1.4 in, there is a clear direct relationship between CA top size and *LTE* for all of the hardness levels. Increasing the aggregate top size results in an increase in the VSTR.

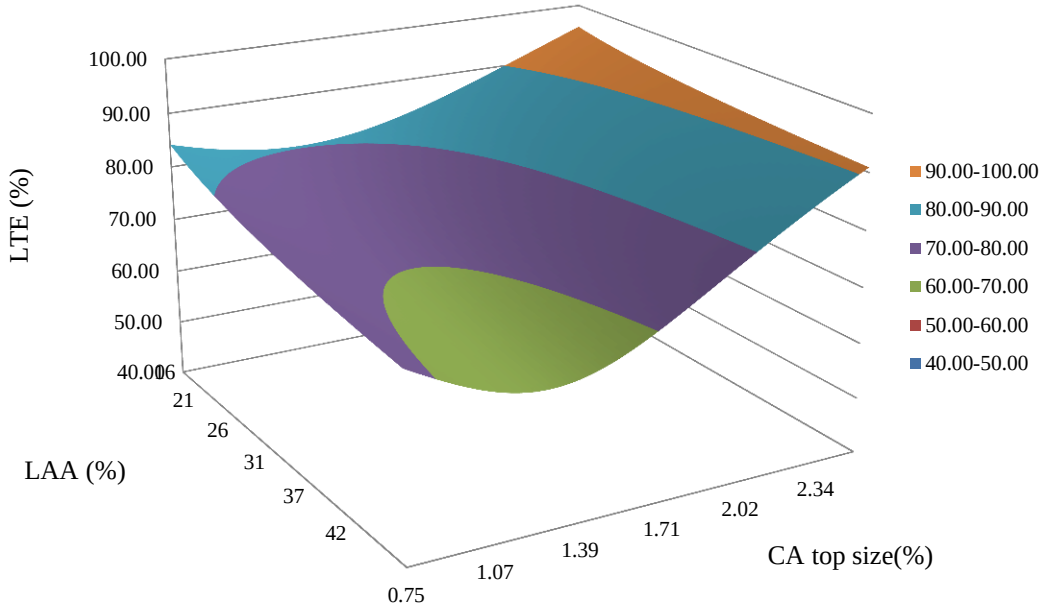

Figure 39. Predicted *LTE* as a function of CA top size and CA LA abrasion for w/c ratio of 0.45, a crack width of 0.08 in, and a slab thickness of 11 in.

5.2.1.4 Predicted *LTE* as a function of Crack Width

The variation of the predicted *LTE* with respect to the crack width is presented in Figure 40. The results shown in the figure correspond to a 10-in thick PCC pavement with four concrete mixtures having a constant w/c ratio of 0.45, a constant aggregate LA abrasion of 45 percent, and a range aggregate top sizes (i.e. 0.75 in, 1 in, 1.5 in, and 2.0 in). It can be seen in Figure 40 that the *LTE* curve is flat until a certain point where it starts to drop non-linearly with respect to the crack width. As observed in Figure 40 the crack width for which the *LTE* drops is different

depending on the aggregate top size. This critical crack width tends to be higher when increasing the aggregate top size. However, in this specific case, for the concrete mixtures with an aggregate top size of 0.75 in and 1 in this critical crack width is the same (i.e. approximately 10 mils). This condition is associated with the non-linearity of the model prediction. As discussed before, this behavior implies that similar surface textures can be obtained for mixtures with two different aggregate top sizes depending on the interaction with the rest of the concrete constituents. For the mixture with aggregate top size of 1.5 in the critical crack width is approximately 20 mils while this value for the mixture with aggregate top size of 2 in is approximately 35 mils. Additionally, it can be observed that concretes with larger aggregate top sizes maintain a higher *LTE* when the crack width is increased in comparison with concretes containing a smaller aggregate top size. These conditions reflect the important contribution of the aggregate top size to the load transfer mechanism and the pavement long-term performance.

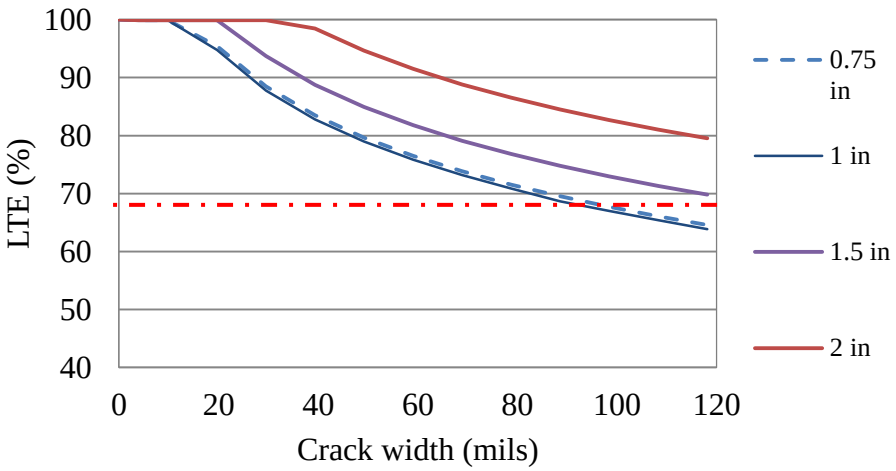

Figure 40. Variation of predicted *LTE* with respect to crack width for four concrete mixture with different aggregate top sizes, a w/c ratio of 0.45, a CA LA of 45 percent, and a slab thickness of 10 in.

Jensen and Hansen (Jensen & Hansen, 2001) measured the *LTE* of 10 in-thick large-scale slabs with respect to the crack width for concretes with two aggregate types and a range of top sizes. The slabs were placed on a typical Michigan highway foundation (i.e. 4 in open-graded drainage course on a 16 in thick subbase).This foundation is similar to the foundation used in the development of Equation (2-8) This similarity allows a comparison between the predicted values using the LTE model, presented in Equation (5-3), and the measured values by Jensen and Hansen.

Figure 41 shows the measured and predicted values for a concrete having an aggregate top size of 1 in (limestone, LA abrasion of 34 percent) and w/c ratio of 0.45; and for a concrete with aggregate top size of 2 in (glacial gravel, LA abrasion of 22 percent) and w/c ratio of 0.45. As observed in Figure 41, the prediction of the *LTE* is fairly accurate in comparison with the measured values, especially for the concrete with an aggregate top size of 1in. Although the analysis of more cases is necessary to validate the *LTE* model developed in this study, these results give an insight of the adequacy of the model.

The Stages I and II of the *LTE* proposed by Jensen and Hansen can also be seen in Figure 41. Stage I, occurs for crack widths smaller than 0.5 mm (20 mils) and the *LTE* is almost 100 percent, Stage II which occurs for crack widths between 0.6 mm (24 mils) and 2.5 mm (99 mils) is the crack width range where aggregate interlock plays a major role. Nevertheless it can be observed that aggregate top size plays an important role in the determination of these stages. For the case when the concrete with aggregate top size of 2 in the predicted *LTE* is maintained at almost 100 percent for crack widths between 0 and 20 mils. Conversely, for the cases when the concrete has an aggregate top size of 1 in, the predicted *LTE* is maintained for crack widths between 0 and 4 mils.

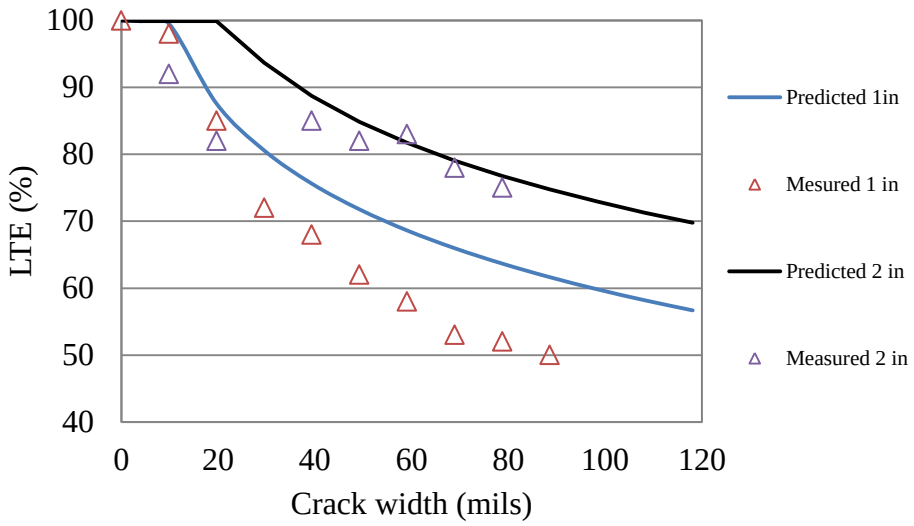

Figure 41. Predicted *LTE* vs. measured *LTE* with respect to crack width for two concrete mixture with different aggregate top sizes, different CA LA abrasion, a constant w/c ratio of 0.46, and a slab thickness of 10 in.

5.2.1.5 Predicted *LTE* as a function of Slab Thickness

Figure 42 shows the variation in the predicted *LTE* with respect to slab thickness. The results presented in the figure correspond to a PCC pavement constructed of a concrete containing and aggregate with top size of 0.75 in and a constant crack width of 79 mils. The *LTE* is the average value of the results for concrete mixtures with the same range of w/c ratio and a LA abrasion mentioned in Section 5.2.1.4. As observed in the figure increasing the slab thickness results in a higher *LTE*. This is related to the augment in the contact area between the faces of the crack.

However, this increase in *LTE* is relatively small. For this specific example increasing the thickness of the slab 1 in results in an *LTE* increase of less than 3 percent.

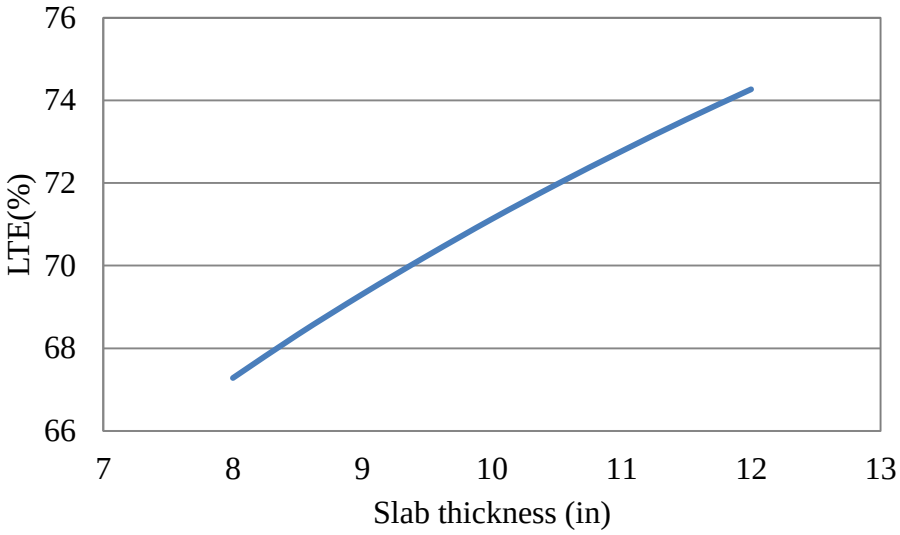

Figure 42. Variation of average *LTE* with respect to slab thickness for a concrete mixture with CA top size of 0.75 in and a crack width of 79 mils.

5.3 DEVELOPMENT OF THE *AGG* MODEL

This section discusses the development of a model that relates *AGG* for cracks and undoweled joints with the concrete mixture w/c ratio, coarse aggregate top size, and hardness, and joint/crack width. This *AGG* model is based on the *AGG* equation presented in Equation (2-9) developed by Vandenbossche (Vandenbossche, 1999).

To directly relate the key concrete mixture properties investigated in this study to the dimensional joint spring stiffness *AGG*, it is necessary to embed Equation (5-2) into Equation (2-9) as follows:

$$AGG = \left[105.72 * e^{2.367 * \log\left(\frac{VSTR * a * ST}{cw} \right)} \right] * b \quad (5\text{-}5)$$

where,

AGG is the joint/spring stiffness expressed in psi/in,

VSTR is Equation (5-2),

a is constant equal to 2.54for units conversion,

b is constant equal to 3.6838 for units conversion

ST is the slab thickness expressed in cm, and,

cw is the crack width expressed in cm.

The resulting equation relates the dimensional joint stiffness with the coarse aggregate top size and hardness, the concrete mixture w/c ratio, the slab thickness, and the crack width.

5.3.1 Analysis of the *AGG* Model Predictions

5.3.1.1 Predicted *AGG* as a function of the Coarse Aggregate LA Abrasion and w/c ratio for Constant Coarse Aggregate Top size, Crack Width, and Slab Thickness.

Figure 43 depicts the predicted *AGG* as a function of the coarse aggregate LA abrasion and the w/c ratio of the concrete mixture for a constant coarse aggregate top size of 1.0 in, a crack width of 0.08 in, and a slab thickness of 11in. The predicted *AGG* seen in the surface plot ranges from 7,800 psi to 47,800 psi. The lowest value corresponds to an *LTE* of 56 percent for a concrete mixture with a w/c ratio of 0.5 and a coarse aggregate with LA abrasion of 46 percent. The largest *LTE* value corresponds to a crack *LTE* of 86 percent for a concrete mixture with a w/c ratio of 0.5 and a coarse aggregate with LA abrasion of 16 percent.

One potential application of this model is the determination of the spring stiffness for modeling of the load transfer mechanism of a pavement using the finite element method. By knowing pavement characteristics such as slab thickness and joint/crack width; and also knowing concrete mixture properties such as w/c ratio and coarse aggregate hardness and top size the spring stiffness can be determined directly by entering those inputs in the *AGG* model.

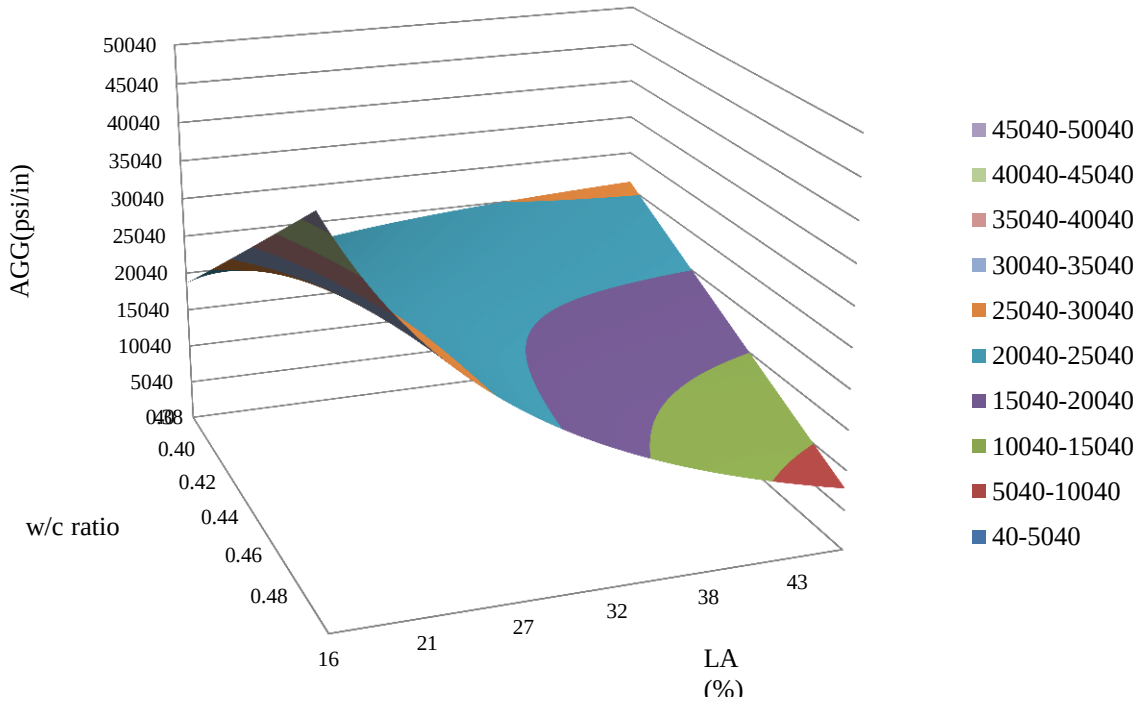

Figure 43. Predicted *AGG* as a function of CA LA abrasion and w/c ratio for CA top size of 1.0 in, a crack width of 0.08 in, a slab thickness of 11 in.

5.3.1.2 Predicted *AGG* as a function of the Coarse Aggregate Top size and w/c ratio for Constant Coarse Aggregate LA Abrasion, Crack Width, and Slab Thickness

Figure 44 presents the predicted *AGG* as a function of the coarse aggregate top size and the w/c ratio of the concrete mixture for a constant coarse aggregate LA abrasion of 20 percent, a crack width of 0.08 in, and a slab thickness of 11in. The predicted *AGG* seen in the surface plot ranges from 20,500 psi to 108,000 psi. The lowest value corresponds to a crack *LTE* of 70 percent for a concrete mixture with a w/c ratio of 0.38 and a coarse aggregate with top size of 0.88 in. The largest *LTE* value corresponds to a crack *LTE* of 98 percent for a concrete mixture with a w/c ratio of 0.38 and a coarse aggregate top size of 2.50 in.

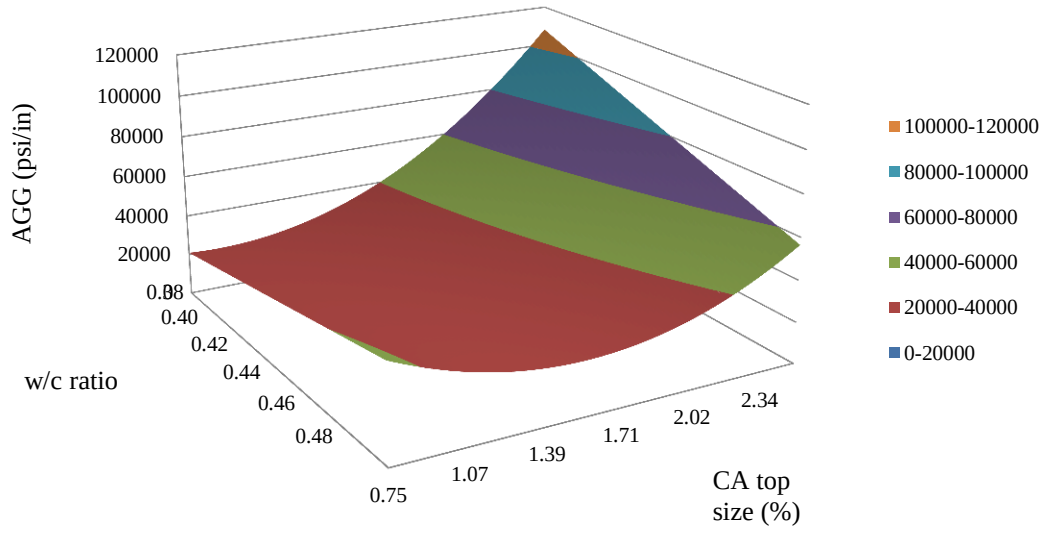

Figure 44. Predicted *AGG* as a function of CA top size and w/c ratio for CA LA abrasion of 20 percent, a crack width of 0.08 in, a slab thickness of 11 in.

5.3.1.3 Predicted *AGG* as a function of the Coarse Aggregate Top size and Coarse Aggregate LA Abrasion for a Constant w/c ratio, Crack Width, and Slab Thickness.

Figure 45 shows the predicted *AGG* as a function of the coarse aggregate top size and the coarse aggregate LA abrasion for a constant w/c ratio of 0.45, a crack width of 0.08 in and, a slab thickness of 11 in. The predicted *AGG* represented by the surface plot ranges from 12,800 psi to 84,000 psi. The lowest value corresponds to a crack *LTE* of 63 percent for a concrete mixture with coarse aggregate LA abrasion of 46 percent and a coarse aggregate top size of 1.25 in. The largest *LTE* value corresponds to a crack *LTE* of 96 percent for a concrete mixture with a coarse aggregate LA abrasion of 16 percent and a coarse aggregate top size of 2.50 in.

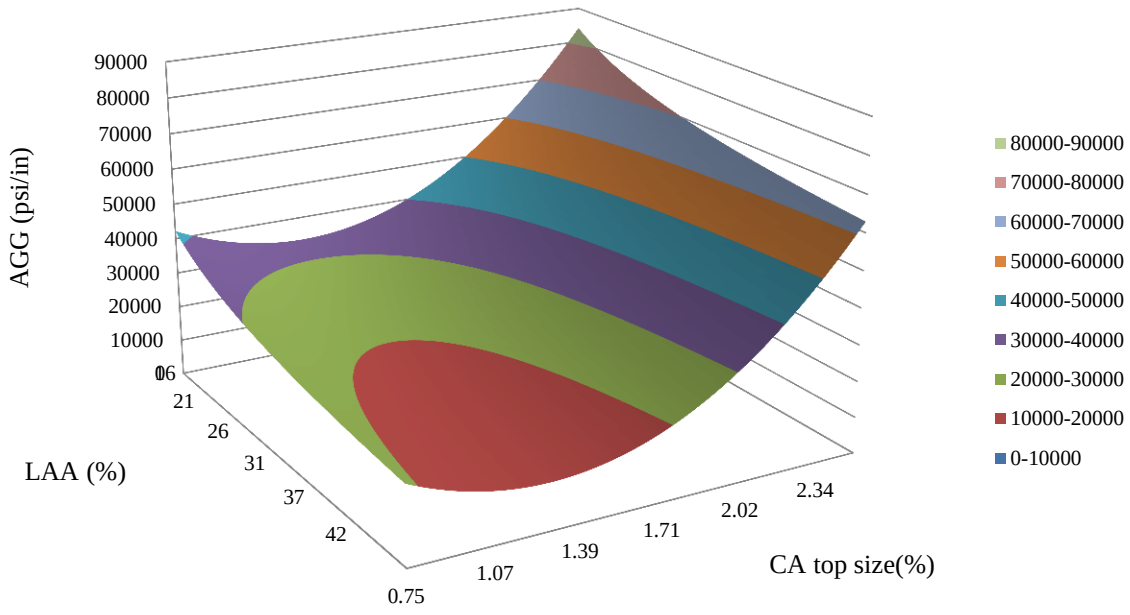

Figure 45. Predicted *AGG* as a function of CA top size and CA LA abrasion for a w/c ratio of 0.48, a crack width of 0.08 in, and a slab thickness of 11 in.

6.0 ANALYSIS OF THE EFFECT OF CRITICAL CONCRETE MIXTURE PROPERTIES ON CONCRETE FRACTURE PARAMETERS FOR THE COMPLETE DATA SET

This chapter discusses the effect of the coarse aggregate hardness and top size as well as the w/c ratio on concrete fracture parameters such as the critical stress intensity factor or fracture toughness(K_{IC}^{S}),the critical tip opening displacement ($CTOD_c$), and the initial fracture energy (G_{IC}). Additionally, the relationship between these fractures parameters and the VSTR is also discussed in this chapter. The data used to establish the mentioned relationships was extracted from the Study No. 3 and fracture energy tests executed as part of the present study. The data is the results of tests executed at two different ages: 1 day and 28 days.

6.1 ANALYSIS OF THE CONCRETE FRACTURE PARAMETERS OBTAINED IN THE PRESENT STUDY AND STUDY NO. 3

As mentioned in Section 3.2.4, the two parameter method (RILEM Comitee on Fracture Mechanics of Concrete-Test Methods, 1990) was used to determine several concrete fracture parameters (i.e. intensity factor or fracture toughness (K_{IC}^{S}), the critical tip opening displacement ($CTOD_c$), and the initial fracture energy) for the 5 concrete mixtures utilized in this study and the

4 concrete mixtures used in Study No.3. This section presents the results of the fracture energy testing executed in the Pavement Mechanics and Materials Laboratory (PMML) of the University of Pittsburgh for the present study and Study No.3.

The results for the concrete mixture containing a maximum aggregate size of 1.25 in (SL_1.25_34_0.4), used in the present study, are not included here because it was determined that due to an error in the dimensions of the specimens for that particular mixture the parameters and fracture properties deviated in comparison with the rest of the mixes. Table 23 presents the results of the fracture energy test executed at day 1 for the five concrete mixtures investigated in the present study. These results correspond to parameters obtained from the plot of *CMOD* vs load such as the maximum load (P_{MAX}), as well as the properties calculated using the equations presented in Section 3.2.4.1 such as, the stress intensity factor or fracture toughness(K_{IC}^{S}),the critical tip opening displacement ($CTOD_c$), the initial fracture energy (G), and the effective critical crack length (a_c). As seen in Table 23and Table 24 the coefficient of variation (COV) is considerably higher for some of the parameters obtained, especially for the $CTOD_c$ and the initial fracture energy (G). This high variability has been reported by several researchers and it is affected by different factors such as the inherent variability in the determination of the loading and unloading compliances from the load vs. *CMOD* plot among others. The load vs *CMOD* plots for all of the specimens are presented in Appendix A.

Table 23. Results for the fracture energy test executed at day 1 for the present study.

Parameter		LS_0.75_17_0.4	SL_0.75_34_0.40	SL_0.75_34_0.45	LS_0.75_17_0.45
P_{MAX}	Average (lbf)	750	741	652	691
	STD (lbf)	95	60	82	78
	COV (%)	13	8	13	11
K_{IC}	Average (psi $in^{0.5}$)	746	823	715	773
	STD (psi $in^{0.5}$)	109	42	99	159
	COV (%)	15	5	14	21
G_{IC}	Average (lb/in)	0.22	0.22	0.17	0.18
	STD (lb/in)	0.11	0.02	0.04	0.07
	COV (%)	48	11	26	37
$CTOD_c$	Average (in)	0.00051	0.00060	0.00047	0.00048
	STD (in)	0.00022	0.00002	0.00008	0.00022
	COV (%)	44	3	17	46
a_c	Average (in)	2.32	2.57	2.69	2.57
	STD (in)	0.18	0.05	0.13	0.34
	COV (%)	8	2	5	13

Table 24 presents the results of the fracture energy test executed at day 28 for the four concrete mixtures containing an aggregate top size of 0.75 in. In addition to the results presented for the 1-daytesting at, the concrete modulus of rupture (MR) measured at 28 days is included in this table. A discussion of the results obtained for the fracture energy testing at days 1 and 28 for the present study and Study No.3 is presented below.

Table 24. Results for the fracture energy and flexural strength tests executed at day 28 for the present study.

Parameter		LS_0.75_17_0.4	SL_0.75_34_0.40	SL_0.75_34_0.45	LS_0.75_17_0.45
MR	Average (psi)	967	834	737	779
	STD (psi)	21	38	13	34
	COV (%)	2	5	2	4
P_{MAX}	Average (lbf)	1131	876	1079	919
	STD(lbf)	83	35	123	73
	COV (%)	7	4	11	8
K_{IC}	Average (psi $in^{0.5}$)	1182	853	1172	966
	STD (psi $in^{0.5}$)	137	62	195	212
	COV (%)	12	7	17	22
G_{IC}	Average (lb/in)	0.36	0.23	0.30	0.27
	STD (lb/in)	0.06	0.01	0.09	0.07
	COV (%)	16	3	30	25
$CTOD_c$	Average (in)	0.00065	0.00049	0.00056	0.00052
	STD (in)	0.00008	0.00004	0.00011	0.00020
	COV (%)	12	7	20	38
a_c	Average (in)	2.54	2.59	2.38	2.48
	STD (in)	0.19	0.15	0.05	0.40
	COV (%)	8	6	2	16

6.1.1 Analysis of the Results of the Maximum Load for the Fracture Energy Test

The average of the maximum loads for each of the four concrete mixtures of this study is presented in Figure 46. As seen in the figure, and as expected, for all of the mixtures there was an increase in the maximum load with respect to the age of the concrete. On average this increase is slightly more than 40 percent, and obviously is related to the development of the strength in the cement paste. For day 1 testing, the maximum load obtained for the mixtures with w/c ratio of 0.4 is slightly higher than that of the mixtures with a w/c ratio of 0.45. However, it can be seen

that the variation in the maximum load between the four mixtures tested at day 1is low (COV 6%) which may imply that at this early age the variation in properties do not significantly affect the fracture behavior of concrete for the range of variables considered. In the case of the maximum load at 28 days, the variation between concrete mixtures is higher than that of 1-day testing (COV 12%), however, there is no common characteristic for the mixtures with a higher maximum load.

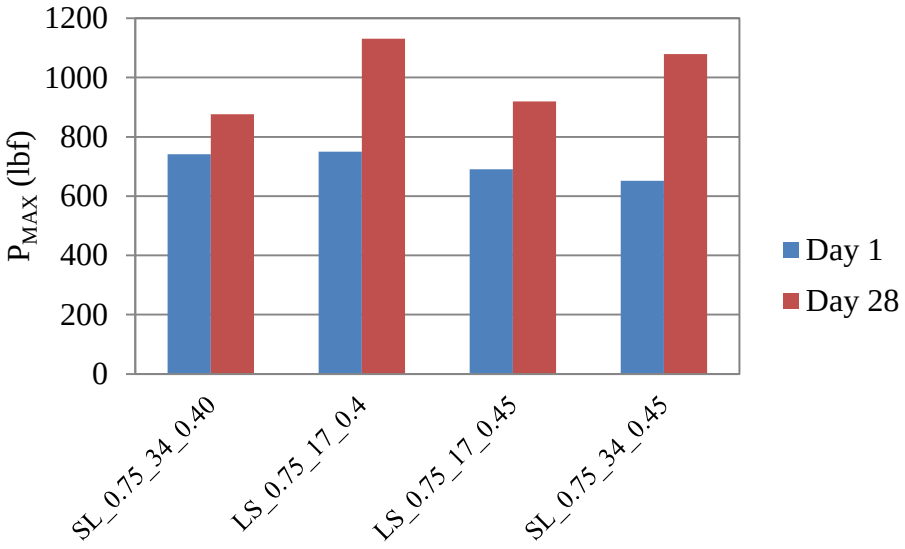

Figure 46. Fracture energy test maximum load for day 1 and day 28.

Comparing the maximum load with the modulus of rupture (see Figure 47) it can be observed that there is no strong relationship between them; the two concrete mixtures with higher values of maximum load present the largest and also the smallest modulus of rupture. Despite the absence of a clear relationship between maximum load and modulus of rupture it is important to note that the modulus of rupture is higher for the mixtures containing the lower w/c ratio (i.e. 0.4) in comparison with mixtures with a w/c ratio of 0.45. Also when comparing the mixtures

with the same w/c ratio, the modulus of rupture is higher for the mixtures containing the stronger coarse aggregate (i.e. limestone).

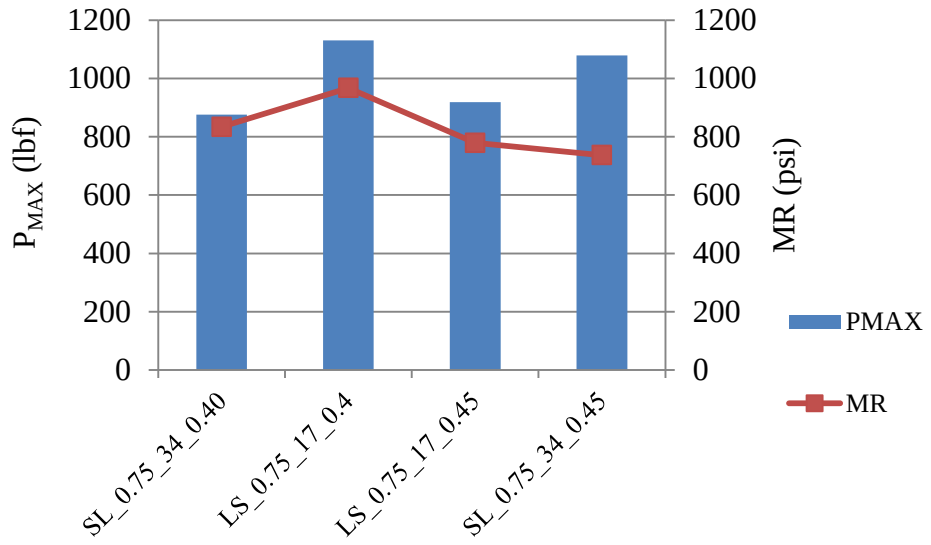

Figure 47. Fracture energy test maximum load and modulus of rupture for 28-day testing.

6.1.2 Analysis of the Results for the Two Parameters: Concrete Fracture Toughness (K_{IC}) and Critical Tip Opening Displacement ($CTDO_c$)

For a quasi-brittle material like concrete, the fracture toughness parameter, K_{IC}, itself is not sufficient to characterize the fracture process of concrete. Several investigators have reported that when fracture toughness is evaluated from notched specimens using conventional LEFM a significant size effect is observed. This size effect has been attributed to nonlinear slow crack growth occurring prior to the peak load. This nonlinear crack growth needs to be included in order to accurately characterize the fracture process. For this reason, and as mentioned in Section 0 , the two parameter model includes the $CTOD_c$ parameter which dictates the critical effective

crack extension. By considering these two parameters, K_{IC} and $CTOD_c$, the critical fracture load and the critical crack length of a structure can be determined. Furthermore, for concrete if only one parameter is considered, then one observes that the fracture toughness increases with increasing compressive strength or increasing strain rate. Such a one-parameter representation is misleading since concrete in fact becomes more brittle as its compressive strength increases. This situation highlights the importance of including the $CTOD_c$ in the characterization of the concrete fracture behavior. The $CTOD_c$ along with critical crack extension decrease with increasing the compressive strength, in fact for an ideally brittle material the critical crack extension is zero.

Figure 48 presents the concrete critical stress intensity factor or fracture toughness for days 1 and 28. This figure includes the results from the present study and the available results from Study No. 3. As observed in the figure, for day 1 testing, the fracture toughness of the concrete mixtures with a lower w/c ratio (< 0.5) exhibit a considerably higher fracture toughness in comparison with the concrete mixtures with a higher w/c ratio (> 0.5) (Study No.3). In the case of the results for the 28 day testing, the higher values do not share a similar property, however, it can be highlighted that the 3 lowest values of fracture toughness correspond to concrete mixtures containing coarse aggregates with lower hardness (i.e. LA > 34%). These observations agrees with the fact that at early ages the crack grows mainly through the ITZ and the matrix, whereas at later ages the crack path depends much more on the interaction of the three concrete components rather than only on the strength of the matrix.

The highest fracture toughness was obtained for the concrete mixture with the largest top size (i.e. 2.5 in). Although the difference is not dramatic, this result agrees with observations made by other researchers as commented in Section 2.3.2.3.

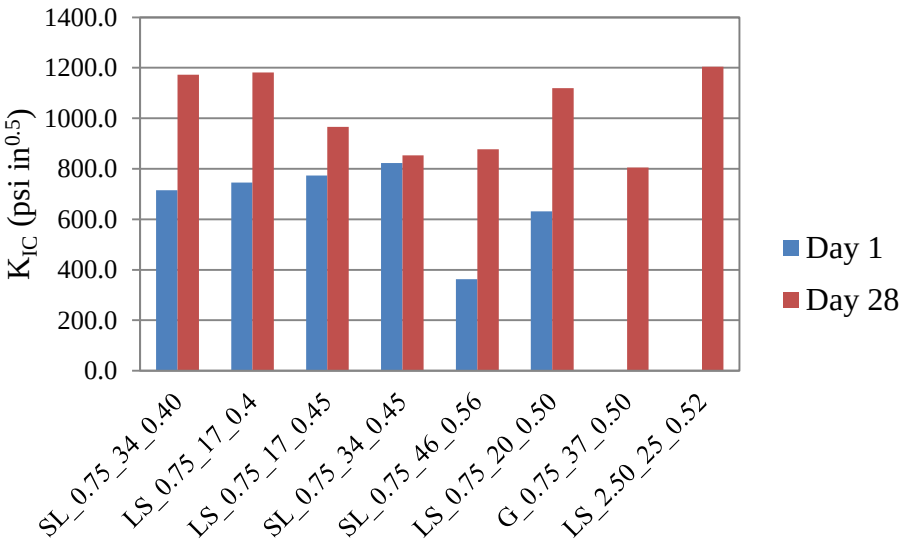

Figure 48. Fracture toughness (K_{IC}) for 1-day and 28-day testing for the present study and Study No.3.

Figure 49 shows the concrete fracture toughness as well as the $CTOD_c$ for the concrete mixtures investigated in the present study and tested at day 1. As the figure shows, the values of $CTOD_c$ follow a similar trend in comparison with the $K_{IC,}$ however, it can be seen that the $CTOD_c$ is almost the same for the three mixtures on the right side of the plot. This might imply that even though the critical failure stress is different for the three mixes, the critical effective crack length, or the crack length where uncontrollable crack dissipation takes place, is similar as well as the brittleness of the three concrete mixtures. According to these results the concrete mixture (SL_0.7_ 34_0.45) exhibits a more ductile behavior in comparison with the rest of the mixtures and a better cracking resistance.

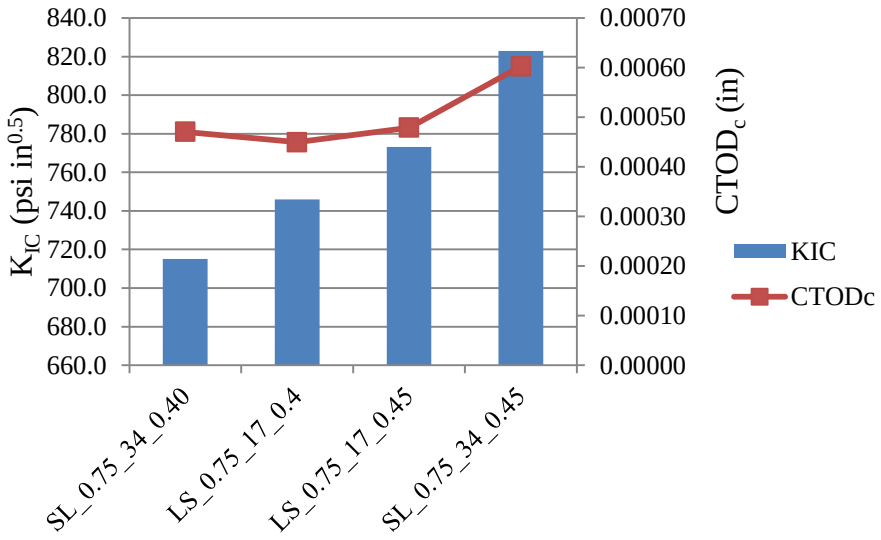

Figure 49. Fracture toughness (K_{IC}) and $CTOD_c$ for 1-day testing for the present study.

Figure 50 presents the concrete fracture toughness as well as the $CTOD_c$ for the concrete mixtures investigated in the present study and tested at day 28. As with the results for the 1 day testing, the values of $CTOD_c$ follow a similar trend in comparison with the K_{IC},. It can be seen in the figure, that for mixtures with the same w/c ratio the $CTOD_c$ is higher for the mixtures containing the hardest aggregate (i.e. limestone). This implies that the for the same w/c ratio the concrete mixtures with slag as aggregate tend to be more brittle in comparison with the concretes using limestone. For the concrete mixtures with w/c of 0.4, the stress for failure is almost the same but the critical crack length for the mixture containing limestone is larger which correspond to a more ductile mixture. For the concrete mixtures containing the same coarse aggregate it can be observed that the higher fracture toughness as well as the larger critical crack length is given by the mixtures with a higher w/c ratio. It can be concluded that, for the concrete mixtures considered, the cracking resistance is more sensitive to the matrix strength than it is the coarse aggregate hardness.

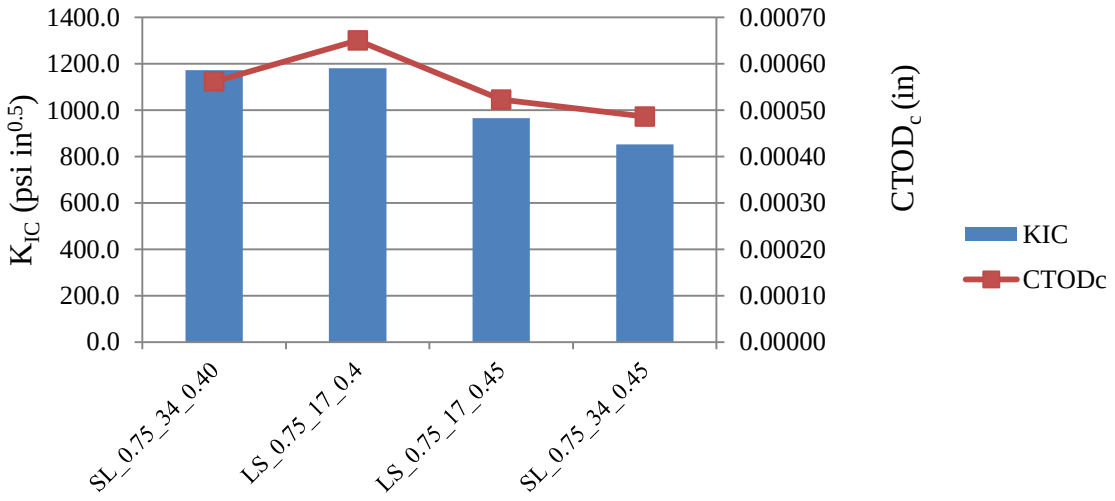

Figure 50. Fracture toughness (K_{IC}) and $CTOD_c$ for 28-day testing for the present study.

6.1.2.1 Relationship between Concrete Fracture Toughness (K_{IC}) and Critical Tip Opening Displacement ($CTDO_c$) with Concrete Mixture Properties and VSTR

This section presents the relationship between K_{IC} and $CTDO_c$ with the key concrete mixtures properties investigated as well as the relationship with the VSTR. These relationships are obtained for the results of K_{IC} and $CTDO_c$ corresponding to day 1 and day 28 testing. As presented in Figure 48, for day1 there are 6 available data points whereas for day 28 there are 8 available data points. Since only one data point represents coarse aggregate top size of 2.5 in (i.e. LS_2.50_25_0.52 concrete mixture Study No.3), the analysis did not include the aggregate top size as a variable and this data point was not considered in the regression for the rest of the variables. Consequently, for the 1-day results 6 data points were considered, whereas for the 28-day results 7 data points were considered.

A regression analysis was executed to determine the numerical relationship between the concrete properties investigated and the fracture toughness. For the early age cracking (i.e. day 1) it was found that the LA abrasion does not significantly impact the response. This was established by a high p-value for the LA term in the regression (i.e. 0.5) and the fact that excluding the LA abrasion from the terms in the regression increased the adjusted R^2 from 94 percent to 95 percent. This negligible contribution of the LA abrasion to the relationship between the concrete properties and the fracture toughness might be related to the variability inherent with the method used for characterizing aggregate strength that. Consequently, a regression was performed with the fracture toughness as the response and the w/c ratio as the only predictor. The obtained equation relating the fracture toughness to the w/c ratio for early age (i.e.1 day) cracking is as follows:

$$K_{IC} = -28964 \cdot w\_c^2 + 25393 \cdot w\_c - 4784.8 \quad (6\text{-}1)$$

where K_{IC} is the fracture toughness expressed in psi* $in^{0.5}$ and w_c is the w/c ratio. This equation exhibits an R^2 of 97 percent, an adjusted R^2 of 95 percent, and a p-value for the quadratic and linear terms of 0.014 and 0.017, respectively. Figure 51 shows the plot of the mentioned relationship. As seen in the figure, for the mixtures with w/c ratio higher than 0.45, the fracture toughness increases as the strength of the matrix increases. This result agrees with results from Jenq and Shah (Jenq & Shah, 1985) who found that the fracture toughness increases with increasing the concrete compressive strength or increasing strain rate. However, as seen in Figure 51, for concrete mixtures with a w/c ratio lower than 0.45 the fracture toughness decreases with a decrease in the strength of the matrix. This particular trend might be the result of the high variation in the fracture energy test itself and should be validated with more experimental results.

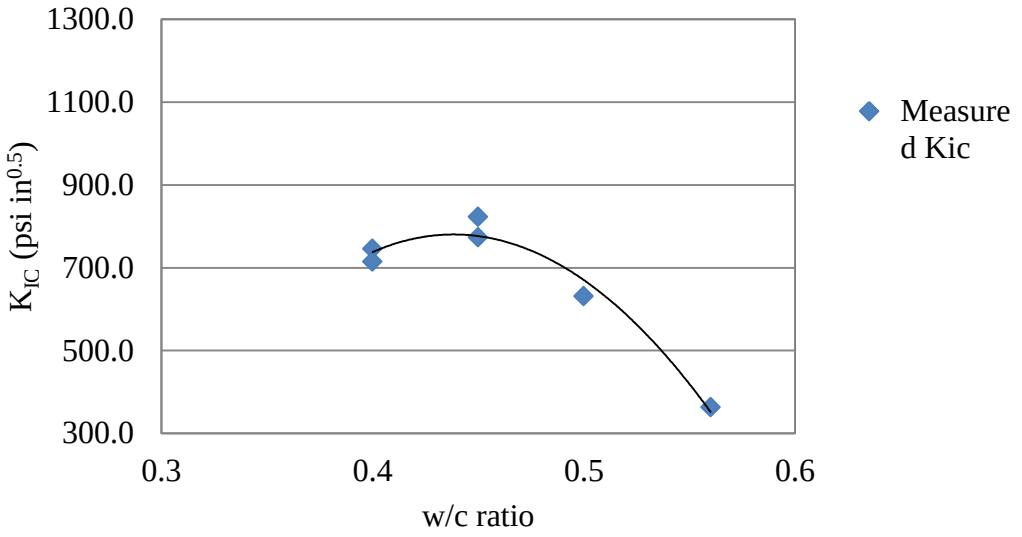

Figure 51. Relationship between fracture toughness *(K_{IC})* and concrete w/c ratio for 1-day testing.

Figure 52 presents the relationship between the concrete fracture toughness and the w/c ratio for the testing executed at 28 days. Similar to the relationship for the day-1 testing, the LA abrasion was not included in this relationship due to the negligible impact it had on the response. As a result, a regression was carried out with fracture toughness as the response and w/c ratio as an isolated predictor. The linear equation obtained from the regression model is as follows:

$$K_{IC} = -1280.9 \cdot w\_c + 1637.5 \qquad (6\text{-}2)$$

Unlike the equation describing the relationship between fracture toughness and w/c ratio for early age cracking, the equation for the 28-day testing exhibited a poor coefficient of determination R^2 (i.e. 25 percent). Additionally, the p-value of the linear term is considerably above the cutoff value of 0.05 (i.e. 0.2). As seen in the figure the scattering of the data points is significant, however, the general trend agrees with the fact that the fracture toughness is directly related to the strength of the matrix. The higher dispersion of the data for the 28-day testing in

comparison to that of the 1-day testing, and the fact that the average variation for the results of both days was the same (i.e. COV 15percent), supports the idea that at early ages the crack grows mainly through the ITZ and the matrix, whereas at later ages the crack path depends much more on the interaction of the three concrete components rather than only on the strength of the matrix.

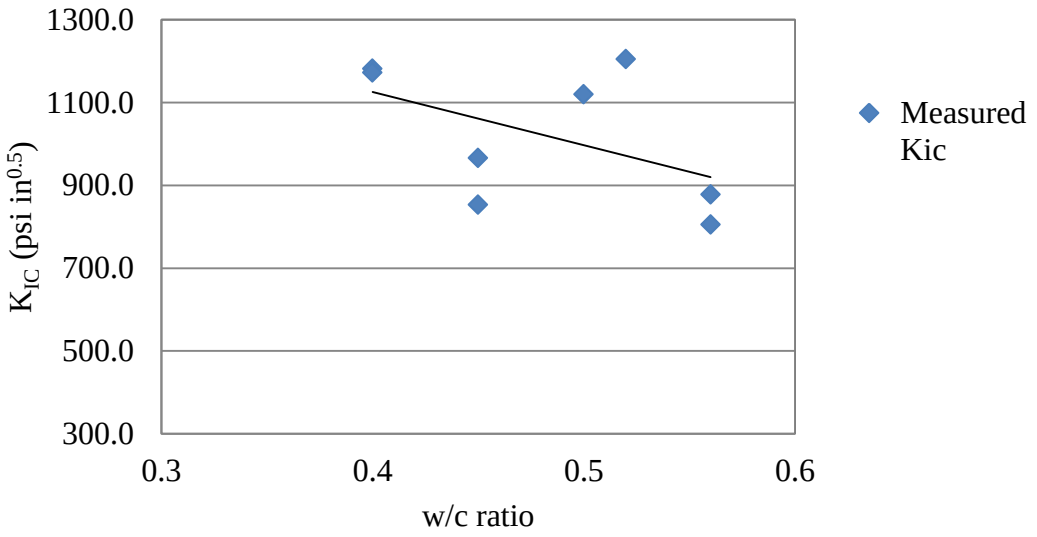

Figure 52. Relationship between fracture toughness *(K_{IC})* and concrete w/c ratio for the 28-day testing.

A relationship between the critical crack tip opening displacement *($CTOD_C$)* and the concrete properties was also investigated. Similar to the fracture toughness, the LA abrasion was not included in the final regression equation due to the same statistical considerations already discussed. The *$CTOD_C$* results were not available for Study No.3 , therefore, only four data points were included in the relationship between *$CTOD_C$* and w/c ratio. As a result of the regression, the following linear equation was obtained to relate the mentioned variables for the results of the fracture energy test executed at day 1:

$$CTOD_C = 0.0016 \cdot w\_c - 0.0002 \quad (6\text{-}3)$$

where $CTOD_C$ is the critical crack tip opening displacement expressed in inches, and w_c is the w/c ratio. This linear equation exhibits a poor fit to the measured data as the obtained R^2 was45 percent, and a p-value for the significance of the regression was 0.33. This poor approximation is derived from the small amount of data points as well as the high variation in the results for the $CTOD_C$ (i.e. average COV of 29 percent). This variation was not a surprise considering the small magnitude of the $CTOD_C$ and the variation reported by other researchers. Despite the small quantity of data points, it can be noticed (see Figure 53) a general trend where increasing the w/c ratio results in a higher $CTOD_C$. This trend agrees with the idea that the critical crack length for an ideally brittle material is zero and increases as the ductility augments.

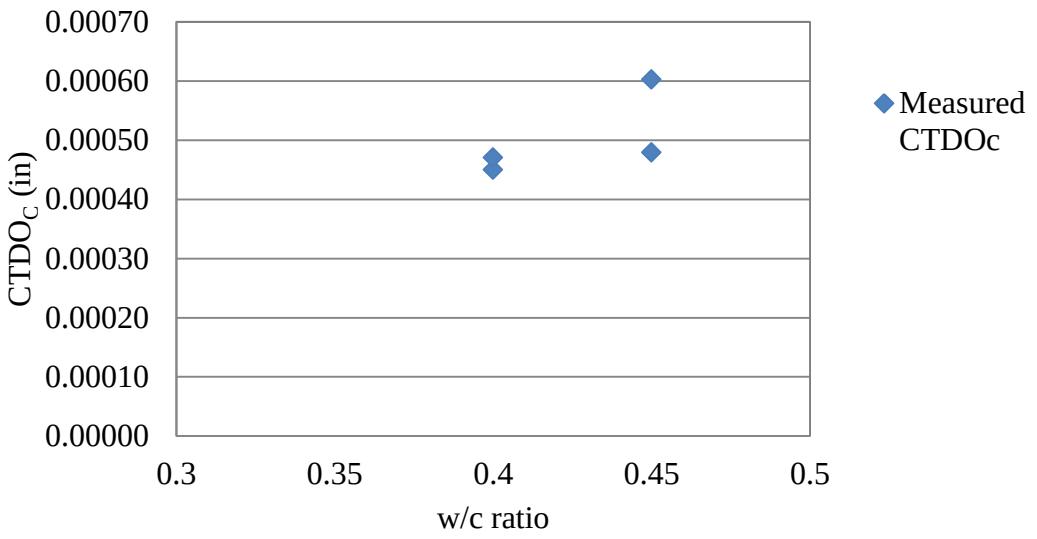

Figure 53. Relationship between the $CTOD_C$ and concrete w/c ratio for the 1-day testing.

Figure 54 presents the relationship between $CTOD_C$ and w/c ratio for the results of the fracture energy test executed at 28 days. The regression equation obtained for the measured data is as follows:

$$CTOD_C = -0.002 \cdot w\_c + 0.0014 \quad (6\text{-}4)$$

This regression equation has an R^2 of 69 percent, and adjusted R^2 of 54 percent and a p-value of the regression of 0.169. Although the linear equation for the 28-day results approximates the measured data better than the regression for the results of the 1-day testing, the trend observed in Figure 54 does not agree with the theory and the observations made by other researchers where the critical crack length decreases as the material tends to be more brittle. This result might be affected by the small quantity of data points and the variability of the results (i.e. average COV 20%).

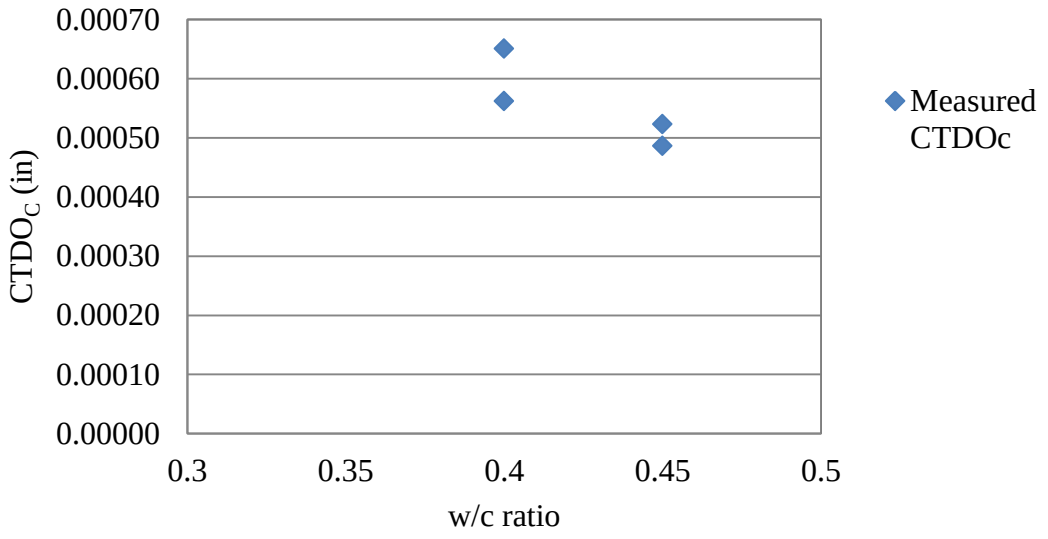

Figure 54. Relationship between the $CTOD_C$ and concrete w/c ratio for the 28-day testing.

The relationship between the concrete fracture parameters and the roughness of the crack face quantified by the VSTR was also investigated. As observed in Figure 55, the eight data points included in the complete data set are well dispersed and do not follow an apparent trend and a regression including the totality of the points does not contribute in understanding the relationship between these two factors. Therefore, the data was separated in two groups depending on the w/c ratio (i.e. w/c> 05 and w/c<0.5). As Figure 55 shows, the data points for the concrete mixtures with w/c ratio greater than 0.5 exhibit a trend that implies a direct relationship between VSTR and fracture toughness. As the fracture toughness increases the roughness of the crack face increases. The linear regression equation describing this relationship is as follows:

$$VSTR = 0.0003 \cdot K_{IC} - 0.1293 \qquad (6\text{-}5)$$

where *VSTR* is the volumetric surface texture ratio expressed in in^3/in^2 and K_{IC} is the concrete fracture toughness expressed in psi $in^{0.5}$. This regression equation has an R^2 of 62 percent, and adjusted R^2 of 43 percent and a p-value of the regression of 0.21. The data points for the concrete mixtures with w/c lower than 0.5 do not follow any trend at all. This condition may be caused by the fact that the cross sectional area of the fracture energy specimens was not sufficiently large for the VSTR test to capture a representative area of the cracked face. The total cross sectional area of the fracture energy specimens used was 3 in by 6 in.

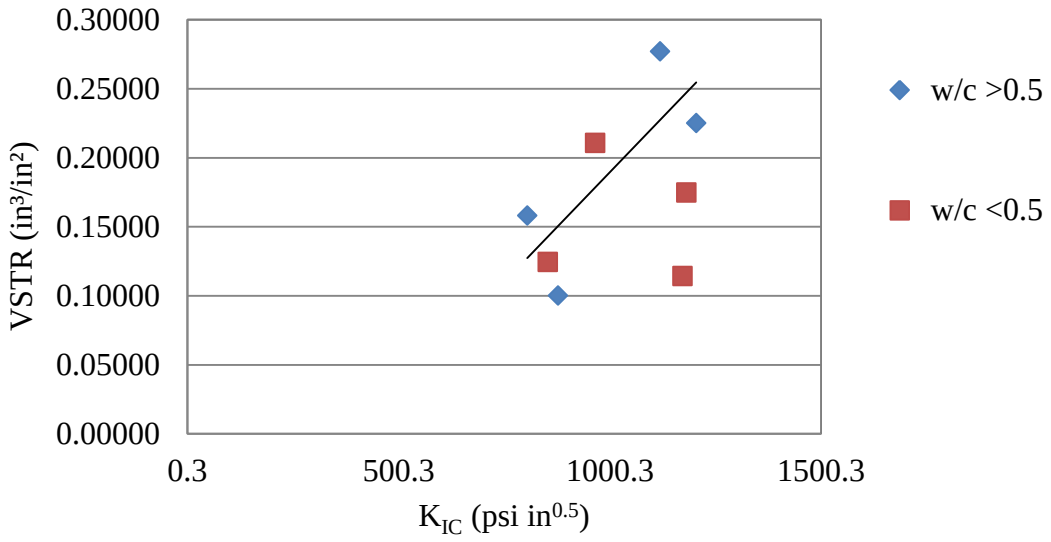

Figure 55. Relationship between the K_{IC} and the VSTR for the 28-day testing.

Figure 56 presents the relationship between the $CTOD_C$ and the *VSTR* for the tests executed at day 28. As observed in the figure only four points are included due to the absence of data for this parameter from the Study No.3. It can be seen in the figure that the data points are so scattered that it is not possible to establish a trend to describe the relationship between $CTOD_C$ and the *VSTR*. This might be caused by the small quantity of data points, the high variation in the $CTOD_C$ and the small cross sectional area of the specimens where the VSTR was quantified.

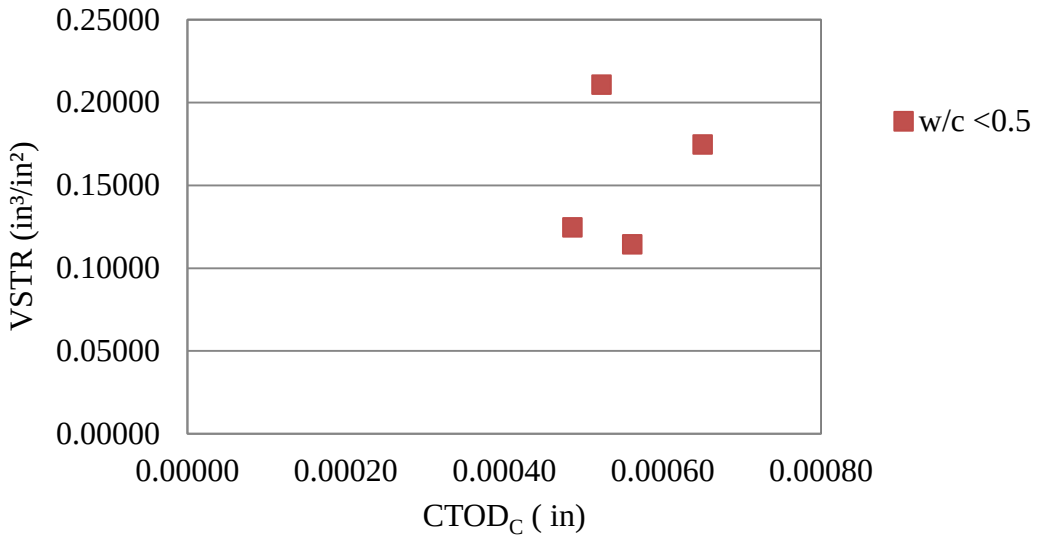

Figure 56. Relationship between the *CTOD*$_C$ and the VSTR for the 28-day testing.

6.1.3 Analysis of the Results for the Initial Fracture Energy

The initial fracture energy, also called the strain energy release rate, represents the amount of energy required for propagation of a unit area of the crack surface. Figure 57 shows the average of the initial fracture energy (G_{IC}) for the tests executed at the present study and Study No.3. As seen in the figure the data for 1-day testing of the mixtures G_0.75_37_0.50 and LS_2.50_25_0.52 is not presented due to the unavailability of it. In comparing Figure 57 and Figure 50 it can be seen that the fracture energy and the fracture toughness follow the same trend with respect to the properties of the concrete mixtures investigated. This condition is established by the definition of the fracture energy (see Equation (3-13)) where the fracture energy is obtained by dividing the square of the fracture toughness into the concrete elastic modulus.

It can be observed in Figure 57 that for 1-day testing the fracture energy of the concrete mixtures with w/c ratio lower than 0.5 is considerably higher than that of the mixtures with w/c

ratio higher than 0.5. The 1-day average fracture energy for the four mixtures with a lower w/c ratio is 0.197 lb/in whereas this value for the mixtures with w/c ratio higher than 0.5 is 0.09 lb/in. As mentioned in the previous section, this might be related to the fact that for early age cracking the crack propagates through the ITZ and matrix rather than through the aggregate. In the case of the fracture energy results for the 28-day testing, it can be seen that the difference in the magnitude of the energy for the mixes with a w/c ratio higher and lower than 0.5 is considerably small. The average of the 28-day fracture energy for the mixtures with w/c ratio lower than 0.5 is 0.289 lb/in whereas this average for the mixtures with w/c ratio higher than 0.5 is 0.27 lb/in. This small difference, as mentioned in the analysis of the fracture toughness, might be caused by the combined effect of all of the concrete components on the development of the crack.

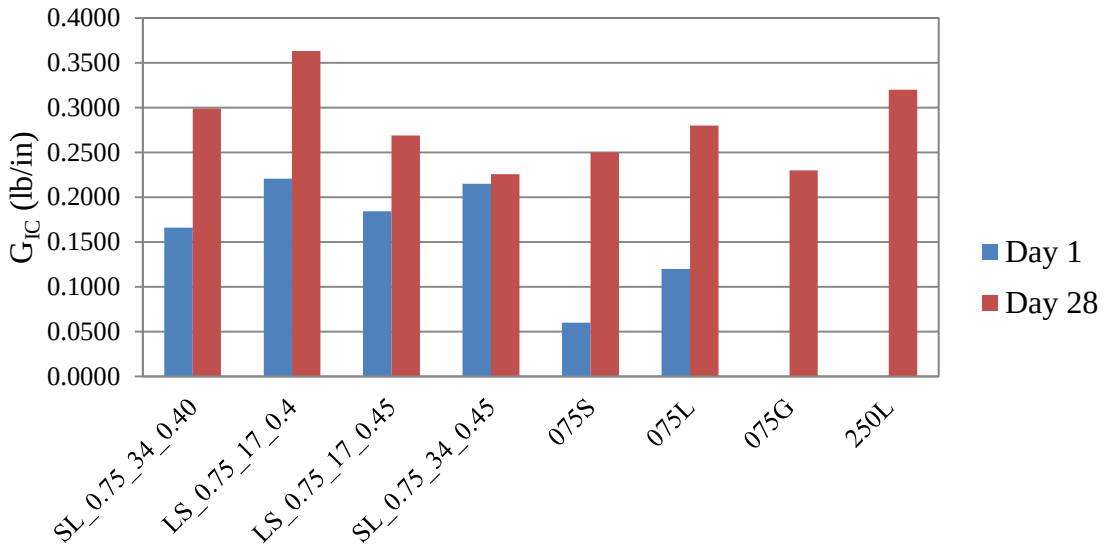

Figure 57. Initial fracture energy *(G_{IC})* results for 1-day and 28-day testing for the present study and Study No.3.

6.1.3.1 Relationship between Initial Fracture Energy (G_{IC}) with Concrete Mixture Properties and VSTR

The relationship between the initial fracture energy and the key concrete properties studied was investigated along with the relationship between fracture energy and the VSTR. The regression performed to fit the G_{IC} experimental data with the critical concrete properties yielded the same result discussed in the previous section in regards to the contribution of the variable LA abrasion to the regression equation. In this particular case for fracture energy, removing the LA abrasion term from the regression equation increased the adjusted R^2 from 61 percent to 68 percent, for the 1-day results and from 14percent to 20 percent in the case of the 28-day results. Additionally, removing the LA abrasion variable form the regression resulted in an improvement of the p-value of the regression from 0.248 to 0.19. Therefore, only the w/c ratio variable was utilized to describe the behavior of the initial fracture energy with respect to concrete properties.

Figure 58 shows the relationship between initial fracture energy and w/c ratio for the results obtained for 1-day testing. As seen in the figure, the general trend suggests an indirect relationship between initial fracture energy and the w/c ratio. As the w/c ratio decreases the initial fracture energy increases. This trend agrees with the theory in that the energy required for propagation of a unit area of crack surface increases with the strength of the material. The linear regression equation relating fracture energy and w/c ratio is as follows:

$$G_{IC} = -0.863 \cdot w\_c + 0.558 \quad \text{(6-6)}$$

where G_{IC} is the initial fracture energy expressed in lb/in and w_c is the w/c ratio.

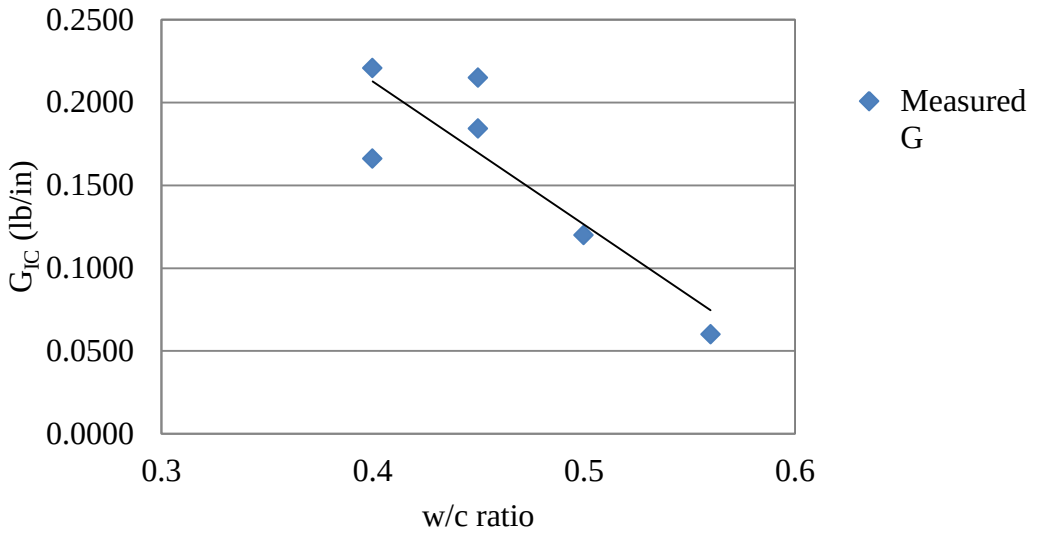

Figure 58. Relationship between the G_{IC} and the w/c ratio for the 1-day testing.

Figure 59 presents the relationship between the fracture energy and the w/c ratio for the results obtained at 28-day testing. As seen in the figure, the trend described by the data points follow the same orientation presented in Figure 58 for the data points of day-1 testing. However, and considering the slope of the regression line, the effect of the w/c ratio on the response is not as pronounced as it is for the results of early age cracks presented in Figure 58. This can be caused by the role that the interaction of all of the concrete components plays in the development of cracks for more mature concrete. The regression equation describing the relationship between initial fracture energy and w/c ratio is as follows:

$$G_{IC} = -0.3727 \cdot w\_c + 0.4584 \qquad (6\text{-}7)$$

This regression equation presents a poor coefficient of determination R^2 (i.e. 27 percent). This can be the result of the high variation in the results for the initial fracture energy (i.e. COV 20 percent).

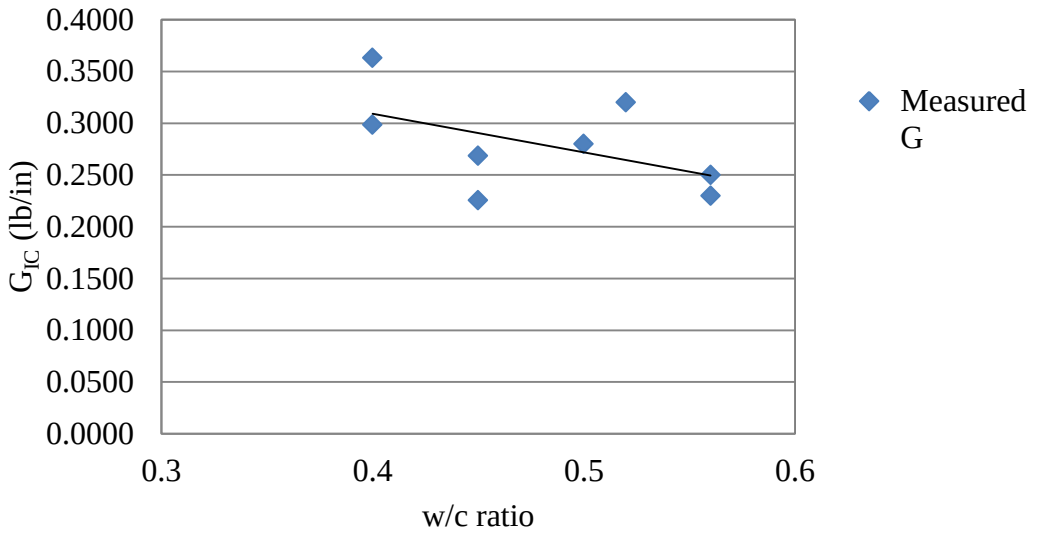

Figure 59. Relationship between the G_{IC} and the w/c ratio for the 28-day testing.

Figure 60 presents the relationship between the initial fracture energy and the VSTR for the 28-day results. Similar to the observation made for the fracture toughness, the dispersion of the data makes it necessary to separate the data in two groups as a function of the w/c ratio (i.e. w/c> 05 and w/c<0.5) in order to recognize a trend. The linear regression describing the relationship between these two variables for the data set with a w/c ratio higher than 0.5 is as follows:

$$VSTR = 1.2391 \cdot G_{IC} - 0.1446 \qquad (6\text{-}8)$$

where *VSTR* is the volumetric surface texture ratio expressed in in^3/in^2 and G_{IC} is the initial fracture energy expressed in lb/in. This regression equation exhibits a coefficient of determination, R^2, of 39 percent.

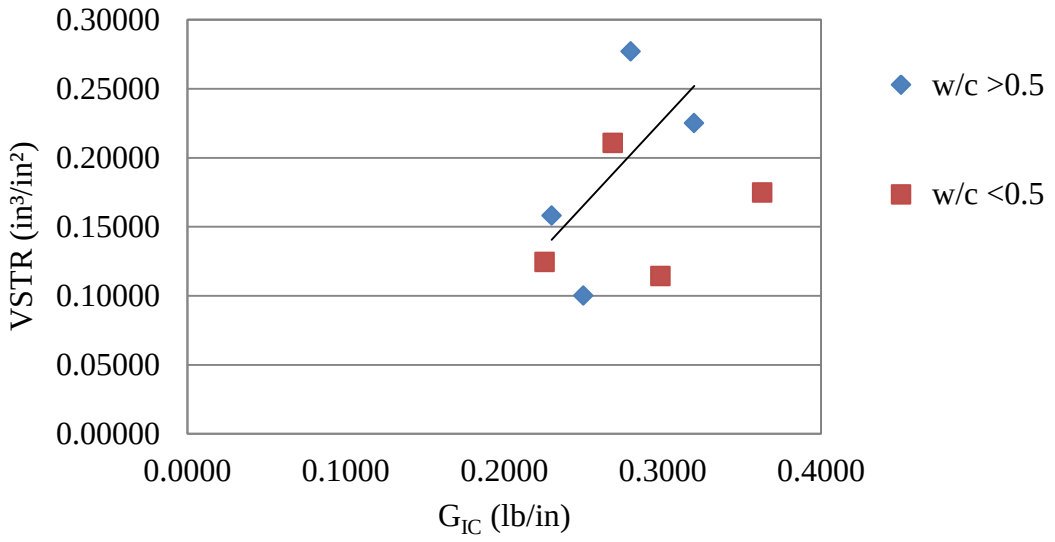

Figure 60. Relationship between the G_{IC} and VSTR for the 28-day testing.

7.0 CONCLUSIONS AND RECOMMENDATIONS

The surface texture of cracked specimens (i.e. 28-day flexural beams) with different concrete mixtures were measured using the VST method. The results of this laboratory experiment were combined with laboratory and field data from previous studies to develop an empirical model that relates key concrete mixture properties (i.e. water–to-cement ratio and coarse aggregate type, top size, and hardness) with the load transfer efficiency, *LTE*, of joints and cracks and the spring stiffness of the joint, *AGG*, for a concrete pavement systems. In addition, concrete fracture parameters for different concrete mixtures and their relationship with the key concrete properties were investigated. The results of this study provide a better understanding of the effects of the critical concrete properties on the aggregate interlock behavior of joints and cracks for concrete pavements. The following section presents a summary of the conclusions derived from this study. Furthermore, recommendations for future research will be presented in the subsequent section.

7.1 CONCLUSIONS

The main conclusions reached as a result of this study and are presented as follows:

1. The VST method has the potential to accurately capture the surface texture of cracked concrete specimens. This method makes it possible to identify and compare important

features of crack propagation for concrete mixtures with different constituent properties or different cracking times (Section 4.2).

2. The surface texture is affected by key concrete properties such as water–to-cement ratio and coarse aggregate type, top size, and hardness. This texture is sensitive not only to the isolated effect of each of the concrete constituents but to the combined interaction between them (Section 4.2).
3. An empirical model that relates water–to-cement ratio, coarse aggregate top size, and hardness with VSTR was developed. This model can be used to predict VSTR without having to cast and test specimens for each mixture (Section 5.1).
4. The relationship between aggregate top size and the predicted surface texture is direct. Increasing the aggregate top size results in a higher surface texture (Section 5.1.1).
5. The effect of varying the matrix strength on the surface texture depends on the aggregate hardness. For concrete mixtures with strong aggregates increasing the matrix strength (i.e. decreasing the w/c ratio) results in a lower predicted surface texture. In the case of concrete mixtures with weak aggregates, increasing the matrix strength results in a higher predicted surface texture. This variation appears to be controlled by the strength/stiffness ratio between the aggregates and the matrix (Section 5.1.1.1).
6. The variation in the predicted surface texture as a result of varying the aggregate hardness depends on the strength/stiffness ratio between the aggregates and the matrix. The relationship between surface texture and aggregate hardness can be direct or indirect depending on the mentioned ratio. The surface texture for concrete mixtures with a low-strength matrix is more sensitive to variations in the aggregate hardness than concrete mixtures with a high-strength matrix (Section 5.1.1.1).

7. The effect of varying the matrix strength is more pronounced for concrete mixtures with larger aggregates than it is for concrete mixtures with smaller aggregates (Section 5.1.1.2).
8. Based on a previously developed model that relates *LTE* with VST, a model that predicts *LTE* based on the critical concrete properties investigated in this study (i.e. water–to-cement ratio, coarse aggregate top size, and hardness) was developed. This *LTE* model can be used to predict load transfer based on the key concrete properties and an estimated or calculated crack width and slab thickness. Additionally, this model can be useful in the selection of concrete mixture properties based on performance requirements (Section 5.2).
9. The predicted *LTE*, using the proposed *LTE* model, exhibited a good correlation with results from a large-scale laboratory study for two concrete mixtures with different properties (Section 5.2.1.4).
10. Based on a previously developed model that relates surface texture with the spring joint stiffness parameter *AGG*, a model that predicts the joint spring stiffness *AGG* based on the key concrete properties (i.e. water–to-cement ratio, coarse aggregate top size, and hardness) was developed. This *AGG* model can be used to predict load transfer based on the key concrete properties, and on estimated or calculated pavement properties such as slab thickness and crack width. (Section 5.3)
11. Concrete mixtures with larger aggregates exhibit a higher fracture toughness, K_{IC}, than mixtures with smaller aggregate particles. This behavior is related to the tendency of these mixtures toward crack bridging and the greater path length as the crack propagates around the aggregate particles (Section 6.1.2).

12. Concrete mixtures with weak aggregates exhibit lower fracture toughness, K_{IC}, in comparison with concretes using stronger aggregates (Section 6.1.2).
13. The matrix strength has a significant effect on the concrete fracture toughness, K_{IC}, as evidenced in the remarkable difference between the results obtained from days 1 and 28. (Section 6.1.2).
14. For concrete mixtures with the same w/c ratio, the $CTOD_c$ is higher for the mixtures containing the hardest aggregate.

7.2 RECOMMENDATIONS

The following recommendations for future work focus on understanding the effect of concrete constituents on the aggregate interlock mechanism were made:

1. The VSTR model should be validated with additional laboratory and field data that include combinations of concrete constituent properties not included in the development of the model.
2. Further work is needed to study the effect of aggregate surface texture and angularity on the surface texture.
3. The *AGG* model can be incorporated into the MEPDG faulting model to predict the aggregate interlock *LTE* based on concrete mixture properties and pavement characteristics.

4. The results of the concrete fracture parameters obtained for this study can be used in future research projects to establish the effects of these parameters on the aggregate interlock mechanism.

APPENDIX A

COARSE AGGREGATE GRADATION CURVES

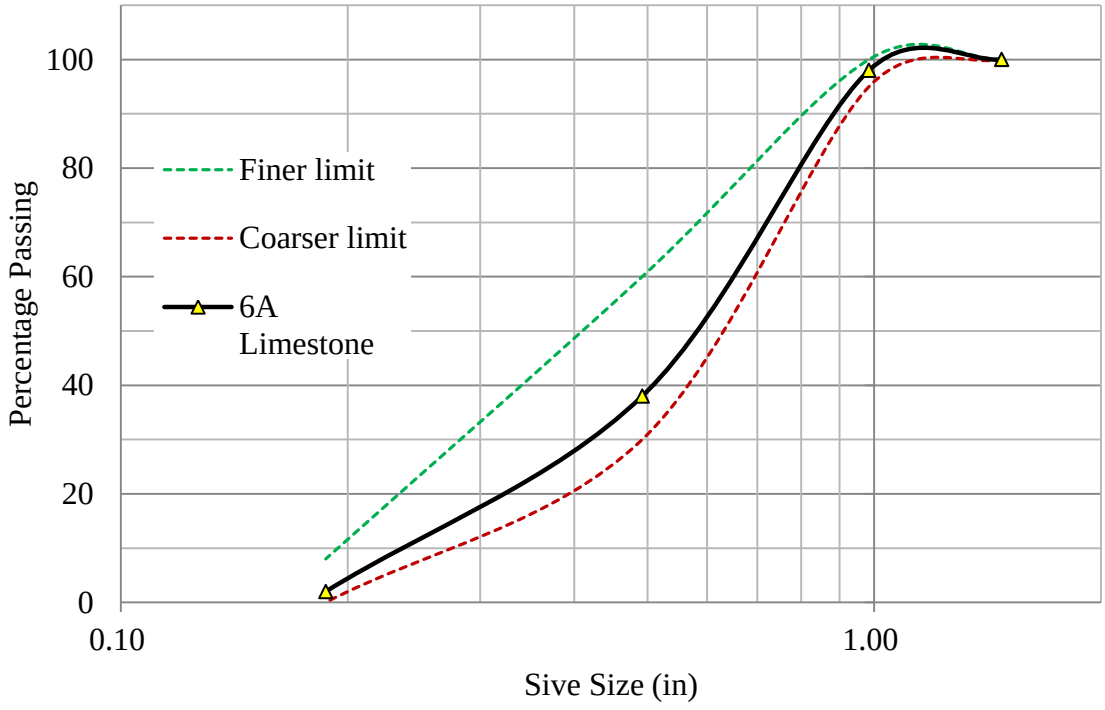

Figure A 1. Gradation curve for coarse aggregate 6A limestone used for Study No.1.

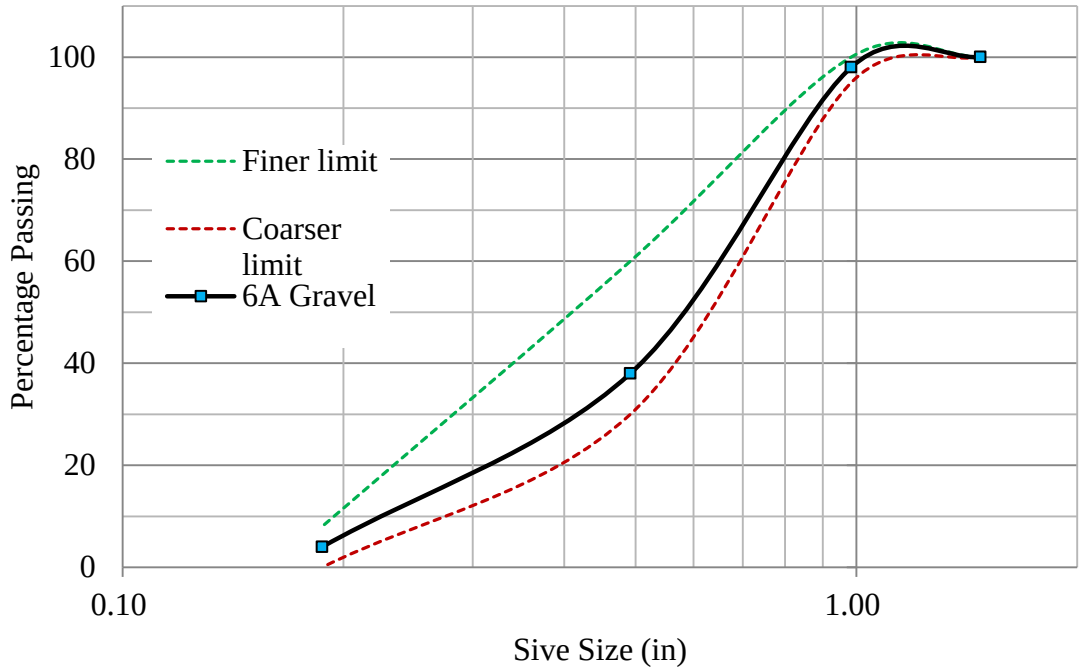

Figure A 2. Gradation curve for coarse aggregate 6A gravel used for Study No.1.

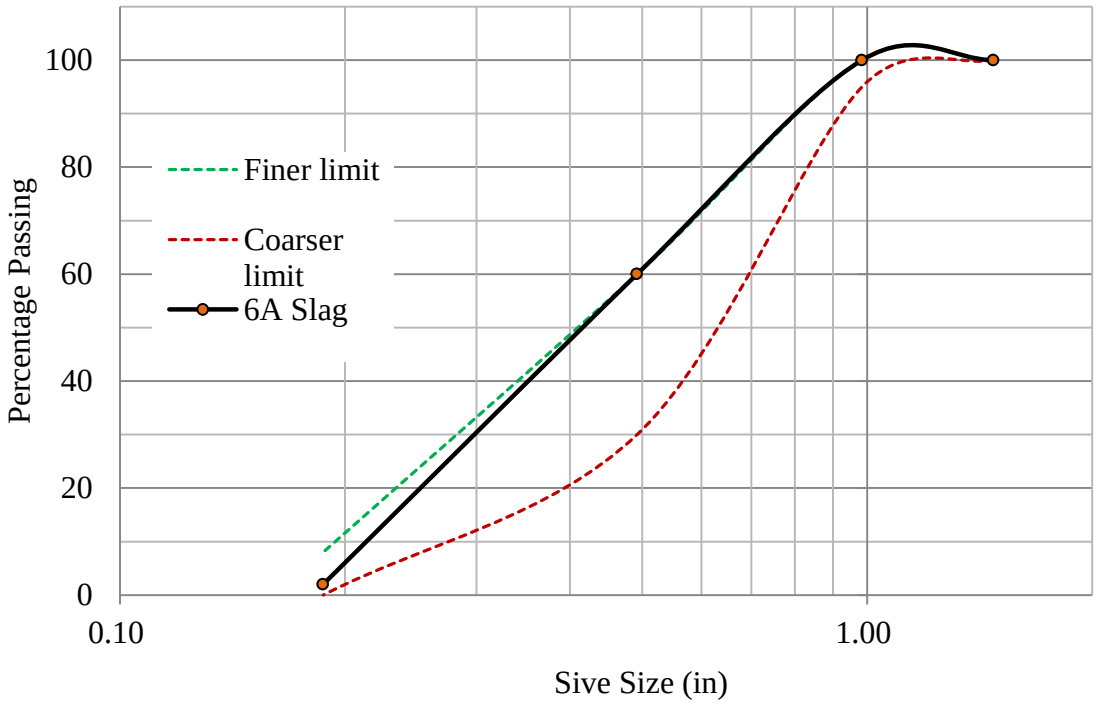

Figure A 3. Gradation curve for coarse aggregate 6A slag used for Study No.1.

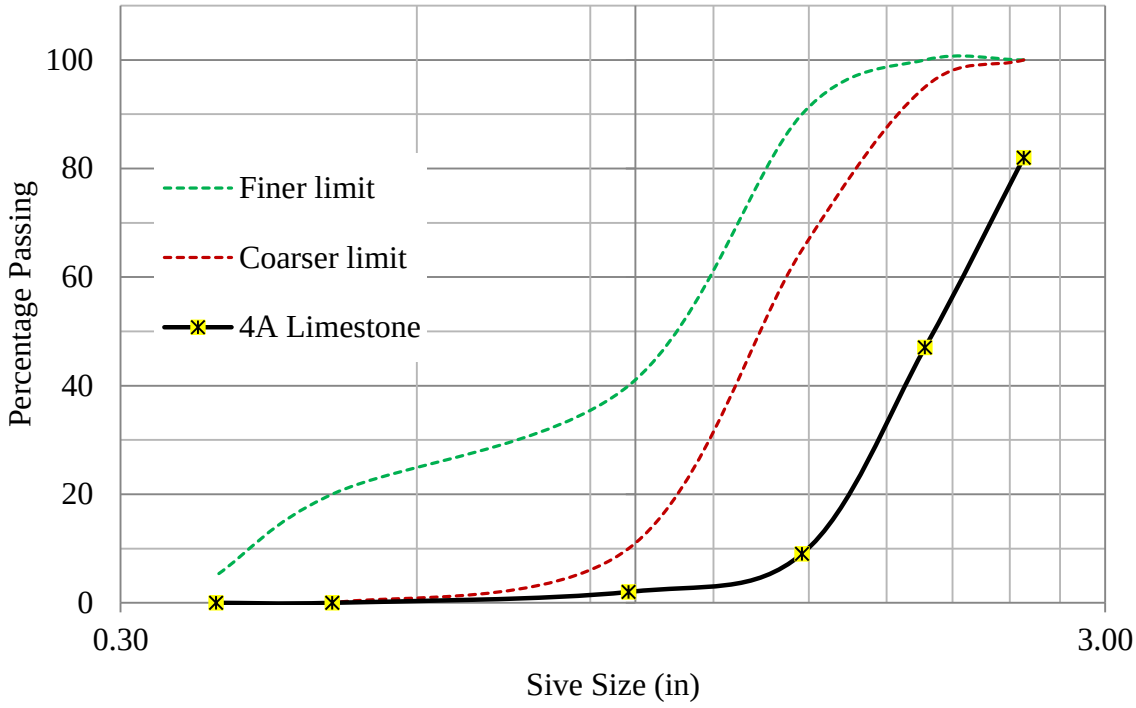

Figure A 4. Gradation curve for coarse aggregate 4A limestone used for Study No.1.

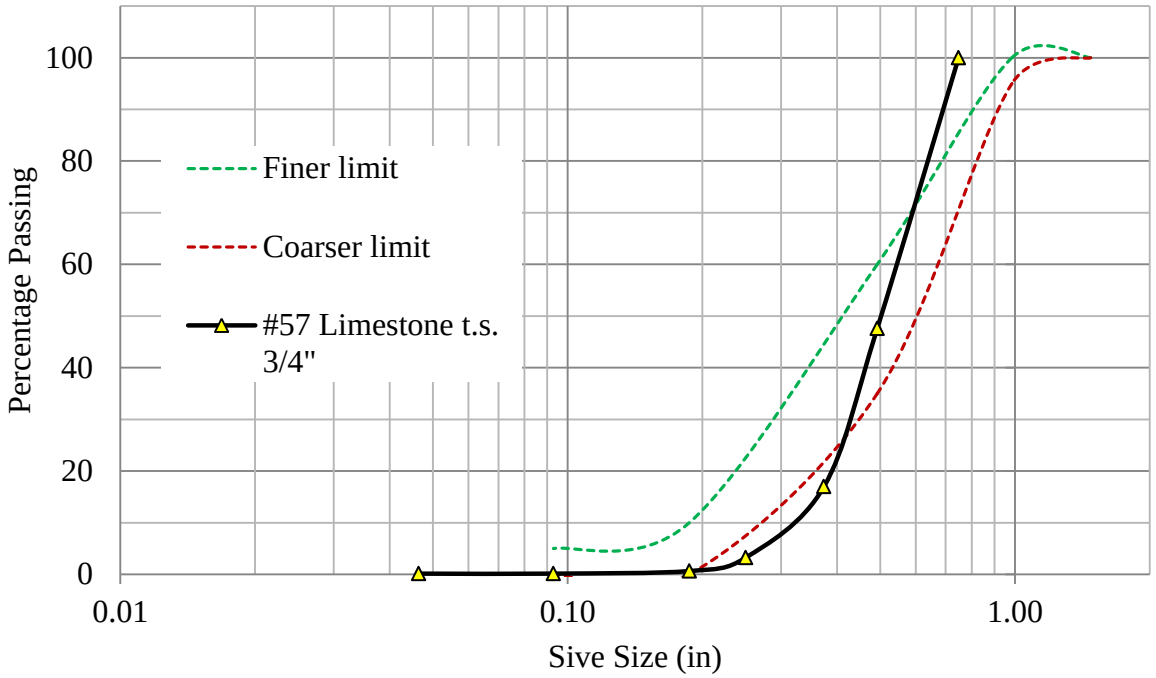

Figure A 5. Gradation curve for coarse aggregate #57 top size 3 /4 in limestone used for the present study.

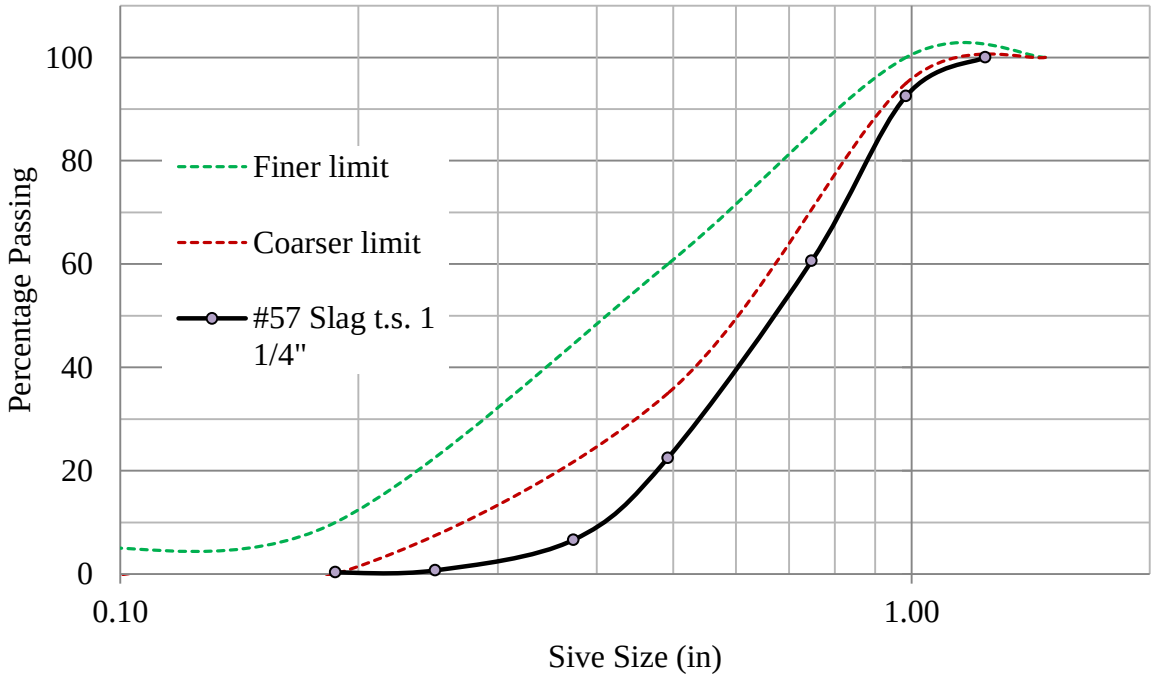

Figure A 6. Gradation curve for coarse aggregate #57 top size 1 1/4 in slag used for the present study.

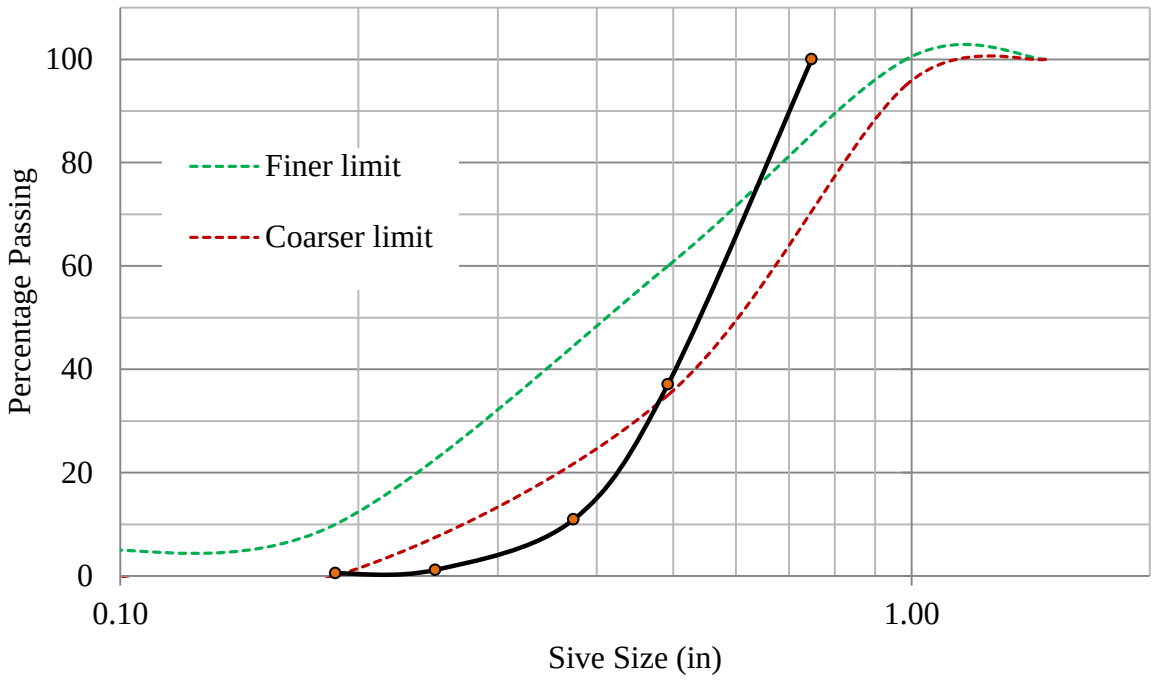

Figure A 7. Gradation curve for coarse aggregate #57 top size 3/4 in slag used for the present study.

APPENDIX B

FRACTURE ENERGY TEST LOAD VS *CMOD* PLOTS

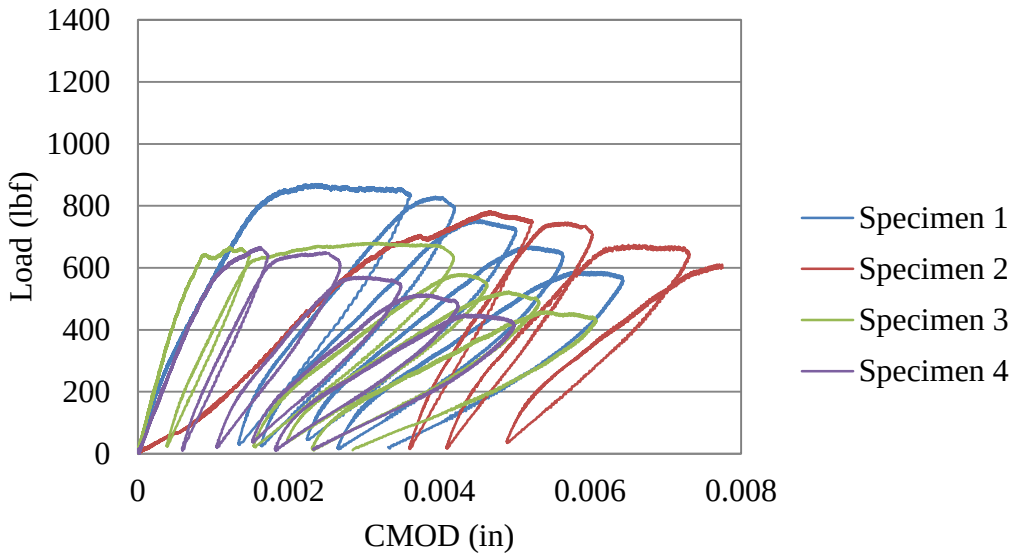

Figure B 1. Load vs *CMOD* plot for concrete mixture LS_0.75_17_0.4 tested at day 1.

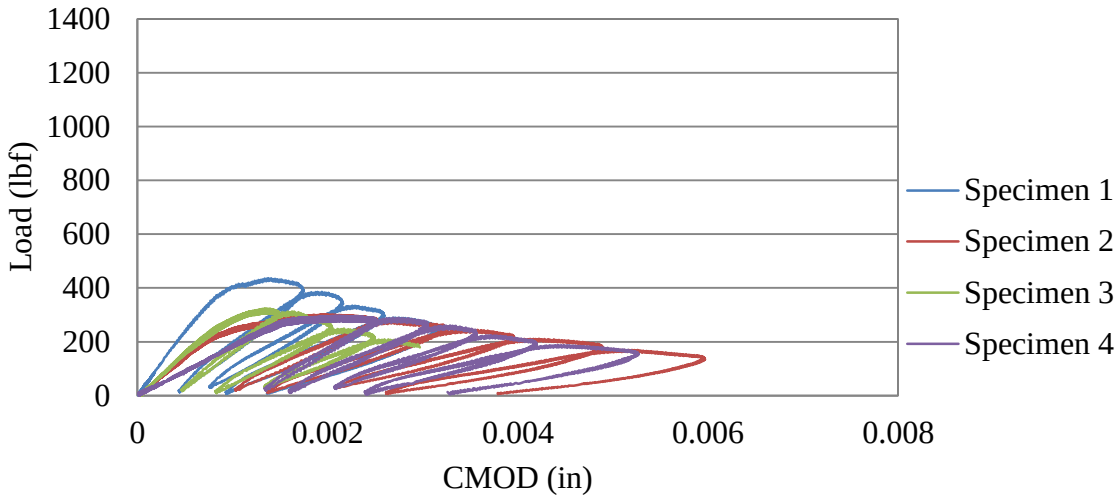

Figure B 2. Load vs *CMOD* plot for concrete mixture SL_1.25_34_0.4 tested at day 1.

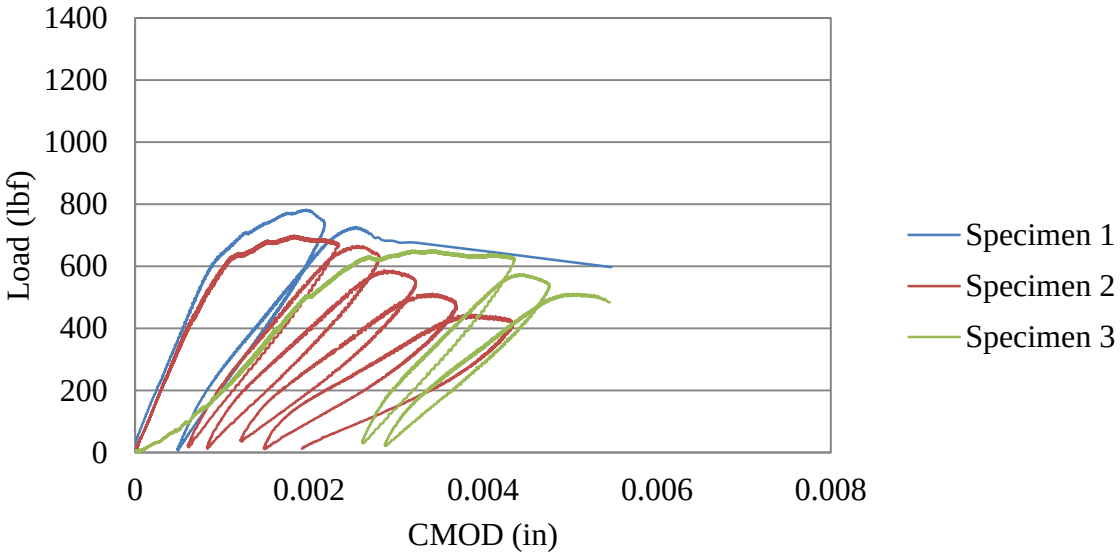

Figure B 3. Load vs *CMOD* plot for concrete mixture SL_0.75_34_0.45 tested at day 1.

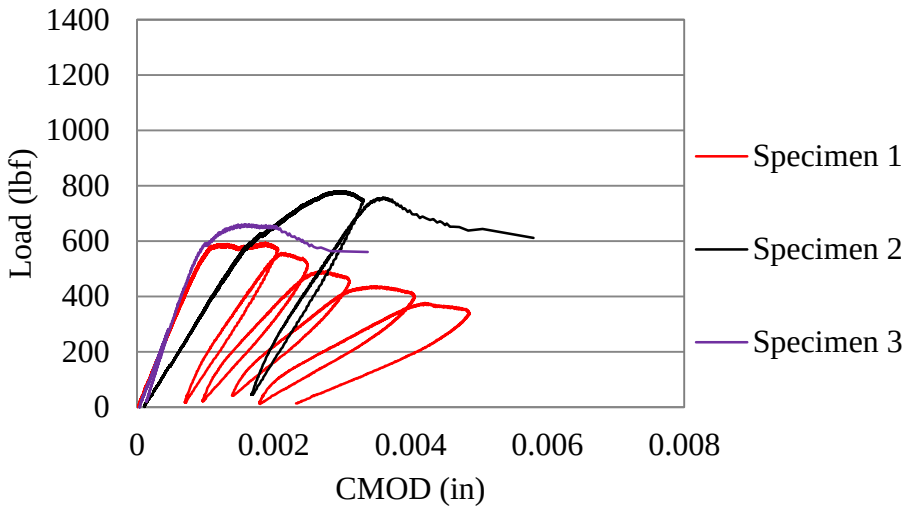

Figure B 4. Load vs *CMOD* plot for concrete mixture SL_0.75_34_0.40 tested at day 1.

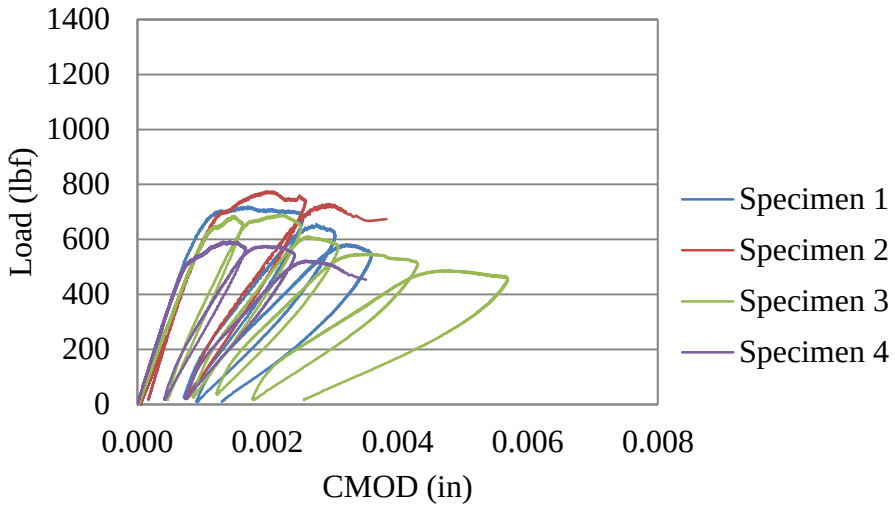

Figure B 5. Load vs *CMOD* plot for concrete mixture LS_0.75_17_0.45 tested at day 1.

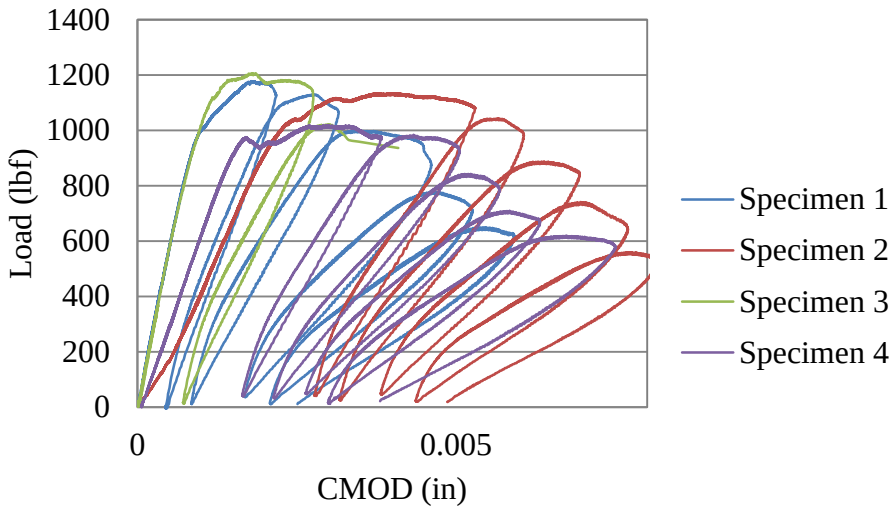

Figure B 6. Load vs *CMOD* plot for concrete mixture LS_0.75_17_0.4 tested at day 28.

.

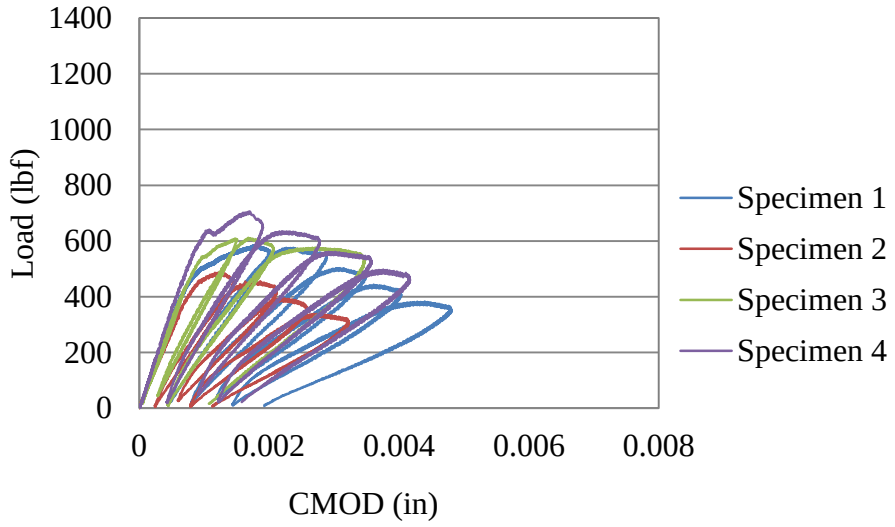

Figure B 7. Load vs *CMOD* plot for concrete mixture SL_1.25_34_0.4 tested at day 28.

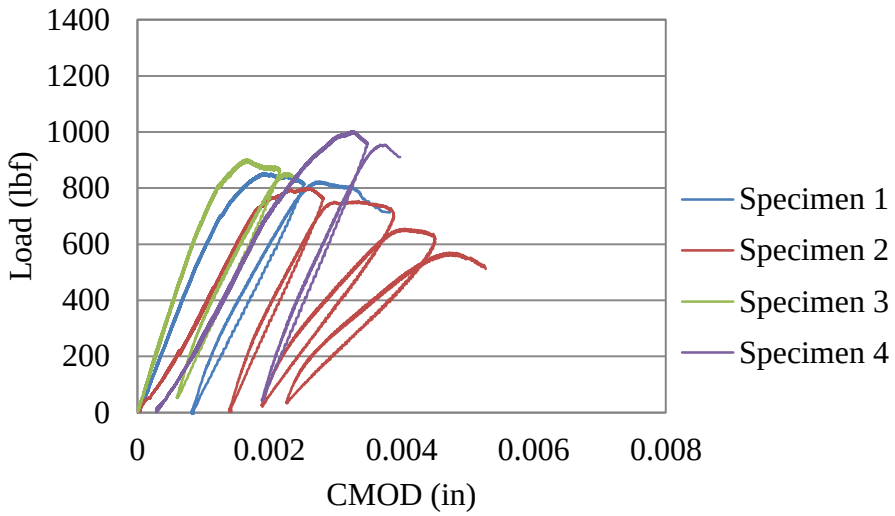

Figure B 8. Load vs *CMOD* plot for concrete mixture SL_0.75_34_0.45 tested at day 28.

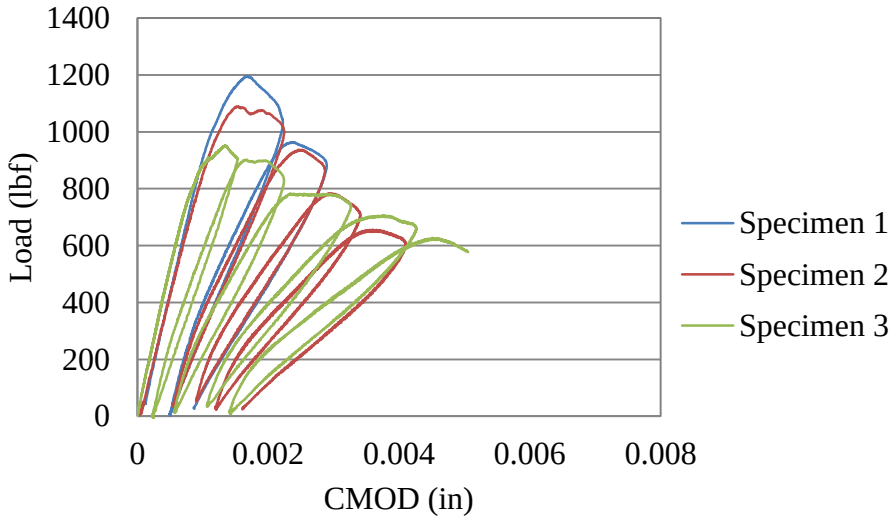

Figure B 9. Load vs *CMOD* plot for concrete mixture SL_0.75_34_0.40 tested at day 28.

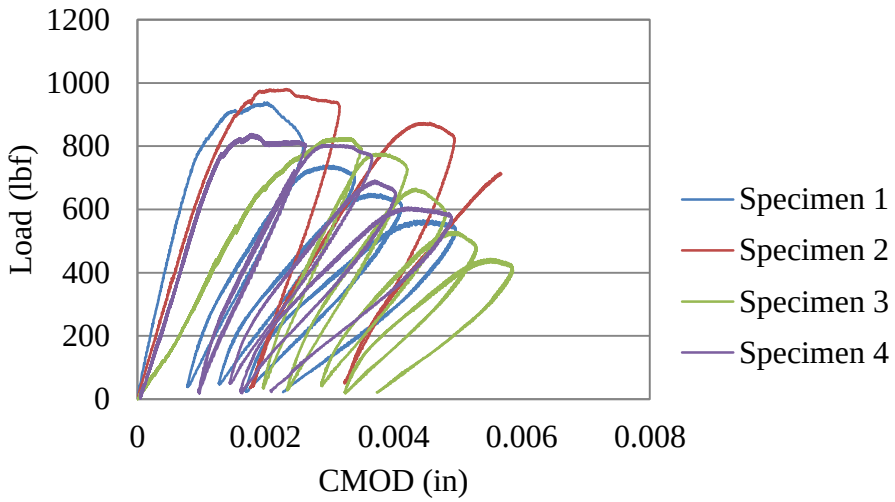

Figure B 10. Load vs *CMOD* plot for concrete mixture LS_0.75_17_0.45 tested at day 28.

APPENDIX C

PICTURES OF LABORATORY SETUP

Figure C 1. Fracture energy test setup.

Figure C 2. MTS clip gauge.

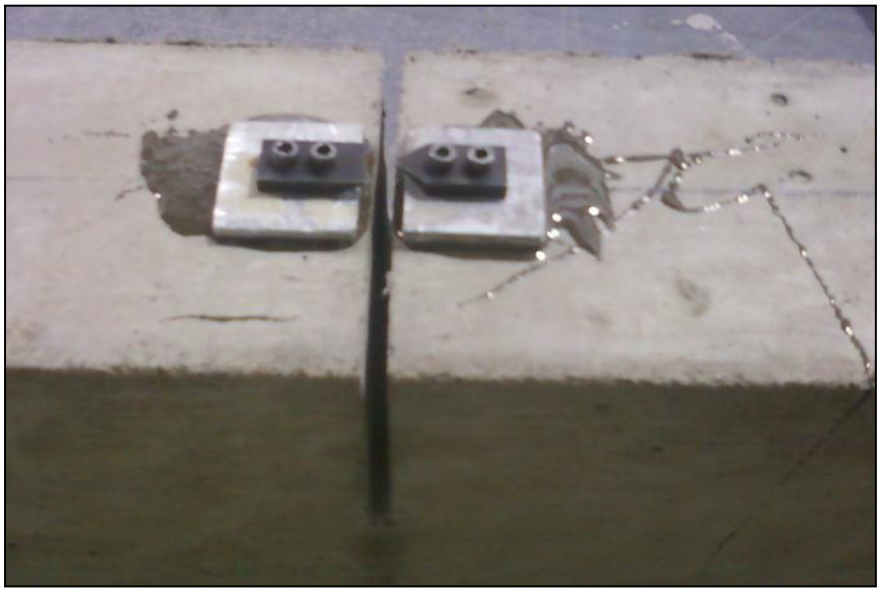

Figure C 3. Detail aluminum and steel plates.

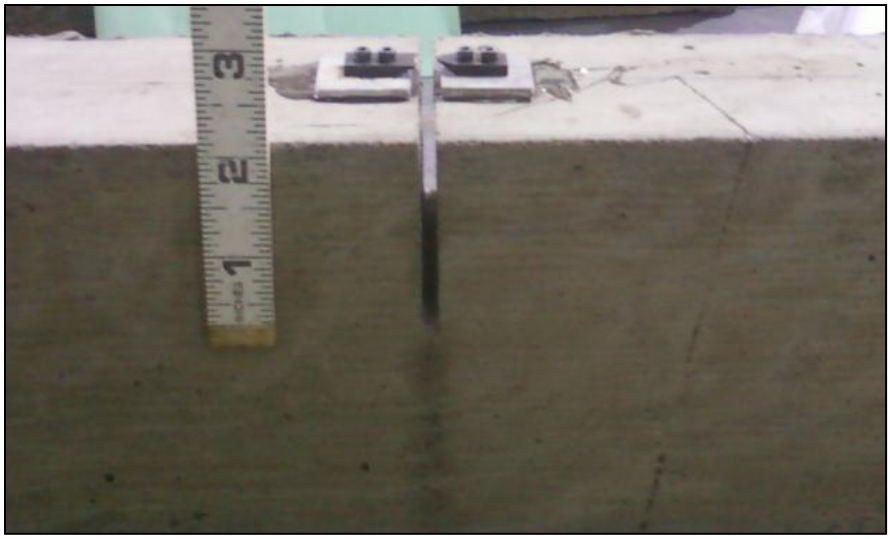

Figure C 4. Saw-cut notch of fracture energy beams.

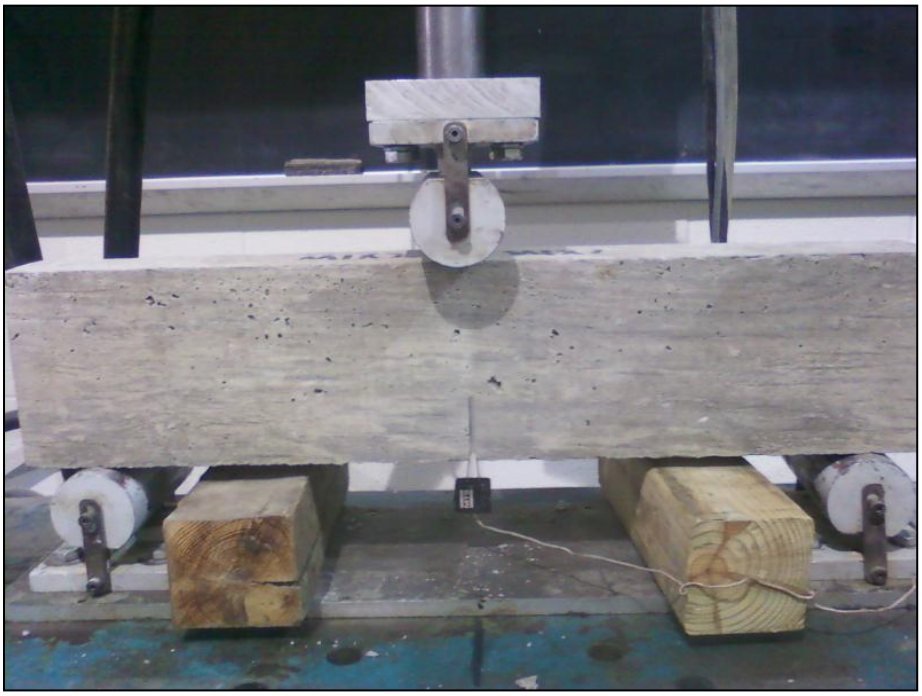

Figure C 5. Fracture energy test in progress.

Figure C 6. Flexural strength test setup.

BIBLIOGRAPHY

ARA,I.,ERES Consultants Division. (2004). *Guide for the Mechanistic-Empirical Pavement Design Guide of New and Rehabilitated Pavement Structures.* Transportation Research Board. Champaign, Illinois: National Cooperative Highway Research Program.

ASTM. (2004). *Annual Book of ASTM Standards, Section 4 Construction.* Philadelphia, Pennsylvannia: American Society for Testing and Materials International.

Bazant, Z., & Gambarova, P. (1980). Rough Cracks in Reinforced Concrete. *Journal of Structural Division* , 819-842.

Benkelman, A. C. (1933). Tests of Aggregate Interlock at Joints and Cracks. *Engineering News Record , 111* (NO.8), 227-232.

Bruinsma, J. E., Raja, Z. I., Snyder, M. B., & Vandenbossche, J. M. (1995). *Factors Affecting the Deterioration of Transverse Cracks in JRCP.* Michigan State University, Department of Civil and Environmental Engineering. East Lansing, Michigan: Michigan Department of Transportation and Great Lakes Center for Truck Transportation Research University of Michigan.

Chowdhury, J. P. (2005). *Tests to Identify Poor Quality Coarse Limestone Aggregates and Acceptable Limits for Such aggregates in bituminous mixes.* Austin, TX: Texas Transportation Institute.

Chupanit, P. (1999). Characterization of Concrete Pavement Joint Surfaces. *Ph.D. thesis* . University of Illinois at Urbana-Champaign.

Chupanit, P., & Roesler, J. R. (2005). Improvement of Concrete Cracking Resistance and Joint Load Transfer Through Coarse Agregate Selection. *Transportation Research Record: Journal of the Transportation Research Board No.1913 ,* 3-10.

Colley, B. E., & Humphrey, H. A. (1967). Aggregate Interlock at Joints in Concrete Pavements. *Highway Research Record* (198), 1-18.

Crovetti, J. A. (1994). Design and Evaluation of Jointed Concrete Pavemet Systems Incorporating Open-Graded Permeable Bases. *Ph.D. Dissertation* . University of Illinois at Urbana Champaign.

Ed Levy Natural Materials. (2010). Retrieved May 21, 2010, from http://www.edwclevy.com/home.aspx

Fabrizzio, M. A., & Buch, N. J. Performance of Transverse Cracking in Jointed Concrete Pavements. *ASCE Journal of Performance of Constructed Facilities , 13* (4), 172-180.

Giaccio, G., & Zerbino, R. (1998). Failure Mechanism of Concrete, Combined Effects of Coarse Aggregate and Strength Level. *Advanced Cement Based Materials , 7,* 41-48.

Hillerborg, A., Modeer, M., & Peterson, P. (n.d.). Analysis of Crack Formation and Crack Growth in Concrete by Means of Fracture Mechani.

Ioannides, A. M., & Korovesis, G. T. (1990). Aggregate Interlock: A Pure-Shear Load Transfer Mechanism. *Transportation Research Record: Journal of the Transportation Research Board No.1286* , 14-24.

Ioannides, A. M., Alexander, D. R., Hammons, M. I., & Davis, C. M. (1996). Application of Artificial Neural Networks to Concrete Pavement Joint Evaluation. *Transportation Research Record 1540* , 54-64.

Jenq, Y. S., & Shah, S. P. (1985). A Two Parameter Fracture Model for Concrete. *Journal of Engineering Mechanics , Vol. 111* (No.4), 1227-1241.

Jensen, D. C., Weiss, W. J., & Schleuchart, S. H. (2000). Simplification of the Testing and Analysis Procedure for the Two Paramater Fracture Model. *14th Engineering Mechanics Conference Proceeedings.*

Jensen, E. A., & Hansen, W. (2001). Mechanisms of Load Transfer-Crack width relation in JPCP: Influence of CA properties. *Procedures 7th Int. Conf. on Concrete Pavements, International Society* .

Jeong, J., & Zollinger, D. (2001). Characterization of Stiffness Parameters in Design of Continuosly Reinforced and Jointed Pavements. *Transportation Research Record* (No.1778), 54-63.

Johnson, R. (2005). *Probability and Statistics for Engineers.* Upper Saddle River: Pearson Prentice Hall.

Kahmaran, S., & Fener, M. (2007). Predicting the Los Angeles Abrasion Loss os Rock Aggregates From the Uniaxial Compressive Strength. *Materials Letters , 61* (26), 4861-4865.

Khazanovich, L., & Gotlif, A. (2003). *Evaluation of joint and Crack Load Transfer Final Report.* Champaign , IL: FHWA.

Ledolter, J., & Hogg, R. (2010). *Applied Statistics for Engineers and Physical Scientists.* Upper Saddle River, NJ: Pearson Prentice Hall.

Maitra, S. R., Reddy, K., & Ramachandra, L. (2010). Load Transfer Characteristics of Aggregate Interlocking in Concrete Pavement. *Journal of Transportation Engineering ASCE* , 190-195.

Mindess, S., Young, J., & Darwin, D. (2003). *Concrete* (Second ed.). Upper Saddle River: Prentice Hall.

Minitab. (2010). *Minitab*. Retrieved from http://www.minitab.com

Nassiri, S., & Vandenbossche, J. M. (2009). *Establishing Appropriate Inputs When Using the Mechanistic-Empirical Pavement Design Guide (MEPDG) To Design Rigid Pavements in Pennsylvania.* Pittsburgh: Pennsylvania Department of Transportation.

Noureldin, A. S. (1990). Evaluation of Steel Slag Asphalt Surface Mixtures. *69th Annual Meeting, Transportation Research Board.* Washington.

Nowlen, W. J. (1968). Influence of Aggregate Properties on Effectiveness of Interlock Joints in Concrete Pavements. *Journal of the PCA, Research and Development Laboratories , 10* (No.2), 2-8.

Raja, Z. I., & Snyder, M. B. (1995). *Factors Affecting the Deterioration of Transverse Cracks in JRCP*. Michigan State University, Department of Civil and Environmental Engineering. East Lansing, Michigan: Michigan Department of Transportation and Great Lakes Center for Truck Transportation Research University of Michigan.

RILEM Comitee on Fracture Mechanics of Concrete-Test Methods. (1990). Determination of the Fracture Parameters (K and CTODc) of Plain Concrete Using Three-Point Bend Tests. *Materials and Structures , 23*, 457-460.

Shah, S. P., Swartz, S. E., & Ouyang, C. (1995). *Fracture Mechanics of Concrete Applications of Fracture Mechanics to Concrete, Rock, and other Quasi-Brittle Materials.* New York: Jhon Wiley & Sons Inc.

Vandenbossche, J. M. (1999). Estimating Potential Aggregate Interlock Load Transfer Based on Measurements of Volumetric Surface Texture of the Fracture Plane. *Transportation Research Record: Journal of the Transportation Research Board No.1673* , 59-63.

Wade, M. J., Cutell, G. D., Vandenbossche, J. M., Yu, H. T., Smith, K. D., & Snyder, M. B. (1997). *Performance of Concrete Pavements Containing Recycled Concrete Aggregate.* Mc Lean, VA: Federal Highway Administration.

Walraven, J. (1981). Fundamental Analysis of Aggregate Interlock. (ASCE, Ed.) *Journal of Structural Engineering , 107* (No. ST11).

Wattar, S. W., Hawkins, N. M., & Barenberg, E. J. (2001). *Aggregate Interlock Behavior of Large Crack Width Concrete Joints in PCC Airport Pavements.* FAA Center of Excellence for Airport Technology.

Yu, H. (2005). Dowel Bar Alignments of Typical In-Service Pavements. *Yu, H.T. 2005. Dowel Bar Alignments of TR&D Serial No. 2894. Portland Cement Association, Skokie, IL*.

Zollinger, D., & Soares, J. (1999). *Performance of Continuosly Reinforced Concrete Pavements: Volume VII: Summary.* Federal Highway Admnistration.